

75 2

K5

logged in 7/23/8

LA-10299-PR
Progress Report

Los Alamos National Laboratory is operated by the University of California for the United States Department of Energy under contract W-7405-ENG-36

*Research and Development Related to
the Nevada Nuclear Waste Storage
Investigation*

July 1—September 30, 1984

HYDROLOGY DOCUMENT NUMBER 236

Los Alamos Los Alamos National Laboratory
Los Alamos, New Mexico 87545

The four most recent reports in this series, unclassified, are LA-10006-PR, LA-10032-PR, LA-10154-PR, and LA-10297-PR.

This report was prepared by the Los Alamos National Laboratory as part of the Nevada Nuclear Waste Storage Investigations managed by the Nevada Operations Office of the US Department of Energy. Based upon their applicability to the investigations, some results from the Radionuclide Migration Project, managed by the Nevada Operations Office of the US Department of Energy, are included in this report.

Prepared by Lia Mitchell, Group INC-7

DISCLAIMER

This report was prepared as an account of work sponsored by an agency of the United States Government. Neither the United States Government nor any agency thereof, nor any of their employees, makes any warranty, express or implied, or assumes any legal liability or responsibility for the accuracy, completeness, or usefulness of any information, apparatus, product, or process disclosed, or represents that its use would not infringe privately owned rights. Reference herein to any specific commercial product, process, or service by trade name, trademark, manufacturer, or otherwise, does not necessarily constitute or imply its endorsement, recommendation, or favoring by the United States Government or any agency thereof. The views and opinions of authors expressed herein do not necessarily state or reflect those of the United States Government or any agency thereof.

Research and Development Related to the Nevada Nuclear Waste Storage Investigations

July 1—September 30, 1984

Compiled by
A. E. Ogard and D. T. Vaniman

Contributors

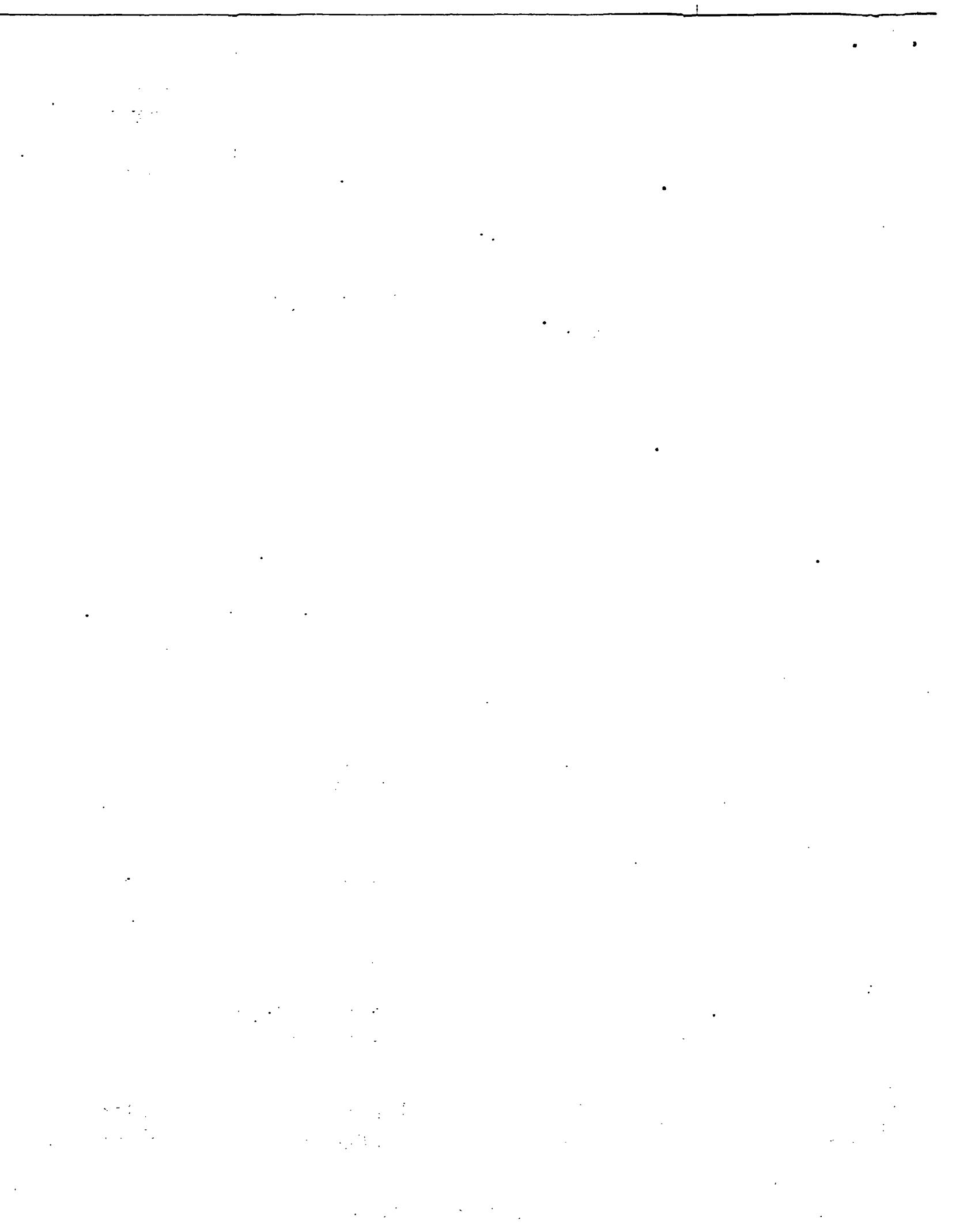
B. P. Bayhurst	F. O. Lawrence
D. L. Bish	S. S. Levy
J. D. Blacic	A. J. Mitchell
L. Brown	E. J. Mroz
D. E. Broxton	T. W. Newton
F. M. Byers, Jr.	H. Nitsche*
F. Caporuscio	A. E. Norris
B. A. Carlos	E. Nuttall†
M. R. Cisneros	A. E. Ogard
B. M. Crowe	P. Palmer
C. J. Duffy	D. M. Roy‡
N. Edelstein*	R. S. Rundberg
S. K. Gifford**	K. W. Thomas
L. S. Hersman	J. L. Thompson
D. E. Hobart	B. J. Travis
S. Hodson	D. T. Vaniman
J. W. Jones**	P. L. Wanek
J. F. Kerrisk	K. Wolfsberg
S. D. Knight	

*Materials and Molecular Research Division, Lawrence Berkeley Laboratory, Berkeley, CA 94720.

**HydroGeoChem, Inc., 1430 North 6th Avenue, Tucson, AZ 85705.

†Chemical-Nuclear Engineering Department, University of New Mexico, Albuquerque, NM 87131.

‡Materials Research Laboratory, Pennsylvania State University, University Park, PA 16802.



CONTENTS

ABSTRACT	1
EXECUTIVE SUMMARY	2
I. INTRODUCTION	12
II. GEOCHEMISTRY.	12
A. Groundwater Chemistry	12
1. Groundwater Composition of Well USW H-6	12
2. pH Buffer Capacity of Well J-13 Water	20
B. Natural Isotope Chemistry	22
1. Results of the June 25-29 Field Trip	22
2. August 13-15 Field Trip	31
C. Hydrothermal Geochemistry	35
D. Solubility Determinations	37
1. New Version of EQ3/6	37
2. Actinide Chemistry in Near-Neutral Solutions	37
3. Solubility of Actinide Compounds	39
E. Sorption and Precipitation	42
1. Groundwater Composition Effects	42
2. Long-Term Technetium Sorption Measurements	42
3. Neptunium Sorption Isotherm Measurements	44
4. Plutonium and Americium Sorption Measurements	44
5. Sorption Measurements of Uranium and Selenium	47
6. Microbial Activity at Yucca Mountain	47
F. Dynamic Transport Processes	49
1. Crushed-Tuff Columns	49
2. Particulate Studies	52
G. Retardation Sensitivity Analysis	55
1. Colloids	55
2. Colloids in Nuclear Waste	57
3. Population Balance	60
4. Application to Nuclear Waste Repository Assessment-Scenarios	61
5. Conclusions	65
H. Applied Diffusion	65

III.	MINERALOGY-PETROLOGY OF TUFF	66
	A. Iron and Manganese in Oxide Minerals and in Glasses . . .	66
	1. Redox Interactions	66
	2. Retardation of Manganese Oxides	68
	B. Zeolite Dehydration Experiments	69
	C. Summary of Mineralogic Data for Yucca Mountain	71
	1. Glass	74
	2. Silica Polymorphs	75
	3. Smectite	75
	4. Clinoptilolite and Mordenite	76
	5. Analcime and Albite	77
IV.	TECTONICS AND VOLCANISM	78
	A. Mechanism of Emplacement of Shallow Intrusions	78
	B. Volcanic Patterns Through Time: DV-PR Volcanic Zone . . .	79
V.	TUFF LABORATORY PROPERTIES	84
	A. History	85
	B. Current Research	86
VI.	SEALING MATERIALS EVALUATION	88
	A. Experimental Results	89
	1. Grout Mixture 82-22	91
	2. Grout Mixture 84-12	91
	B. Comparison of the 82-22 and 84-12 Formulations	92
	C. Conclusions	93
	REFERENCES	93

RESEARCH AND DEVELOPMENT RELATED TO THE NEVADA NUCLEAR
WASTE STORAGE INVESTIGATIONS

July 1--September 30, 1984

Compiled by

A. E. Ogard and D. T. Vaniman

Contributors

B. P. Bayhurst	F. O. Lawrence
D. L. Bish	S. S. Levy
J. D. Blacic	A. J. Mitchell
L. Brown	E. J. Mroz
D. E. Broxton	T. W. Newton
F. M. Byers, Jr.	H. Nitsche
F. Caporuscio	A. E. Norris
B. A. Carlos	E. Nuttall
M. R. Cisneros	A. E. Ogard
B. M. Crowe	P. Palmer
C. J. Duffy	D. M. Roy
N. Edelstein	R. S. Rundberg
S. K. Gifford	K. W. Thomas
L. S. Hersman	J. L. Thompson
D. E. Hobart	B. J. Travis
S. Hodson	D. T. Vaniman
J. W. Jones	P. L. Wanek
J. F. Kerrisk	K. Wolfsberg
S. D. Knight	

ABSTRACT

This report summarizes the contribution of the Los Alamos National Laboratory to the Nevada Nuclear Waste Storage Investigations for the fourth quarter of FY 1984.

EXECUTIVE SUMMARY

This report summarizes some of the technical contributions from the Los Alamos National Laboratory to the Nevada Nuclear Waste Storage Investigations (NNWSI) project managed by the Nevada Operations Office of the US Department of Energy (DOE) during the period July 1 through September 30, 1984. The report is not a detailed technical document but does indicate the status of the investigations being performed at Los Alamos.

GEOCHEMISTRY

The objective of this work is to determine the geochemical properties of Yucca Mountain tuff and groundwater. These properties will be used as a basis for predicting the migration of radionuclides to the accessible environment and for assessing the geochemical response of a potential repository site in Yucca Mountain in the southwest portion of the Nevada Test Site to the emplacement of a repository.

Groundwater Chemistry

In the quarterly report for the second quarter of FY 1984, we reported on the composition of the groundwater pumped from Well USW H-3 located at the south end of the repository block at Yucca Mountain. Two features of this groundwater were different from other groundwaters of the area: the pH was higher and the water was reducing. These results could have important consequences for the solubility of some of the waste elements if it could be shown that these groundwater conditions are general for the repository area and can be expected to continue in the future.

Well USW H-6 is immediately west of the repository block and may be along the recharge pathway to the repository block area. There are two separate and distinct permeable zones in this well; in the Bullfrog Member and the Tram Unit. Groundwater from these separate zones would yield information on the vertical distribution of water compositions and also on the expected composition of possible recharge water to the saturated zone beneath Yucca Mountain.

Both zones were individually packed off and each pumped at over 13 l/s until formation water was established. Samples were periodically taken and analyzed in the usual manner reported for other wells.

The results are different from what was expected.

- The groundwaters cleared of detergent very quickly by pumping. Apparently, less detergent was used in the drilling of this well compared to others.
- The groundwater from permeable zones in the Bullfrog Member and the Tram Unit are both oxidizing.
- Very little difference exists in the composition of the groundwaters of the permeable zones in the Bullfrog Member and the deeper Tram Unit. Calcium and bicarbonate ions are ~0.1 meq/l higher in the upper Bullfrog Member; all other constituents are quite similar between the two waters.

The amount and identification of particulates moving with the groundwater are insufficiently known. Small-sized mineral particulates from tuff and natural colloids, such as iron hydroxides, are possible transporters of sorbed or coprecipitated waste elements if the solids move through the fractures or open porosity of the tuff along with the natural water flow. Studies on particulates in the laboratory and in the field pumping tests will be our major emphasis for the remainder of FY 1984 and FY 1985.

The pH buffer capacity of Well J-13 water and water plus local minerals has been estimated. The results indicate that the water alone and the water plus minerals commonly found at Yucca Mountain have a relatively good buffer capacity. This is particularly true for the water-mineral system subject to H^+ addition such as might result from oxidation of iron pyrite.

Natural Isotope Chemistry

Two field trips to Yucca Mountain were undertaken to collect samples for measuring rainfall infiltration by the "bomb pulse" ^{36}Cl technique. The bomb pulse refers to the greatly increased ^{36}Cl global fall-out that resulted from high-yield nuclear weapons tests conducted in the Pacific Ocean testing area between 1952 and 1959. The first field trip this quarter resulted in the collection of samples for ^{36}Cl analyses from a trench bulldozed in the alluvial fill at the Exploratory Shaft site in Coyote Wash and from the Yucca Wash 6 trench, which is located about 4 km east of the Exploratory Shaft site. In addition, survey work of two types was performed to help locate a suitable site to measure ^{36}Cl infiltration into fractured tuff. One type

consisted of sampling the thin soil overlying the fractured tuff at four sites on the crest of Yucca Mountain and at one site at the mouth of Coyote Wash. These soil samples were analyzed for chloride concentrations. The low chloride contents and the lack of increased chloride contents adjacent to the underlying tuff indicate well-drained soils. Presumably, rainfall drains into the fractured tuff. The second type of survey involved measurements of the electromagnetic conductivity of the 10 to 20 m of tuff closest to the surface at two sites on the crest of Yucca Mountain and at three sites adjacent to Coyote Wash. Measurements at 30° increments about the surveyed points showed that the tuff is electrically anisotropic in the direction of fracturing. A potential site for collecting fractured tuff samples for ^{36}Cl measurements was identified at the mouth of Coyote Wash from these electromagnetic survey results. The site was determined to contain no archeological artifacts and no endangered plant or animal species. A backhoe and a pneumatic hammer were used to collect samples to a depth of 0.8 m, when heavy rains forced the termination of sampling at this location. The excavation was backfilled as well as the muddy conditions would permit, to prevent the hole from becoming a local recharge point.

Hydrothermal Geochemistry

A thermodynamic model has been constructed for analcime as a start to our understanding the controls on its stability. Modeling analcime stability leads to insights about the parameters that affect the stability of other zeolites and the probable relative importance of kinetics versus chemical equilibrium.

The thermodynamics of analcime are directly important because analcime is a probable breakdown product of clinoptilolite. The thermodynamics of analcime as well as those of clinoptilolite must, therefore, be known before the possible reaction of clinoptilolite to analcime phases can be modeled. The model for analcime can also be used to clarify the present chemical conditions in portions of Yucca Mountain where analcime is present and to examine the possibility that these portions of the mountain may have been heated to higher temperatures in the past.

The model indicates that the analcimes present in Yucca Mountain crystallized under conditions where the silica activity was only slightly below that in equilibrium with cristobalite. The fact that they presently

coexist with quartz indicates that the rock is not in overall equilibrium. The model suggests that the analcimes did not crystallize at temperatures above about 150°C but does not indicate a specific temperature. The model predicts that analcime will crystallize at higher silica activities when the pressure on the crystal is closer to the fluid pressure. This implies that, as the mountain evolves toward silica activities more closely in equilibrium with quartz, albite may be converted to analcime that will tend to crystallize in void space where the pressure on the analcime would be equal to the fluid pressure. Such an occurrence would tend to decrease permeability.

Solubility Determinations

A new version of the EQ3/6 chemical equilibration computer program has been received and brought up on the Livermore Time Sharing System (LTSS) at Los Alamos.

Data collected on the solubility behavior of colloidal Pu(IV) are being reviewed in our attempt to understand the reactions that are occurring and the controlling mechanisms. An upper limit for the solubility product has been estimated, but a lower limit is still uncertain.

Solubility measurements of NpO_2^+ , NpO_2^{2+} , Am^{3+} , Pu^{4+} , PuO_2^+ , and PuO_2^{2+} in Well J-13 groundwater have been started by Heino Nitsche at Lawrence Berkeley Laboratory. To avoid the loss of CO_2 from the J-13 water during the experiment, a partial CO_2 -pressure of 0.014 atmospheres is being maintained above the solution surface at all times. The pH of the solution is held at 7.0 ± 0.1 through the use of a pH-stat.

Work on the solubility of $\text{Am}(\text{OH})\text{CO}_3$ has been started. $\text{Am}(\text{OH})\text{CO}_3$ was prepared by the formation and subsequent hydrolysis of the trichloroacetate complex in aqueous solution. The material is being characterized by x-ray powder diffraction (XRD) analysis.

Sorption and Precipitation

Sorption experiments testing the effects of possible variations in groundwater composition are being conducted. In addition to water from Well J-13, we are using waters from Wells UE-25p#1 (P-1), which has much higher concentrations of calcium, magnesium, strontium, barium, sodium, bicarbonate, and sulfate, and USW H-3 and deionized water. Sorption measurements of strontium, cesium, barium, and europium were performed this quarter with

UE-25p#1 and deionized waters, using USW G-1-2901 tuff (devitrified). Sorption ratios for strontium, cesium, and barium are lower for the P-1 water than for the deionized water, indicating the expected ionic-strength effect. Barium and europium ratios were high in both cases.

Sorption measurements with technetium and J-13 groundwater show no increases with contact times up to 1 yr and are close to zero. Final measurements will be made at 15 months.

Batch measurements with ^{235}Np for long-term sorption measurements are continuing. Neptunium isotherm sorptions in a CO_2 controlled atmosphere are finished, and as much of the counting as is presently possible has been completed. Counting of the samples will resume soon.

Serial sorption measurements with plutonium have been started, and the first phase has been completed. The measurements are being made on drill hole USW GU-3-916 crushed rock. The sorption ratio determined in the first phase is 260 ± 14 , which agrees quite well with the value of 250 ± 25 reported previously. The second phase, which is sorption on freshly crushed rock using the aqueous phase of a previous sorption, will be completed within the next few weeks. This will indicate whether the species of plutonium remaining in solution after a sorption experiment behaves any differently than the plutonium that sorbed initially.

There has recently become available a well-characterized solution of Am(III) in carbonate solution. Batch sorptions will be run with this material as well as that used previously for americium batch sorptions, and the results will be compared with those for fast-flow columns.

There will soon be available to us carbonate solutions of Pu(V) and of Pu(VI). Batch sorptions are planned using feed solutions made by adding a spike of the carbonate solutions to the rock-equilibrated water. A comparison will be made by using plutonium solutions prepared in our usual manner.

Batch sorption measurements of uranium were carried out at a pH of 6.0 to 6.4 in a controlled partial pressure of CO_2 . This gives conditions comparable with those found in Yucca Mountain groundwaters. An effect on uranium sorption because of the change from pH 8 may be possible because of the change in the carbonate complexing of uranyl ion. We are observing R_d values 3 to 8 times higher than at pH 8.3, indicating that previous measurements gave conservative results. Similar experiments with selenium indicated no change from previous work carried out in the ambient atmosphere.

Work is continuing on the study of anaerobic degradation of drilling fluids with an investigation of gas evolution from an anaerobic growth from Yucca Mountain on Turco-5622. The purpose of this work is to determine if microbial activity can influence the mobility of waste elements, such as plutonium, at Yucca Mountain. Preparations for a new plutonium sorption experiment were made this quarter, and a series of experiments was carried out. Pure cultures, capable of degrading ASP-700 or Turco-5622 drilling fluids, were prepared and used. Results will be presented in the future.

Dynamic Transport Processes

The anion exclusion effect was observed in the 2-m-long USW G-2-2017 crushed-rock column. The anions chloride, sulfate, and nitrate were found to elute approximately 22 per cent earlier than tritiated water. The magnitude of the observed effect is in approximate agreement with the internal volume of the intracrystalline channels in clinoptilolite and mordenite. The one exception is fluoride that arrived slightly later than tritiated water. This may be due to the small ionic radius of fluoride, which may be small enough to penetrate the intracrystalline channels. If the tuff/J-13 system is near fluorite saturation, however, the retardation may be due to fluorite precipitation. Pertechnetate has not been run through the columns, but, based on the above observations, it is not expected to be retarded because the ionic radius is larger than fluoride.

The code INVPOS was modified to invert the Laplace transform generated in autocorrelated photon spectroscopy (APS). The method of Butler et al.* would not optimize the smoothing factor at first. This was found to be due to the assumption used in deriving the auxiliary equation $H(\alpha)$ that all errors are equal so that the standard deviation could be used. Because the errors are larger for the early correlation data, the $H(\alpha)$ function could not be minimized. The standard deviation was, therefore, replaced by the vector dot product of the individual errors in $H(\alpha)$. The code now inverts APS data with optimal smoothing.

Monodisperse polystyrene particles with diameters from 60 nm to 1.0 micron have been acquired for testing the APS system. The particle size distribution for these suspensions has been determined by electron

* J. P. Butler, J. A. Reeds, and S. V. Dawson, "Estimating Solutions of First Kind Integral Equations With Nonnegative Constraints and Optimum Smoothing," SIAM J. Numer. Anal. 18, 381 (1981).

microscopy. Fluorescent polystyrene particles have also been purchased for testing as possible colloids for use in field testing. The fluorescent particles are carboxylated so they would be expected to have a negative charge and, therefore, are not expected to adhere to mineral surfaces. The fluorescence makes them easy to detect at very low concentrations by fluorimetry.

Retardation Sensitivity Analysis

There are many recent papers on the geological disposal of waste and repository assessment, but they have not quantitatively addressed the impact of colloid formation and transport.

Since about 1979, the question of colloid formation and migration has increased in importance and is now a topic of major interest in the scientific community. To date, several experimental studies have shown the presence of radioactive colloids under simulated waste disposal conditions, but their impact on repository assessment, however, has not been addressed because the existing geo-transport codes used to assess geologic waste disposal cannot treat this problem. Additional theory and equations are required to mathematically describe colloid formation and migration. The population balance equations and submodels can be added to the existing radionuclide transport theory and codes to accomplish this goal.

Through the correct use of the population balance equations coupled with the existing theory, problems of colloid formation and migration can be assessed quantitatively. The well-established theory of the population balance can be applied to the difficult radioactive colloid problem with the same success with which it has been used to treat many physical and biological particulate problems over the past 20 years.

We have reviewed the key experimental research on radioactive colloids and developed the population balance. Its application to waste assessment is illustrated by modeling two postulated repository scenarios: (1) a near-field study and (2) a far-field problem involving colloids from when the backfill is breached and waste leakage occurs during the thermal repository, and from natural sources.

Applied Diffusion

Work to characterize the properties of bromide anions as a tracer in field measurements of diffusivity was impeded by problems with the necessary analytical instrumentation. Parts of one ion chromatograph required repair at the factory. The parts have been returned, and the apparatus will be usable as soon as some minor leaks are fixed. A new ion chromatograph required samples too large for routine use in these bromide tracer studies. The sampling system of the new ion chromatograph is being modified to permit the use of this analytical instrument in addition to the other ion chromatograph for the tracer studies in this program.

Mineralogy/Petrology of Tuff

Mineralogy/petrology studies this quarter concentrated on the oxidation-reduction (Eh) buffering potential of iron and manganese in Yucca Mountain minerals and glasses, on zeolite dehydration studies, and on a compilation of current x-ray diffraction data for rocks in the vicinity of the Yucca Mountain exploration block. The iron-manganese study concludes that the oxide minerals may have little potential for removing oxygen from groundwater. Ferrous iron occurs only in oxide phenocrysts that have been isolated from past water interaction; it remains to be determined whether these phenocrysts could have any active role in water interactions during future transport. The manganese oxides that occur within the tuff, primarily along fractures, consist of minerals (todorokite, cryptomelane, and possibly lithiophorite) that contain predominantly Mn^{4+} rather than Mn^{2+} and, therefore, have almost no capacity for removing oxygen from groundwater. Ferrous iron in glasses may have some potential for removing oxygen from groundwater. Studies of zeolite dehydration reactions have progressed from experiments in vacuum (to establish limits of concentration) to experiments under controlled humidity. It has been found that zeolite composition has a strong effect on dehydration reactions. Sodium-saturated clinoptilolite underwent the greatest contraction (8.4%), calcium-saturated compositions contracted less (3.6%), and potassium-saturated clinoptilolite underwent the least contraction (1.6%). However, clinoptilolites in partially saturated rocks at temperatures below 100°C should not decrease in volume significantly. The summary of x-ray diffraction data emphasizes, as in previous studies, that the Yucca Mountain region consists of three principal mineralogic categories:

primary rocks that consist mostly of silica minerals and alkali feldspar, primary rocks that consist mostly of glass, and altered rocks that may contain relatively sorptive minerals (zeolite and clay) or nonsorptive minerals (analcime, albite). This summary shows that the transition from tridymite to quartz occurs about midway in the densely welded portion of the Topopah Springs Member, that four principal zeolitization intervals can be mapped beneath Yucca Mountain, and that sorptive clays (smectites) occur in abundance either near major vertical structures (the Claim Canyon cauldron rim, or the structure of Drill Hole Wash) or as a "sandwich" bounding the proposed repository horizon.

Tectonics and Volcanism

Sills and discordant basalt intrusions are present at two localities in the Nevada Test Site (NTS) region. Formation of these types of intrusions during disruption of a repository could greatly increase the consequences of its disruption. Field and drill hole data suggest that narrow dikes are the more common intrusion structure. However, the stress regime of Yucca Mountain could favor the formation of sill-like intrusions and data on frequency of occurrence of basalt intrusion structures in the southern Great Basin may be biased by the level of erosional dissection of basalt landforms.

Three major petrological groups of basalt are recognized in the basalt episodes of the NTS region. These include straddle-type hawaiite, hypersthene hawaiite, and basaltic andesite. No distinct time-space trends are recognized in the geochemical patterns of these basalt groups.

Tuff Laboratory Properties

This study is being terminated this quarter. The preliminary part of this study has been completed in zeolitized tuff, and shows that time-dependent mechanical properties (creep) can significantly degrade zeolitized tuff stability. Preliminary estimates indicate that the long-term strength of devitrified tuff, such as the Topopah Spring devitrified samples, may also be significantly decreased. Unfortunately, the termination of this project will not permit these estimates to be tested.

Sealing Materials Evaluation

During this quarter, work has been carried out on a new cementitious grout mixture (84-12) having lower calcium sulfate content, because of concern about the possible adverse effect on waste element solubility from introduction of sulfate in the repository water. Work was also completed on a previously prepared, higher sulfate grout (82-22). Both formulations were developed with the objective of minimizing the chemical potential differences between the bulk tuff composition and the bulk grout composition without the extensive use of locally derived (local to the NTS) tuffaceous materials.

Comparisons of the data for the 200°C experiments show relatively small differences in the compositions of calcium, sodium, and sulfate in the fluid phases in contact with the two formulations in combination with tuff. The 84-12 formulation exhibits a generally lower concentration of silicon than the 82-22 formulation, possibly reflecting the physical properties of the silica-rich admixtures that were utilized in the formulation. The pH values of liquids in contact with both formulations appear to decrease with time, except for the 84-12 mixture at 200°C (based on a single point at 600 hours, which is slightly higher again). The alteration of the two concretes appears to be slightly different. The 82-22 formulation maintains a pH value almost one unit lower than the 84-12 formulation.

No major differences were found between the chemical behaviors of grout mixtures 82-22 and 84-12. Despite the lower sulfate content of 84-12, solutions in contact with it showed similar sulfate content to those in contact with 82-22. This is probably due to control of sulfate by anhydrite precipitation in both grouts. Grout 84-12 may, however, be a more appropriate grout for use in Yucca Mountain because its use would introduce less total sulfate. Also, if removal of sulfate from the fault seals were leach rate controlled, the lower sulfate content 84-12 would probably give up its sulfate more slowly.

I. INTRODUCTION

This report summarizes some of the technical contributions from the Los Alamos National Laboratory to the NNWSI project managed by the Nevada Operations Office of the US DOE during the period July 1 through September 30, 1984. The report is not a detailed technical document but does indicate the status of the investigations being performed at Los Alamos.

II. GEOCHEMISTRY

A. Groundwater Chemistry

1. Groundwater Composition of Well USW H-6. (A. E. Ogard, M. R. Cisneros, A. J. Mitchell, and P. L. Wanek). In the quarterly report for January-March 1984¹ we reported on the composition of groundwater pumped from Well USW H-3 located at the south end of the repository block at Yucca Mountain (Fig. 1). Two features of this groundwater were different from other groundwaters of the area; the pH was higher (at ~9.4 rather than ~7.2) and the oxidation-reduction potential was reducing (-143 mV) whereas in other wells it is oxidizing (+250 to 350mV). These results could have important consequences for the solubility of some waste elements² if it could be shown that these groundwater conditions exist generally below the repository area and are expected to continue in the future.

Well USW H-6 is west of the repository block of Yucca Mountain (Fig. 1) and is up-gradient in the hydrologic flow paths³ from Well USW H-3. However, being up-gradient may not mean it is directly in the flow path because the fault in Soltario Canyon between the two wells may redirect the flow path. There are two separate and distinct permeable zones:⁴ the upper zone in the Bullfrog Member at 610 to 635 m and the lower zone in the Tram Unit at 775 to 785 m.

Because of the relationship of the USW H-6 well location to well USW H-3, it was thought that groundwater from separate permeable zones in Well USW H-6 would yield information on

- o the composition of water that may be the precursor of the groundwaters of the permeable zones that exist below Yucca Mountain and
- o the difference in water composition for two well-separated permeable zones in tuff.

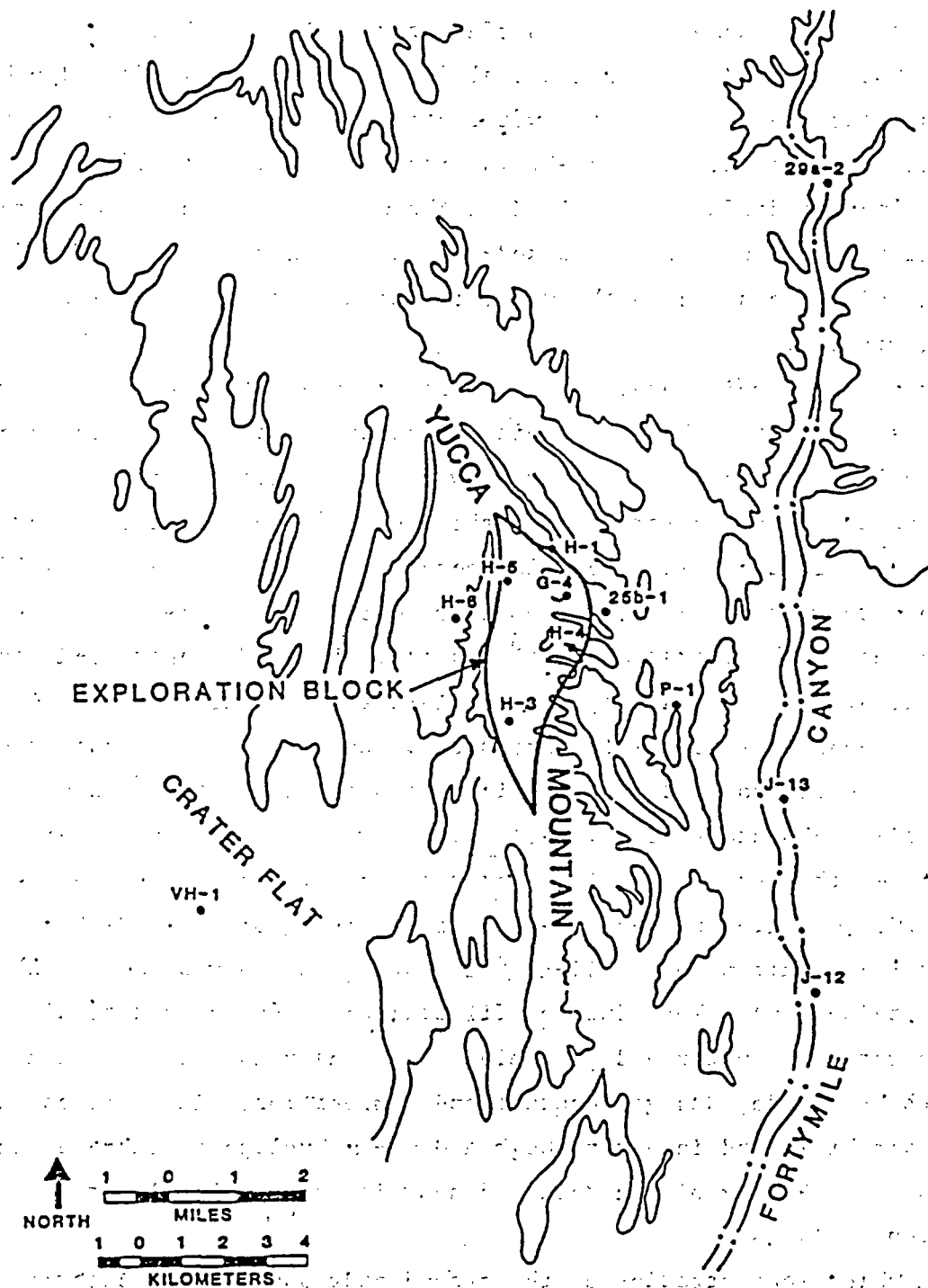


Fig. 1. Location map showing the exploration block outline at Yucca Mountain. Drill hole locations are indicated.

The pumping test was set up in a similar manner to the test in Well UE-25b#1.⁵ A Lynes Inflata-Plug was first set in the Well at ~835 m in depth and a Lynes Pip Packer at ~750 m. Groundwater could then be pumped from between these two packers to the surface for analysis. The pump was set at a 610-m depth, much deeper than normal for pumping wells. This depth was chosen so that the height of the water column inside the casing at the pump locations would be large, thus eliminating any possibility of pump-cavitation and reducing the diffusion of air down through the column of water to the water being pumped out of the packed-off zone. In addition, 20 l of diffusion pump oil were added to the water column over the pump to act as a floating air seal.

During the pumping process, a portion of the well's total flow was continuously directed through a 1-in. Tygon hose into the mobile laboratory at the well site. There the water flow could be directed into the anaerobic filtration equipment and/or through the electrode cell, where measurements of oxygen, pH, oxidation-reduction (Eh) potential, conductance, and sulfide could be made without exposing the water to the atmosphere.

The anaerobic filtration unit⁵ consists of two Nuclepore 1-l stainless steel filtration units, appropriate stainless steel valves and tubing, and 1-l Pyrex receiver vessels with pressure stopcocks. The filtration unit is mounted on wheels so that the unit is portable and can be taken out of our large mobile laboratory to any well site. Two filtration units are provided in series so that even very dirty water can be filtered in stages, ending with a 0.05- μ m Nuclepore membrane. In the pumping of Well USW H-6, only the top filtration unit with a 0.05- μ m Nuclepore membrane was used. The 1-l Pyrex containers were kept full of filtered water (unexposed to air) to be used for reference water and possible future analyses for concentration of ¹⁴C, carbon-dioxide, and gas content and composition. In addition, daily samples were filtered in air through a 0.05- μ m Nuclepore membrane, acidified with 100 μ l of Ultrex nitric acid and sent in Nalgene bottles to Los Alamos for cation analyses.

The anion concentration of the groundwater usually was determined twice a day, by using a Dionex Model 16 Ion Chromatograph in the mobile laboratory at the well site. This instrument proved to be extremely durable and dependable for such a field operation. Samples of anaerobically filtered water, water taken directly from the well, and water exiting the mobile laboratory:

were all used as samples for anion analysis. Varying sampling procedures did not produce any discernable differences in the samples' anion content. The detergent content of the water was determined spectrophotometrically with a Hach Model DR-EL/4 Portable Laboratory. Detergent was a good indicator or tracer of drilling fluids in the well. The Eh was measured with a Sensorex S500C-ORP electrode; pH, with an Orion "Ross" Model 81-02 combination electrode; sulfide, with a Beckman #39610 Sulfide/Silver Electrode; and oxygen, with a Yellow Springs Instrument Model 54 ARC dissolved-oxygen meter and electrode. Alkalinity was determined (on samples sent to Los Alamos) by using a Metrohm E636 Titroprocessor to titrate unfiltered samples with hydrochloric acid.

Results of our analyses are shown in Tables I and II.

Upon completion of the first pumping test, which was determined by the total disappearance of the detergent used in drilling the well, the Inflata-Plug, Pip-Packer, and pump were removed and relocated to 650, 610, and 580m, respectively, to pump groundwater from the isolated zone in the Bullfrog Member. Again, 20 g of diffusion pump oil were added to the water column in the standpipe over the pump to act as a movable air barrier.

Results of our analyses are given in Tables III and IV.

The results are different from what was expected.

- The groundwaters cleared of detergent very quickly by pumping. Apparently less detergent was used in the drilling of this well compared to others.
- The groundwaters from permeable zones in the Bullfrog Member and the Tram Unit are both oxidizing.
- Very little difference exists in the composition of the groundwaters of the permeable zones in the Bullfrog Member and the deeper Tram Unit. Calcium and bicarbonate ions are ~0.1 meq/g higher in the upper Bullfrog Member; all other constituents are quite similar in the two waters.
- The pH of groundwater from Well USW H-6 is higher (8.2) than other wells with the exception of USW H-3.

These results lead to some important conclusions affecting the groundwater chemistry task plan and performance assessment.

TABLE I
ELEMENTAL CONCENTRATIONS IN GROUNDWATER FROM THE TRAM UNIT OF WELL USW II-6

Sample	Concentration (mg/l)												
	Mg	Mn	Si	Fe	Sr	Ba	V	Ti	Ca	Li	K	Al	Na
06081	0.066	0.026	18.7	0.061	0.005	<0.001	0.014	<0.012	2.47	0.069	1.73	0.147	85
06083	0.026	0.021	18.3	0.080	0.003	<0.001	0.012	<0.012	1.75	0.067	1.42	0.134	86
06085	0.015	0.027	18.5	0.085	0.003	<0.001	0.012	<0.012	1.78	0.055	1.49	0.100	83
06088	<0.008	0.022	17.8	0.077	0.003	<0.001	0.012	<0.012	1.58	0.067	1.41	0.076	80
06094	<0.008	0.017	17.7	0.042	0.003	<0.001	0.014	<0.012	1.48	0.063	1.48	0.064	80
06101	<0.008	0.020	17.6	0.068	0.002	<0.001	0.015	<0.012	1.41	0.053	1.48	0.049	81
06111	<0.008	0.032	19.3	0.334	0.003	<0.001	0.015	<0.012	1.63	0.074	1.69	0.024	78
06112	<0.008	0.029	20.0	0.120	0.003	<0.001	0.015	0.015	1.60	0.082	1.78	0.069	77
06121	<0.008	0.020	19.4	0.074	0.003	<0.001	0.015	<0.012	1.51	0.082	1.59	0.054	75
06122	<0.008	0.024	19.6	0.048	0.003	0.002	0.017	<0.012	1.53	0.072	1.75	0.077	79
06131	<0.008	0.022	19.8	0.037	0.003	<0.001	0.015	<0.012	1.52	0.088	1.83	0.033	80
06132	<0.008	0.024	19.4	0.041	0.003	<0.001	0.014	<0.012	1.48	0.095	1.88	0.124	80
06141	<0.008	0.023	19.3	0.069	0.003	0.002	0.018	<0.012	1.52	0.078	2.18	0.092	83
06142	<0.008	0.026	19.6	0.038	0.003	<0.001	0.017	<0.012	1.51	0.074	2.19	0.084	80
06151	<0.008	0.028	20.3	0.059	0.003	0.002	0.027	0.013	1.61	0.089	2.57	0.087	87
06181	<0.008	0.027	20.1	0.064	0.003	0.004	0.025	<0.012	1.62	0.096	2.70	0.116	85
06183 ^a	<0.008	0.023	20.2	0.095	0.003	0.003	0.021	<0.012	1.61	0.083	2.67	0.144	89
06191	<0.008	0.024	19.8	0.060	0.003	0.003	0.022	0.016	1.57	0.097	2.78	0.097	85
06193 ^a	<0.008	0.024	20.2	0.115	0.003	0.002	0.021	0.022	1.59	0.090	2.81	0.142	90
06201	<0.008	0.022	19.9	0.057	0.003	0.004	0.023	0.021	1.51	0.075	2.68	0.093	80
06203 ^a	<0.008	0.027	19.6	0.090	0.003	0.004	0.024	0.025	1.48	0.090	2.68	0.123	80
06211	<0.008	0.028	20.0	0.070	0.003	0.004	0.026	0.020	1.53	0.087	2.66	0.105	83
06213 ^a	<0.008	0.025	20.0	0.099	0.003	0.004	0.022	0.022	1.53	0.093	2.82	0.154	84
06221	<0.008	0.025	20.4	0.050	0.003	0.005	0.028	0.029	1.55	0.082	2.88	0.112	81
06223 ^a	<0.008	0.025	20.6	0.083	0.003	0.004	0.025	0.036	1.56	0.097	2.93	0.124	82

^a Unfiltered.

TABLE II.
ANION CONCENTRATIONS AND OTHER PARAMETERS IN GROUNDWATER FROM THE TRAM UNIT OF USW H-6

Sample	Concentration (mg/l or otherwise stated)										
	F ⁻	Cl ⁻	NO ₃ ⁻	Detergent	SO ₄ ²⁻	fpl ^a (no units)	pH (no units)	Alk (meq/l)	Eh (mV)	O ₂	Conductivity (µmho/cm)
0607	3.9	6.9	4.5	0.23	28.9		8.46	2.896			
06081	3.7	7.0	4.5		28.7	7.98	8.11	2.956	112		371
06083	3.4	6.6	5.8		27.3		8.06	2.936			
06088	3.6	6.4	5.7		26.7		8.02	2.920			
06094	4.0	6.5	5.5	0.26	26.3	8.16	7.96	2.916	274		335
06101	3.4	6.5	6.1	0.13	27.3	8.23	8.04	2.928	315		340
06111	3.6	6.8	6.5	0.12	28.0	8.12	8.01	2.912	253		
06112	3.3	6.7	7.1	0.15	27.3	8.21	8.16	2.898	278		
06121	3.1	6.6	7.1	0.11	27.2	7.77	8.07	2.894	331		307
06122	3.3	6.6	5.6	0.11	27.4						
06131	3.8	6.7	6.1	0.095	27.4	7.89	8.08	2.866	363		
06132	3.0	6.2	5.8	0.075	26.7	8.24	8.07	2.888	340	2.50	
06141	3.5	6.5	6.1	0.050	26.9	8.22	8.11	2.866	386	1.80	
06142	3.5	6.6	6.1	0.039	26.7	8.21			394	7.50	354
06151	3.3	6.4	6.1	0.037	26.9	8.23	8.16	2.868	426	2.30	329
06181	3.6	6.5	5.6	0.022	26.1	8.21	7.44	2.896	328		290
06183	4.5	6.8	5.7		28.4	8.17			315	9.80	317
06191	3.4	5.8	5.7	0.018	26.2	8.18	7.55	2.908	329	9.00	320
06193	3.3	6.4	5.8		26.8	8.33			330	7.00	307
06201	4.2	6.8	5.9		27.4	8.32	7.43	2.883	243	5.00	
06203	3.8	6.5	5.7		26.3	8.26			340		
06211				0.024		8.24	7.74	2.827	347		317
06221	3.6	6.7	5.6	0.017	26.7	8.30	7.68	2.872	350		306

^afpl is field-determined pll.

TABLE III
 ELEMENTAL CONCENTRATIONS IN GROUNDWATER FROM THE BULLFROG MEMBER OF WELL USW II-6

Sample	Concentration ($\mu\text{g/l}$)												
	Hg	Mn	Si	Fe	Sr	Ba	V	Ti	Ca	Li	K	Al	Na
06281	0.087	0.045	19.5	0.098	0.012	0.006	0.025	0.032	5.36	0.098	3.13	0.114	79
06282	0.030	0.035	20.3	0.088	0.011	0.005	0.028	0.034	5.12	0.090	2.96	0.111	77
06291	0.010	0.034	20.3	0.086	0.010	0.005	0.026	0.033	4.98	0.089	3.00	0.110	75
06294	<0.008	0.033	20.5	0.097	0.010	0.006	0.029	0.034	5.05	0.095	3.18	0.109	76
06295	<0.008	0.028	20.6	0.106	0.010	0.005	0.028	0.035	5.10	0.090	3.20	0.113	77
06301	<0.008	0.028	19.6	0.078	0.010	0.005	0.029	0.034	4.94	0.086	3.03	0.104	82
06302 ^a	<0.008	0.027	20.2	0.117	0.010	0.006	0.031	0.038	5.08	0.085	3.17	0.150	83
06302	<0.008	0.028	20.1	0.080	0.010	0.005	0.029	0.039	5.00	0.089	3.11	0.102	81
07011	<0.008	0.027	20.2	0.101	0.010	0.007	0.033	0.039	5.18	0.092	3.29	0.130	84
07012	<0.008	0.028	20.4	0.121	0.011	0.006	0.032	0.044	5.19	0.096	3.42	0.120	82
07013	<0.008	0.029	19.9	0.103	0.010	0.006	0.033	0.042	5.17	0.098	3.38	0.133	84
07021	<0.008	0.026	19.7	0.102	0.011	0.006	0.030	0.030	5.26	0.094	3.36	0.140	91

^aUnfiltered.

TABLE IV
ANION CONCENTRATIONS AND OTHER PARAMETERS IN GROUNDWATER FROM THE BULLFROG MEMBER OF USW II-6

Concentration
(mg/l or otherwise stated)

Sample	F ⁻	Cl ⁻	NO ₃ ⁻	Detergent	SO ₄ ²⁻	fpH ^a (no units)	pH (no units)	Alk (meq/l)	Eh (mV)	O ₂	Conductivity (μmho/cm)
06281	4.3	8.9	5.6	0.045	32.7	7.82	8.10	3.154	306	2.60	328
06282	4.8	6.8	6.4	0.031	30.2	7.97	8.18	3.072	279	4.10	302
06291	5.0	6.6	6.0	0.010	29.9	8.04			315	6.50	314
06294	4.1	5.9	6.2	0.010	30.0						
06295	3.9	6.5	5.6		30.0	8.17	8.06	2.996	331	6.90	290
06301	4.2	6.5	5.9	0.005	29.7	8.20	8.23	3.014	332		290
06302	4.0	6.4	6.4	0.004	29.3	8.19	8.20	2.998	337	5.20	293
07011	3.8	6.4	6.2	0.004	29.4	8.20	8.10	3.260	351	6.10	
07012	3.7	6.4	6.4		29.4	8.20			352	6.00	258
07013	3.8	6.3	5.8		29.0	8.20	8.26	2.994	356	5.70	
07021	4.0	6.5	6.8	0.004	29.3	8.22	8.20	3.014	369	7.30	242
07022	4.7	6.5	5.4	0.004	29.4	8.21			274	5.10	250

^afpH is field-determined pH.

Up-gradient groundwater that may recharge the area under the repository site at Yucca Mountain is oxidizing. Because the groundwater in Well USW H-3 at the southern end of the repository block was found to be reducing,¹ one must postulate that the reduction process is a localized phenomenon taking place in the impermeable tuffs of Yucca Mountain. The extent of the area that is impermeable and that also contains reduced groundwater cannot be defined without additional wells being drilled in the repository block itself. This would unnecessarily alter the natural state of the site and should not be done if the sole reason is to gain knowledge of the groundwater composition. The conservative approach to performance assessment is to not use the possible reducing qualities of the groundwater below the repository to decrease estimated solubilities of waste elements.

This pumping test of Well USW H-6 together with all the other results presented in LA-10188-MS² contain sufficient data on the dissolved constituents so that the groundwater composition from the repository to the accessible environment--when defined--can be estimated, especially concerning any effects on retardation by sorption or precipitation. No further wells are necessary solely for groundwater composition. However, the groundwater composition of additional wells drilled for other site characterization studies will be sampled and analyzed to increase our detailed knowledge of the site and area.

Groundwater properties that are insufficiently known are the amount and identification of particulates moving with the groundwater. Small-sized mineral particulates from tuff and natural colloids, such as iron hydroxides, are possible transporters of sorbed or coprecipitated waste elements if the solids move through the fractures or open porosity of the tuff along with the natural water flow. Studies on particulates in the laboratory and in the field pumping tests will be our major emphasis in FY 1985.

2. pH Buffer Capacity of Well J-13 Water (J. F. Kerrisk). The water compositions found at Yucca Mountain are at or near equilibrium with the local minerals and would be unlikely to change significantly if conditions remain stable. However, if conditions change, it is of interest to understand the capacity of the water and mineral system to accommodate these changes. One aspect of this general problem, the response of the system to addition of H^+ or OH^- (that is, the pH buffer capacity) is discussed here.

Pure water can undergo large changes in pH after small additions of strong acids or bases. However, dissolved species in the water can significantly reduce pH changes for a given addition of acid or base. In water from Yucca Mountain, the aqueous carbonate, aqueous silica, and sulfate species have significant buffer capacity. Carbonate and aqueous silica exhibit their buffer capacity in the pH range of from 6 to 10. Sulfate would only be an effective buffer at a pH near 2. Solids that are in equilibrium with an aqueous solution or that can precipitate from it also affect the buffer capacity of the solution. Reactions involving the clays, zeolites, and feldspars that are found at Yucca Mountain generally include the production or consumption of H^+ and should thus provide additional buffer capacity. Precipitation or dissolution of calcite or dolomite can also affect water pH.

The most likely cause of pH changes in water at Yucca Mountain is oxidation of iron pyrite (FeS_2), if present; this process is responsible for acid waters associated with many mines. Calculations of the effects of oxidizing iron pyrite in Well J-13 water alone and in water, plus the local minerals, have been done. In Well J-13 water alone, about 0.5 mmol of iron pyrite can be oxidized per litre of water with only moderate pH change (from 7 to 5). This process would add about 1 mmol/l of sulfate to the water, a factor of 5 more than the normal Well J-13 water sulfate content. When the appropriate local minerals are present, the water pH would be stabilized near 7 by the conversion of clinoptilolite to nontronite and kaolinite; this indicates a very large buffer capacity associated with the minerals. Similar calculations were done for addition of H^+ and OH^- by unspecified processes to the water and to water plus minerals. Well J-13 water alone can accommodate addition of about 2 mmol/l of H^+ or OH^- with only moderate pH changes (about 2 pH units). With minerals present, the behavior for addition of H^+ is the same as for pyrite oxidation; however, the local minerals do not provide much additional buffer capacity for addition of OH^- over the water alone. A more detailed discussion of these results is given in LA-10188-MS.²

The results represented here indicate that Well J-13 water alone and water plus the minerals commonly found at Yucca Mountain have a relatively good pH buffer capacity. This is particularly true for the water-mineral system subject to H^+ addition. However, these calculations have assumed

equilibrium behavior. This is a good assumption for reactions involving only aqueous species, but kinetic constraints may limit rates of aqueous-solid reactions such as precipitation or dissolution. If the buffer capacity of the water-mineral system becomes important, it may be necessary to perform additional experiments or analyses to verify the assumption of near-equilibrium behavior.

Water from Well J-13 is generally similar to water from other wells that tap the tuffaceous aquifer near Yucca Mountain. In particular, water from Wells UE-25b#1, H-1, H-4, H-5, H-6, and G-4 would be expected to have buffer capacities similar to Well J-13. Water from Well USW H-3 has a higher pH and higher carbonate content than Well J-13 water; it would have a higher buffer capacity for H^+ addition.

B. Natural Isotope Chemistry (A. E. Norris, K. Wolfsberg, S. K. Gifford, and J. W. Jones)

Global fallout of ^{36}Cl from high-yield nuclear tests in the Pacific Ocean approximately 25 years ago has provided a tracer for determining the extent of rainfall infiltration since that time. This work seeks to measure the "bomb pulse" ^{36}Cl in two types of surficial material at Yucca Mountain to obtain information about potential recharge. One type is relatively flat-lying alluvial sediment, and the other is fractured tuff that is either exposed at the surface or thinly covered by soil or loose rock. Laboratory analyses of samples collected during a field trip in February indicated that the Yucca Wash 6 trench would be a good location to measure ^{36}Cl . That work was reported in the previous quarterly report.⁶ A field trip was undertaken in June to collect samples from the Yucca Wash 6 trench large enough for ^{36}Cl analyses, to excavate a trench at the Exploratory Shaft site for collecting ^{36}Cl samples at that location, and to perform electromagnetic conductivity surveys at locations on and near Yucca Mountain to aid in selecting a ^{36}Cl sampling site in fractured tuff. The field trip accomplished its goals. The results are discussed below. Another field trip was undertaken in August to collect samples from fractured tuff. Samples were desired as deep as 2.5 m, but heavy rains curtailed sample collection to a depth of less than 1 m.

1. Results of the June 25 - 29 Field Trip.

a. Soil sampling. Soil samples were collected from six locations on or near Yucca Mountain. Five of the locations are shown in Fig. 2. The sixth location was at the Yucca Wash 6 trench, about 4 km east of the Exploratory Shaft site. The chloride concentration in each sample was measured, and the results are listed in Table V. The data are plotted in Figs. 3 through 8. Note that the first and last figures of this set are semilogarithmic, while the remainder are linear.

The chloride concentration data from the four shallow soil samples and from the Yucca Wash 6 trench are similar to those obtained from similar February field trip samples. The low values for the shallow soil samples, with no big increase near the underlying tuff, indicate well-drained soil conditions. The data from the trenches at Yucca Wash 6 and at the Exploratory Shaft site indicate that infiltration may be deeper at the Exploratory Shaft site than at the Yucca Wash 6 trench, but both sets of samples should provide useful samples for ^{36}Cl analyses. The presence of what appears to be a relatively impervious caliche layer in the Yucca Wash 6 trench may account for the shallower depth of chloride leaching in comparison with the Exploratory Shaft site trench, where no impervious caliche layer was evident.

b. Electromagnetic conductivity survey measurements. The electrical conductivity patterns of tuff were measured with a Geonics Model EM34-3 loop-loop inductive electromagnetic survey instrument to help locate an appropriate site in fractured tuff for bomb pulse ^{36}Cl infiltration measurements. The five sites that were surveyed are shown in Fig. 2. The electrical anisotropy of the tuff was measured at each site by collecting data at 30° intervals about a point. Both vertical and horizontal dipole measurements were made. The equipment characteristics are such that the vertical dipole measurements sense to approximately 0.75 of the intercoil spacing, while the horizontal dipole measurements sense to 1.5 times the intercoil spacing. The data from these measurements are listed in Table VI. These azimuthal surveys showed that the tuff is electrically anisotropic in the direction of fracturing, as we inferred from the measured ratios of electrical conductivities as large as 2:1 as a function of azimuth.

BUSTED BUTTE, NEV.
SW/4 TOPOPAH SPRING 15' QUADRANGLE

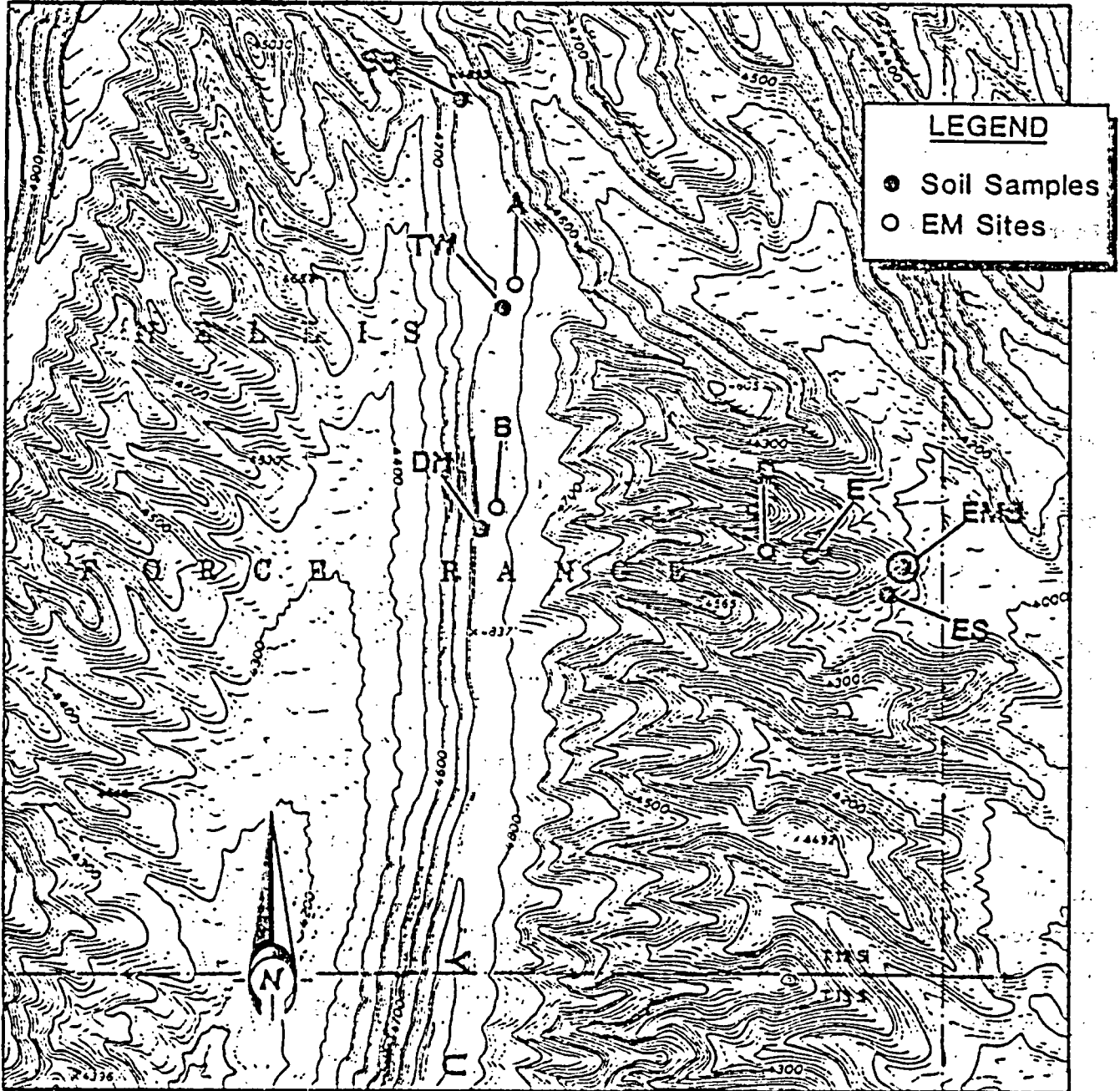


Fig. 2. Location map of soil sampling and electromagnetic (EM) survey sites at Yucca Mountain, Nye County, Nevada.

TABLE V
 CHLORIDE CONCENTRATIONS IN SOILS
 SAMPLES FROM YUCCA MOUNTAIN LOCATIONS

<u>Sample Identification</u> ^a	<u>Depth</u> (meters below land surface)	<u>mg Cl⁻/kg soil</u>
ES-15	0 - 0.152	12.4
ES-14	0.152 - 0.305	4.1
ES-13	0.305 - 0.396	0.75
ES-12	0.457 - 0.549	1.23
ES-11	0.488 - 0.579	1.04
ES-10	0.732 - 0.823	0.85
ES-9	0.579 - 0.671	0.43
ES-8	0.823 - 0.914	0.63
ES-7	0.914 - 1.006	0.25
ES-6	0.975 - 1.097	0.34
ES-5	1.128 - 1.219	0.19
ES-4	1.372 - 1.463	3.0
ES-3	1.798 - 1.920	231
ES-2	2.073 - 2.225	593
ES-1	2.754 - 2.865	659
SS-1	0 - 0.076	7.6
SS-2	0.076 - 0.127	3.7
SS-3	0.127 - 0.178	2.0
SS-4	0.203 - 0.279	2.4
SS-5	0.279 - 0.356	2.5
SS-6	0.356 - 0.381	3.6
TW-1	0 - 0.076	3.1
TW-2	0.076 - 0.152	1.3
TW-3	0.152 - 0.203	0.8
TW-4	0.229 - 0.254	1.0
DN-1	0 - 0.051	3.9
DN-2	0.051 - 0.102	0.5
DN-3	0.127 - 0.152	0.7
DN-4	0.178 - 0.203	1.1
DN-5	0.203 - 0.229	1.5
YWR-15	0 - 0.152	25
YWR-14	0.152 - 0.229	21
YWR-13	0.229 - 0.259	12
YWR-12	0.259 - 0.305	66
YWR-11	0.335 - 0.412	488

TABLE V (cont)

<u>Sample Identification</u> ^a	<u>Depth</u> (meters below land surface)	<u>mg Cl⁻/kg soil</u>
YWR-10	0.427 - 0.488	788
YWR-9	0.518 - 0.549	46
YWR-8	0.549 - 0.579	47
YWR-7	0.610 - 0.640	110
YWR-6	0.640 - 0.701	112
YWR-5	0.762 - 0.793	178
YWR-4	0.884 - 0.945	577
YWR-3	1.067 - 1.158	414
YWR-2	1.463 - 1.524	752
YWR-1	1.676 - 1.829	1699
EMS-1	0 - 0.152	0.6
EMS-2	0.152 - 0.203	0.8
EMS-3	0.203 - 0.254	1.0
EMS-4	0.254 - 0.305	0.3
EMS-5	0.330 - 0.356	1.2
EMS-6	0.356 - 0.381	3.7
EMS-7	0.381 - 0.406	3.2

^aThe letter codes designate the following:

ES = Trench at Exploratory Shaft site, 56 ft in a direction N42°E from the aerial survey marker.

SS = North end of Yucca Mountain, 60 ft west of USGS rain gauge "Sandy."

TW = North end of Yucca Mountain, 0.5 miles south of USGS rain gauge "Sandy."

DN = Middle of Yucca Mountain, 300 ft north of USGS rain gauge "Dianne."

YWR = Yucca Wash 6 trench.

EMS = Electromagnetic survey site at the mouth of Coyote Wash.

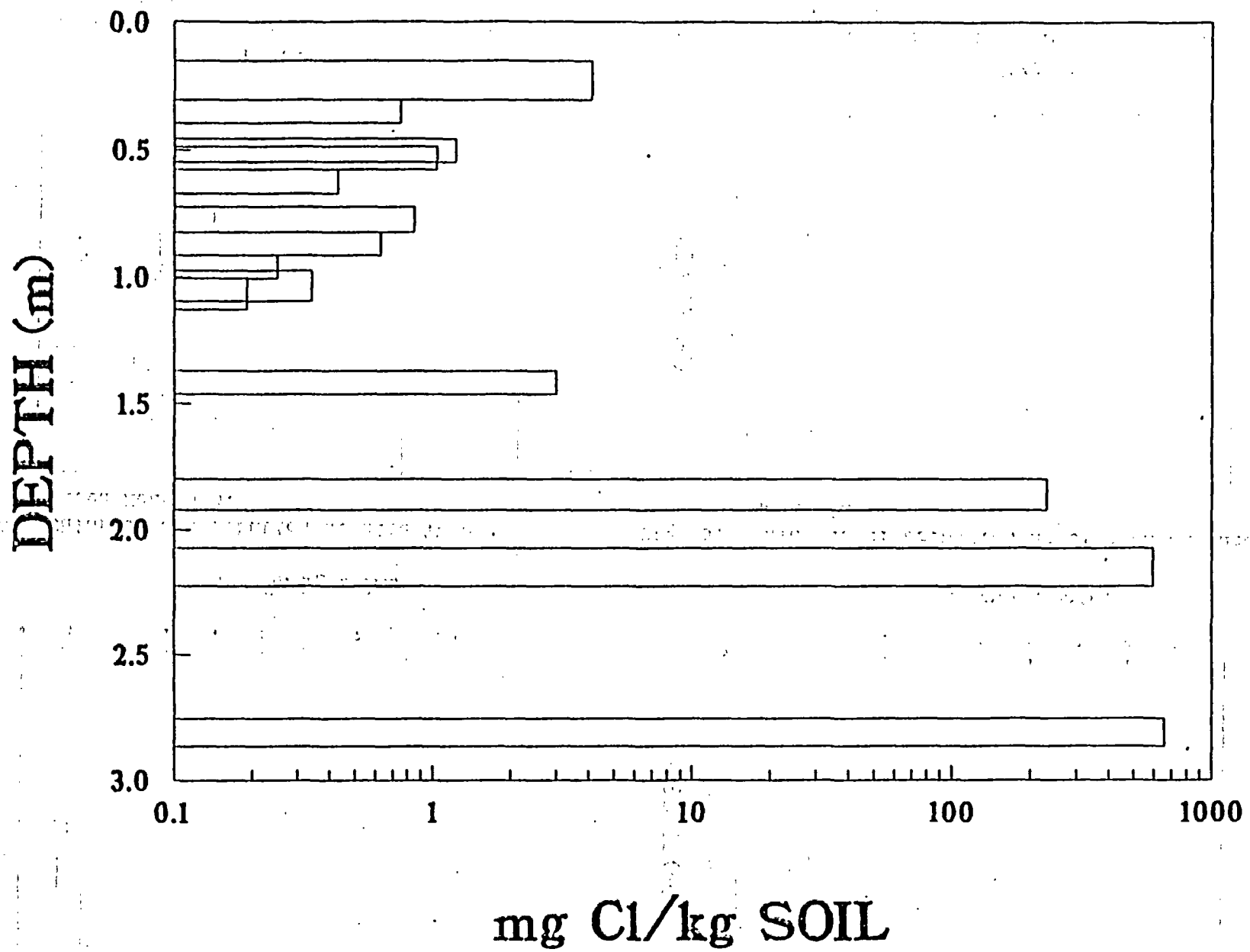


Fig. 3. Chloride distribution in trench at Exploratory Shaft site.

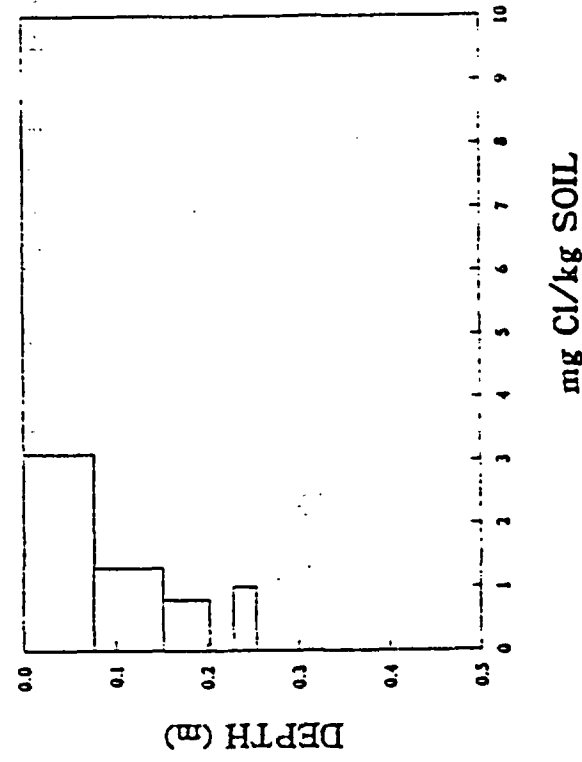


Fig. 4. Chloride distribution at site TW on Yucca Mountain.

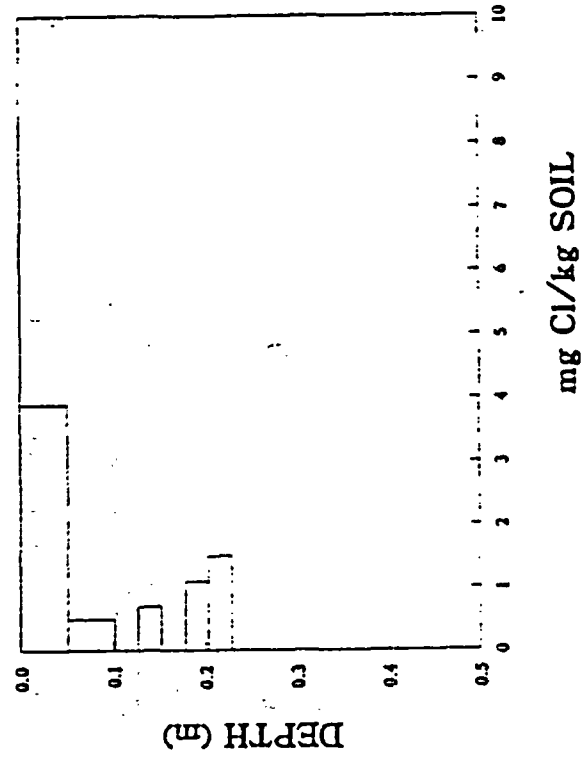


Fig. 5. Chloride distribution at site DN on Yucca Mountain.

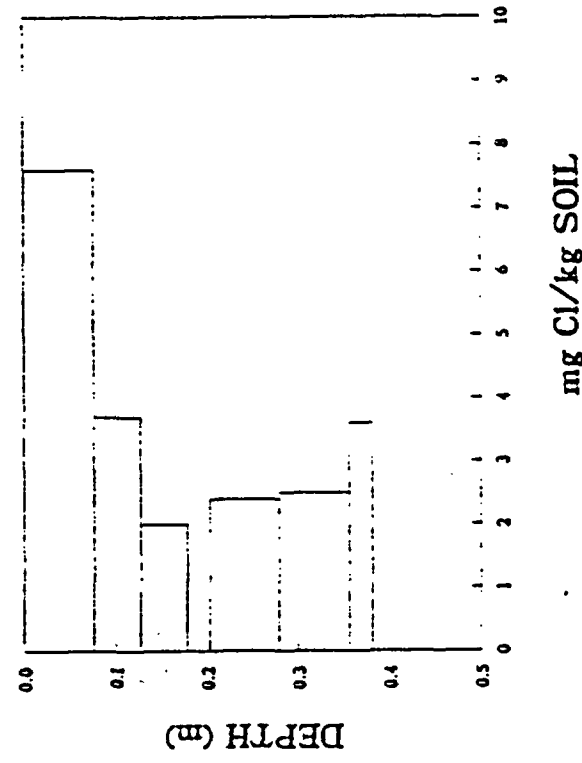


Fig. 6. Chloride distribution at site SS on Yucca Mountain.

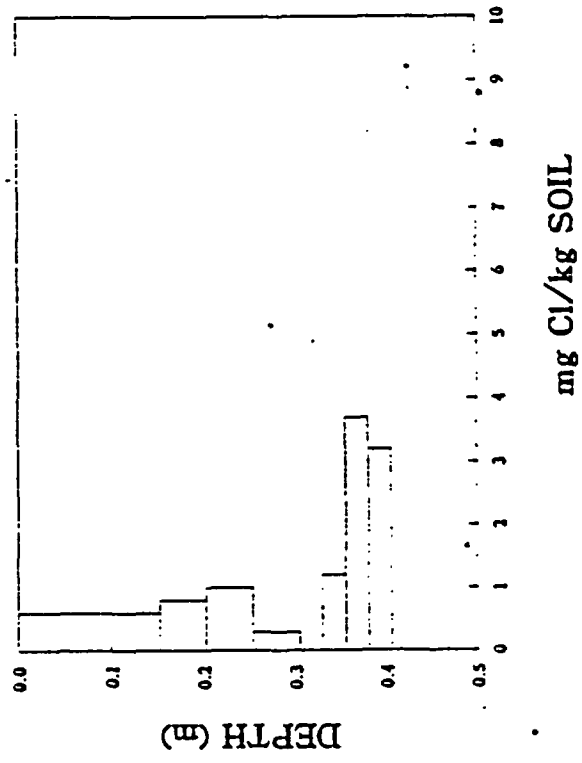


Fig. 7. Chloride distribution at site EMS at Coyote Wash.

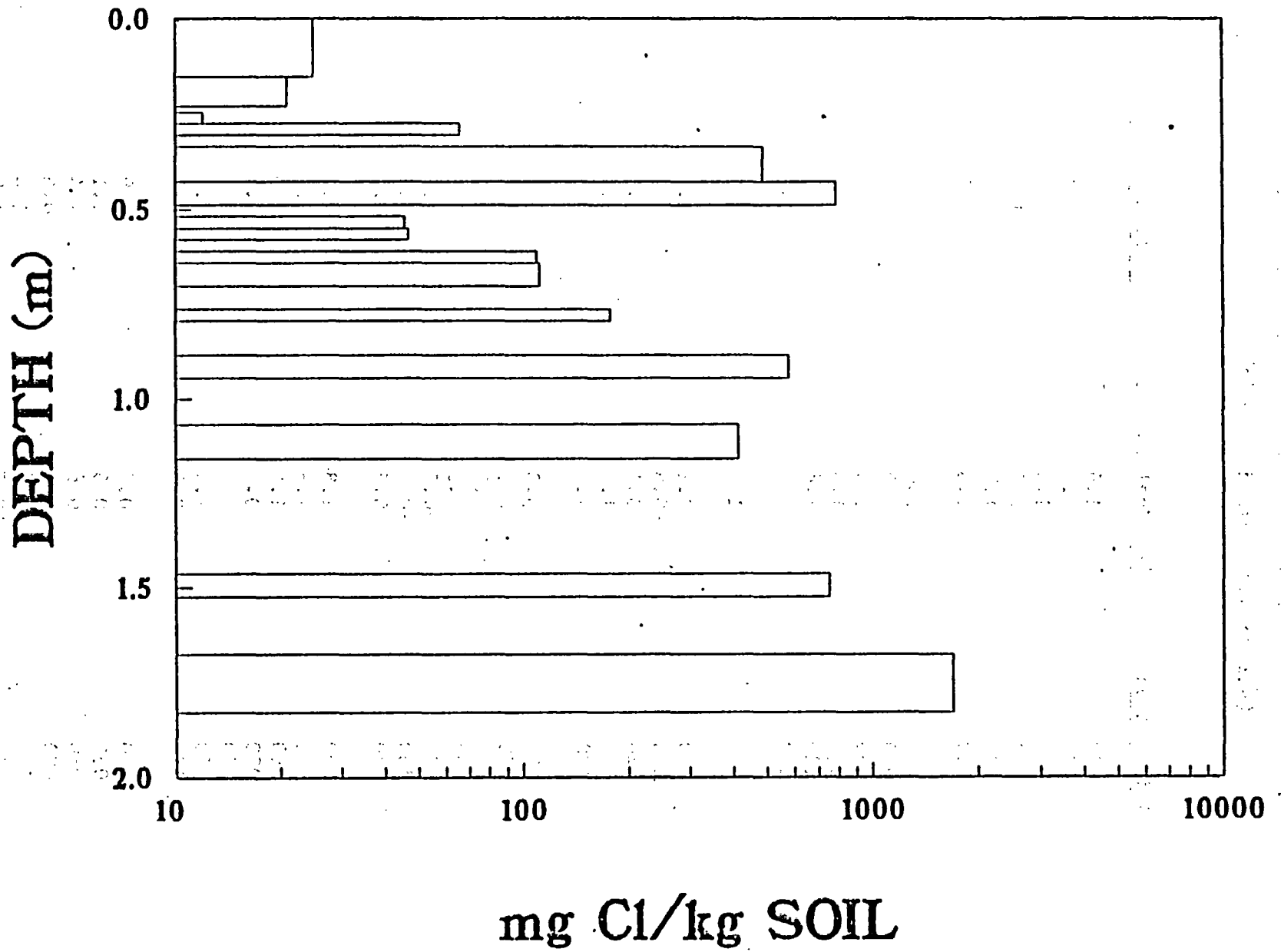


TABLE VI
ELECTROMAGNETIC MEASUREMENTS OF APPARENT ELECTRICAL CONDUCTIVITY
(All measurements in mmho/m)

<u>Location</u> <u>Spacing</u>	<u>Orientation</u>	<u>Vertical Dipole</u>	<u>Horizontal Dipole</u>
D 10 m	000	1.6	1.4
	030	1.4	1.1
	060	1.5	1.0
	090	2.0	1.4
	120	1.7	1.0
	150	1.3	1.2
E 10 m	000	2.0	1.3
	030	2.0	1.4
	060	2.0	1.9
	090	1.5, 1.2	2.7, 2.4
	120	1.6	1.2
	150	2.0	1.2
A 10 m	000	1.5	4.9
	030	0.6	4.3
	060	0.1	3.4
	090	-0.6	2.6
	120	0.1	3.0
	150	1.0	3.0
A 20 m	000	0.3	3.1
	030	0.4	2.0
	060	-0.5	1.0
	090	-0.3	0.8
	120	-0.5	0.8
	150	-0.5	1.6
B 10 m	000	1.8	2.0
	030	1.8	2.1
	060	1.4	2.0
	090	0.7	1.9
	120	1.0	2.4
	150	1.4	2.5
B 20 m	000	0.7	0.9
	030	0.6	1.1
	060	0.6	1.4
	090	0.5	0.6
	120	0.6	1.2
	150	0.8	1.0
180	0.7	0.6	

TABLE VI (cont)

<u>Coordinates</u> <u>Spacing</u>	<u>Orientation</u>	<u>Vertical Dipole</u>	<u>Horizontal Dipole</u>
Tuff Sampling Area (EMS Soil Sampling Area)			
230, 150 10 m	000	3.55	2.8
	030	3.3	3.0
	060	3.5	3.0
	090	3.4	3.0
	120	3.75	3.2
	150	3.6	2.8
	180	3.5	2.8
230, 190 10 m	000	3.4	3.5
	030	3.3	3.2
	060	3.3	2.9
	090	3.3	3.0
	120	4.0	3.0
	150	3.6	3.0
	180	3.6	3.0
200, 170 10 m	000	3.4	2.9
	030	3.3	3.0
	060	2.9	2.5
	090	3.0	2.8
	120	3.6	2.5
	150	3.5	2.4
	180	3.6	2.8

The electromagnetic survey measurements indicated that the site labeled EMS in Fig. 2 is highly fractured. Other characteristics, such as proximity to a road and the gentle slope of the terrain, appeared to make fracture sampling feasible at this location. Therefore, a detailed electromagnetic survey was made along seven north-south lines to produce a 15 ft x 15 ft grid for assessing the spatial variability of shallow tuff conductivity. These data are listed in Table VII and are plotted in Fig. 9. The contours seem to reflect the major set of northwest-trending fractures at the ground surface near the Exploratory Shaft site and perhaps the minor set of northeast-trending fractures.

TABLE VII
 GRID ELECTROMAGNETIC MEASUREMENTS
 NORTH-SOUTH TRAVERSE ON 10-m SPACING
 (See Fig. 9)

<u>X-Coord.</u>	<u>Y-Coord.</u>	<u>Vertical Dipole</u>	<u>Horizontal Dipole</u>
140	100	4.0	3.4
	115	3.3	3.5
	130	3.3	3.4
	145	3.6	3.1
	160	3.6	2.8
	175	3.0	3.0
	190	3.2	3.0
	205	3.7	3.0
	220	3.3	2.8
	235	3.9	2.6

Drift of Machine Measured to be 0.0 mmho/m

155	100	3.6	3.9
	115	3.4	3.9
	130	2.2	3.5
	145	3.8	3.2
	160	3.6	3.0
	175	2.6	3.2
	190	3.2	3.3
	205	3.6	3.4
	220	3.4	3.3
	235	3.3	3.0

Drift of Machine Measured to be 0.0 mmho/m

170	100	3.6	3.8
	115	4.1	3.2
	130	3.1	2.4
	145	3.4	3.4
	160	3.4	3.2
	175	3.7	3.2
	190	3.7	3.2
	205	3.1	2.8
	220	3.3	3.0
	235	3.2	3.0

Drift of Machine Measured to be 0.0 mmho/m

185	100	4.1	3.3
	115	3.6	3.0
	130	3.6	3.0
	145	3.2	3.0
	160	3.4	3.1
	175	3.3	2.9

TABLE VII (cont)

<u>X-Coord.</u>	<u>Y-Coord.</u>	<u>Vertical Dipole</u>	<u>Horizontal Dipole</u>
	190	3.6	3.1
	205	3.3	3.0
	220	3.3	3.7
	235	3.3	4.0
	250	3.6	3.6

Drift of Machine Measured to be 0.1 mmho/m

200	100	3.8	3.6
	115	3.8	3.3
	130	3.0	3.3
	145	3.0	3.3
	160	3.6	3.1
	175	3.9	3.1
	190	3.6	3.2
	205	3.3	3.0
	220	3.5	3.4
	235	3.7	3.3

Drift of Machine Measured to be 0.0 mmho/m

215	100	3.3	3.2
	115	3.4	3.3
	130	3.3	3.2
	145	3.6	3.4
	160	3.5	3.4
	175	2.9	3.6
	190	2.8	3.1
	205	3.6	2.7
	220	3.7	2.5
	235	3.4	2.8

Drift of Machine Measured to be -0.1 mmho/m

230	100	4.0	3.4
	115	3.8	3.1
	130	3.8	2.6
	145	3.2	2.6
	160	4.2	2.8
	175	3.6	2.7
	190	3.6	2.9
	205	3.8	3.0
	220	2.5	2.8
	235	2.7	2.8

Drift of Machine Measured to be -0.1 mmho/m

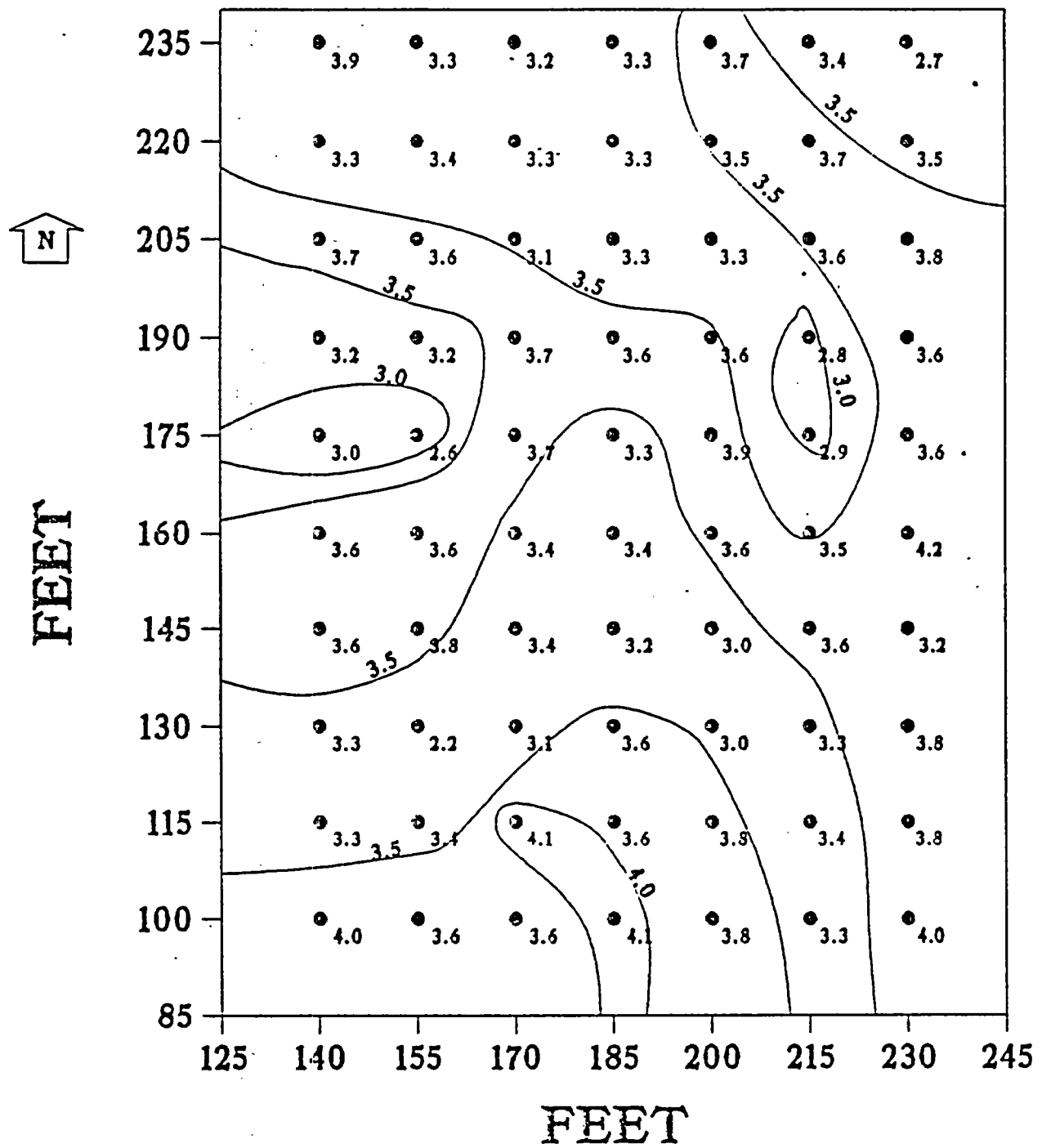


Fig. 9. Contours of apparent electrical conductivity, vertical dipole, 10-m spacing, C.I. 0.5 mmho/m.

2. August 13-15 Field Trip. The site selected for measuring infiltration into fractured tuff was determined to contain no archeological artifacts and no endangered plants or animals. A backhoe and a pneumatic hammer were used to excavate a hole about 0.8 m deep. Four soil samples and two tuff samples were collected. Holes were drilled to permit blasting to deeper levels, but heavy rains resulted in a pool of standing water in the excavation. Water from this pool could have carried chloride and ^{36}Cl to deeper levels than it might have moved during the past 25 years, thus compromising the interpretation of the data if sampling and analyses had continued. Therefore, the sampling was stopped, and the excavation was backfilled as well as the muddy conditions would permit, to prevent the hole from becoming a local recharge point. The chloride concentration measurements on the samples collected will be performed and reported next quarter.

C. Hydrothermal Geochemistry (C. J. Duffy)

Thermodynamics of Zeolites. A thermodynamic model has been constructed for analcime as a start to our understanding the controls on its stability. Analcime is neither the most abundant nor the most sorptive zeolite at Yucca Mountain. It is, however, the most studied and reported upon zeolite in the literature. Modeling analcime stability leads to insights about the parameters that affect the stability of other zeolites, the probable relative importance of kinetics vs chemical equilibrium, and the best approaches to studying the other zeolites.

The thermodynamics of analcime are directly important because analcime is a probable breakdown product of clinoptilolite. The thermodynamics of analcime as well as those of clinoptilolite must, therefore, be known before the possible reaction of clinoptilolite to analcime plus additional phases can be modeled. The model for analcime can also be used to clarify the present chemical conditions in portions of Yucca Mountain where analcime is present and to examine the possibility that these portions of the mountain may have been heated to higher temperatures in the past.

The framework for the analcime thermodynamic model was presented in the April-June Quarterly report.⁶ The parameters necessary to the model have now been evaluated. Because no data were available to unambiguously fix all the parameters, experimental and field data were combined and adjusted within

reasonable constraints until a set of parameters was found that was consistent with all the data.

Volumes were obtained by fitting the data of Kim and Burley⁷ after they had been extrapolated to 25°C. Compressibility data for the $\text{NaAlSi}_2\text{O}_6 \cdot \text{H}_2\text{O}$ end member were taken from Birch.⁸ Thermal expansion was estimated based upon data from Skinner.⁹ Due to lack of data, compressibility and thermal expansion were assumed to be equal for both end members. The resultant volume functions are

$$V = (1 - (1.97e-6)P - (2.77e-10)P^2)(1 + (3.5e-5)T)(9.6914)$$

for $\text{NaAlSi}_2\text{O}_6 \cdot \text{H}_2\text{O}$ and

$$V = (1 - (1.97e-6)P - (2.77e-10)P^2)(1 + (3.5e-5)T)(9.2394)$$

for $\text{Si}_3\text{O}_6 \cdot 1.5\text{H}_2\text{O}$, where V is in J/mol bar, P is in bar, and T is in °C.

The calorimetric entropy of the silica end member was estimated using entropy and volume data and the estimation technique given by Helgeson et al.¹⁰ along with the above volume data. Data for zeolitic water and tridymite were used in the estimation. Tridymite was preferred to the other silica polymorphs because its use resulted in the smallest volume correction. The calorimetric entropy was estimated to be 215.31 J/mol K. This number was combined with data from Johnson et al.¹¹ to obtain a value of 228.43 J/mol K for the calorimetric entropy of the sodium end member. The value given above represents the total entropy for the silica end member, but there are additional configurational components in the sodium end member.

The heat capacity of the silica end member was also estimated using data and techniques given by Helgeson et al.¹⁰ However, quartz was used in the estimation because the other silica polymorphs have phase transitions in the temperature region of interest. Using the same estimation technique, data on an intermediate analcime¹¹ were combined with the derived heat capacity for the silica end member to provide a heat capacity for the sodium end member. The functions are

$$C_p = 236.615 - 0.467373T + (1.66004e-3)T^2 - (1.23551e-6)T^3 + (5.860792e4)/T^2$$

for the sodium end member and

$$C_p = 324.056 - 1.0057T + (2.67422e-3)T^2 - (1.85403e-6)T^3 - (6.3093e5)/T^2$$

for the silica end member, where C_p is in J/mol K and T is in °C.

These data were then combined with field data and hydrothermal experimental data on the albite, quartz, analcime equilibrium to obtain chemical potentials of the end members exclusive of the contributions of configurational entropy. No single data point exists for which all the needed parameters are available; however, the chemical potentials can be constrained by requiring that they be consistent with a broad range of data. The chemical potentials obtained are -3 087 431 J/mol for the sodium end member and -2 908 213 J/mol for the silica end member.

The model indicates that the analcimes present in Yucca Mountain crystallized under conditions where the silica activity was only slightly below that in equilibrium with cristobalite. The fact that they presently coexist with quartz indicates that the rock and water are not in overall equilibrium. The model suggests that the analcimes did not crystallize at temperatures above 150°C, but does not indicate a specific temperature. The model predicts that analcime will crystallize at higher silica activities when the pressure on the crystal is closer to the fluid pressure. This implies that as the mountain evolves toward silica activities more closely in equilibrium with quartz, analcime will tend to crystallize in void space where the pressure on the analcime would be equal to the fluid pressure. Such an occurrence would tend to decrease permeability.

D. Solubility Determinations

1. New Version of EQ3/6 (J. F. Kerrisk). A new version of the chemical equilibrium computer program EQ3/6 was received from Lawrence Livermore National Laboratory. This version is now running on the LTSS system at Los Alamos. The primary addition in this version is the capability to do calculations at constant gas fugacity. This boundary condition may be representative of conditions in the unsaturated zone where the aqueous phase is in contact with a gas reservoir.

2. Actinide Chemistry in Near-Neutral Solutions (D. E. Hobart, T. W.

Newton, and P. Palmer). The chemistry of actinides in the near-neutral waters found in the vicinity of Yucca Mountain will have a significant impact on actinide solubility and transport in water that interacts with nuclear waste stored there. Three aspects of actinide chemistry are being examined. They are (1) complex formation between Pu(IV) and carbonate, (2) solubility product of $\text{PuO}_2 \cdot n\text{H}_2\text{O}$ (solid or colloidal sol), and (3) complex formation between Am(III) and carbonate. During the past quarter, work concentrated on the solubility product of $\text{PuO}_2 \cdot n\text{H}_2\text{O}$.

Work was continued on the solubility behavior of colloidal Pu(IV). A serious difficulty in solubility determinations using ^{239}Pu is the effect of alpha radiation during the long time periods required to reach equilibrium. This effect does not appear to have been considered in previous studies.

The principal reaction being investigated is



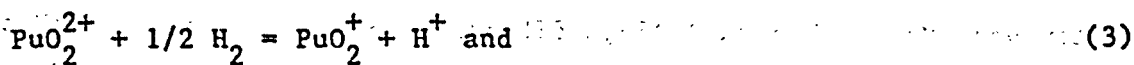
The equilibrium constant for this reaction, together with known thermodynamic data, can be used to calculate the equilibrium constant for the reaction



This equilibrium constant is the solubility product that is fundamental for predicting solubility as a function of pH and complexing anions. Literature values for this constant vary rather widely, so these studies are required.

In our study of reaction (1), three components are important: PuO_2^+ , PuO_2^{2+} , and colloidal Pu(IV). Pu(III) might be expected at high Pu(V) and low Pu(VI) concentrations, but careful examination of the spectra of such solutions shows no evidence of this oxidation state. Solutions starting with the components PuO_2^+ , PuO_2^{2+} , and colloidal Pu(IV) individually and in various combinations have been prepared. These mixtures were stored at room temperature and periodically analyzed spectrophotometrically for Pu(V) and Pu(VI). Values for pH were also determined. Data have been taken over periods up to 260 days. The plan was to determine Q' , the concentration quotient for reaction (1) under conditions where both forward and reverse reactions could be observed and, thereby, bracket the equilibrium constant.

The data indicate that several reactions in addition to (1) are important. These include reduction of Pu(VI) by products of the alpha radiolysis of the solution.



oxidation of the colloid by radiolysis products,



and



Disproportionation, the reverse of reaction (1), readily occurs in solutions with $1.5 < \text{pH} < 5$. For $\text{pH} < 2$, the observed rates are in reasonable agreement with published work for higher acid concentrations. At higher pH values, however, much higher rates are observed. This suggests possible catalysis by the freshly formed colloidal Pu(IV).

Reaction (3) is readily observed in solutions in which Pu(VI) is the predominant oxidation state. Our values for the rate of this reaction are in good agreement with those published previously.¹² Reactions (4) and (5) are observed in solutions initially containing pure colloid. At concentrations $< 1 \times 10^{-4}$ M, reaction (5) is much more important than reaction (4).

Mixtures of the various components or solutions of single components that have stood a long time show wide ranges of average oxidation states, Q' values, and their rates of change with time.

Disproportionation appears important at Q' values as small as 10^{-3} . From this, an upper limit for the solubility product can be estimated as $\log K_{sp} < -56.7$. An estimate for a lower limit requires a value for Q' under conditions where reaction (1) occurs as written. The data provide no direct evidence for this. Thus, it will be necessary to find a satisfactory model for the observed behavior in order to reach conclusions with respect to equilibrium in reaction (1). Plausible models are being investigated and, in addition, data using ^{242}Pu are being collected.

3. Solubility of Actinide Compounds (H. Nitsche and N. Edelstein).

Work concluded on the measurements of the solubilities of $^{237}\text{NpO}_2^+$, $^{237}\text{NpO}_2^{2+}$,

$^{242}\text{Pu}^{4+}$, $^{242}\text{PuO}_2^+$, $^{242}\text{PuO}_2^{2+}$, and $^{243}\text{Am}^{3+}$, individually, in groundwater from the Nevada Test Site and in aqueous NaClO_4 solutions of similar pH.^{1,6,13}

Solubility measurements in Well J-13 groundwater were conducted in a manner similar to the experiment in noncomplexing NaClO_4 solutions. The groundwater was passed through 0.05- μm filters prior to use, and the pH of the solution was held at 7.0 ± 0.1 . In addition, to avoid the loss of CO_2 from the Well J-13 water during the experiment, a partial CO_2 -pressure of 0.014 atmospheres was maintained above the solution's surface at all times. The analytical procedures for the separation of the solids from the solution phase have been described earlier.⁶

The actinide solution concentrations were followed as a function of time, and, after steady-state conditions were reached, the supernates were analyzed to determine the oxidation state distribution of solution species. For the NpO_2^+ , NpO_2^{2+} , and Am^{3+} solutions, we used spectrophotometry. For the plutonium solutions, with their rather low concentrations, we employed a combination of coprecipitation with rare earth fluorides and both thenoyltrifluoroacetone (TTA) and hexone (methyl-isobutyl-ketone) extractions.⁶

The solids were studied by x-ray powder diffraction analysis. Samples were sealed in 0.3-mm quartz capillaries; $\text{CuK}\alpha$ radiation filtered through nickel was utilized. Table VIII lists the analytical results.

The spread in solubility for the plutonium in NaClO_4 solution appears at first rather puzzling because the final solution compositions are similar. One possible reason for the solubility spread may be found in the nature of the precipitating solids. Presumably the solids in all three plutonium-solutions are Pu(IV)-hydroxides or hydrous oxides. This is supported by (a) identically green physical appearance of the precipitates and (b) by the low solubility values for the initially PuO_2^+ and PuO_2^{2+} solutions. If these ions would precipitate as PuO_2OH and $\text{PuO}_2(\text{OH})_2$, respectively, their solubility values should be in the same order of magnitude as the values for the analogous neptunium-hydroxides. The literature value¹⁴ for the solubility at pH 7 for crystalline Pu(IV) oxide is 10^{-8} M and for amorphous hydrous Pu(IV) oxide it is $10^{-6.5}$ M. The values for the solubility seem not only to depend on whether the material is amorphous or crystalline but also on the properties of the amorphous state; that is, various phases from amorphous $\text{Pu}(\text{OH})_4$ to amorphous $\text{PuO}_2 \cdot \text{H}_2\text{O}$ display differences in solubility. Alpha radiolysis effects, as discussed in Section 2, also must be considered.

TABLE VIII
ANALYTICAL RESULTS OF SOLUTIONS IN EQUILIBRIUM WITH THEIR SOLID PHASE (SUPERSATURATED STARTING CONDITIONS)
IN 0.1 M NaClO₄ AND J-13 GROUNDWATER AT pH = 7.0 ± 0.1, 25 ± 1°C

Initial Species	Solubility (M)		Final Oxidation State of Soluble Species		Solid	
	NaClO ₄	J-13	NaClO ₄	J-13	NaClO ₄	J-13
NpO ₂ ⁺	(4.37±0.10) × 10 ⁻⁴	(1.41±0.51) × 10 ⁻³	+5 (100%)	+5 (100%)	amorphous	crystalline Na ₃ NpO ₂ (CH ₃) ₂ x n H ₂ O
NpO ₂ ²⁺	(3.47±0.16) × 10 ⁻⁴	(7.16±0.54) × 10 ⁻⁴	+5 (100%)	+5 (100%)	crystalline unidentified	crystalline unidentified
Am ³⁺	(2.95±0.14) × 10 ⁻⁴	(1.05±0.17) × 10 ⁻⁶	+3 (100%)	+3 (100%)	mostly amorphous	crystalline Am ₂ (CO ₃) ₂ x 2 H ₂ O/ AmOHCO ₃
Pu ⁴⁺	(2.8±2.1) × 10 ⁻⁸	(1.65±0.11) × 10 ⁻⁶	(+3)+(+4)+ polymer ≤ 5% (+5)+(+6)-97% (+5)-60 to 65%	(+3)+(+4)+ polymer ≤ 1% (+5)+(+6)-99% (+5)-40%	amorphous	amorphous
PuO ₂ ⁺	(3.1±1.2) × 10 ⁻⁹	(7.1±3.8) × 10 ⁻⁶	(+3)+(+4)+ polymer ≤ 10% (+5)+(+6)-90 to 98% (+5)-50 to 70%	(+3)+(+4)+ polymer ≤ 1% (+5)+(+6)-98% (+5)-63%	amorphous	crystalline unidentified
PuO ₂ ²⁺	(1.2±0.4) × 10 ⁻⁷	(3.6±1.4) × 10 ⁻⁵	(+3)+(+4)+ polymer ≤ 5% (+5)+(+6)-97% (+5)-65 to 80%	(+3)+(+4)+ polymer ≤ 2% (+5)+(+6)-98% (+5)-70%	amorphous	crystalline unidentified

A topical report on the task is in preparation and will be submitted later.

Work on the measurements of AmOHCO_3 in 0.1-M NaClO_4 solution at atmospheric CO_2 concentrations at 25°C at pH values of 6, 8, and 10 is near conclusion.

The $^{243}\text{Am}(\text{OH})\text{CO}_3$ was prepared through the formation and subsequent hydrolysis of the trichloroacetate complex in aqueous solution.¹⁵ The material was identified by x-ray powder diffraction analysis as crystalline AmOHCO_3 . Solution samples are being analyzed by counting the 75.44-keV ^{243}Am γ -ray with a solid state x-ray counting system.

Details will be given in a topical report on this task.

E. Sorption and Precipitation (K. Wolfsberg)

1. Groundwater Composition Effects (S. D. Knight and K. W. Thomas)

The effects of groundwater composition on the sorptive behavior of tuff have been under study for some time. Most of our sorption data have been obtained with Well J-13 groundwater. New measurements have been added with the Paleozoic-hole groundwater from Well UE-25p#1 (P-1) and with deionized water. The Paleozoic-hole groundwater has a much higher concentration of calcium, magnesium, strontium, barium, sodium, bicarbonate, and sulfate than does the Well J-13 water. The deionized water is more similar in composition to Well J-13 groundwater.

Batch sorption experiments were performed this quarter on tuff sample USW G-1-2901, a devitrified tuff with small amounts of calcite, from the Tram Unit. Measurements were made with the Paleozoic groundwater and with deionized water. Strontium-85, ^{137}Cs , ^{133}Ba , and ^{152}Eu were the radio-nuclides used, and all the contact times were six weeks. Table IX lists all the sorption and desorption ratios determined in these experiments.

Sorption ratios for strontium, cesium, and barium were lower when measured in P-1 water than in deionized water. Because the P-1 water is a higher ionic strength water than the deionized water, it is expected that these three elements that sorb mainly by ion exchange will show lower sorption ratios in the P-1 groundwater. Sorption and desorption ratios for europium on Drill Hole G-1-2901 tuff were very high in both waters, and differences in sorption ratios in both waters were difficult to observe.

TABLE IX
SORPTION RATIOS ON TUFF SAMPLE G1-2901 WITH PALEOZOIC AND DEIONIZED WATERS

Groundwater	Traced Feed (pH)	Element	Traced Feed Concentration (M)	Sorption ^b or Desorption	Sorption Ratios (mL/g)			
					Experimental Value (pH)		Average ^c Value	
UE-25p#1 ^a	8.70	Sr	2×10^{-7}	Sorption	31	57	44	(13)
					(8.92)	(8.99)		
		Cs	4×10^{-9}	Sorption	662	1150	900	(250)
				Ba	6 x 10 ⁻⁸	Sorption	940	1920
		Eu	2×10^{-7}	Sorption	22 000	53 700	38 000	(16 000)
				Sr	Desorption	39	31	35
					(8.90)	(9.03)		
		Cs		Desorption	926	775	850	(76)
				Ba	Desorption	1190	1030	1100
		Eu		Desorption	89 000	49 000	69 000	(20 000)
		DW ^d	8.30	Sr	2×10^{-7}	Sorption	136	137
	(8.57)					(8.39)		
Cs	4×10^{-9}			Sorption	3190	3520	3350	(170)
				Ba	6 x 10 ⁻⁸	Sorption	7290	7100
Eu	1×10^{-7}			Sorption	33 000	41 000	37 000	(4000)
				Sr	Desorption	118	92	105
					(8.74)	(8.45)		
Cs				Desorption	4390	3130	3800	(670)
				Ba	Desorption	6970	5190	6100
Eu				Desorption	34 000	21 000	27 500	(6200)

^aWell UE-25p#1, Paleozoic groundwater.

^bSorption and desorption times were 6 weeks.

^cNumbers in parentheses are the standard deviation of the mean.

^dDeionized water.

Some new experiments have been started with strontium, cesium, barium, europium, and tin in groundwater from Well USW H-3. This water has a higher pH (~9) than other groundwaters studied.

2. Long-Term Technetium Sorption Measurements (S. D. Knight and K. W. Thomas). Batch sorption measurements with technetium in Well J-13 groundwater and three tuff samples have been carried out with times up to 1 yr. Sorption ratios have been determined at 6 wk, 3 months, 6 months, 9 months, and 12 months. Sorption ratios for technetium did not change with time and were all very small, near zero. The last measurements of this series will be made for 15 months contact time. Table X lists the results obtained to date.

3. Neptunium Sorption Isotherm Measurements (F. O. Lawrence, M. R. Cisneros, and K. W. Thomas). Batch measurements, with ^{235}Np , for long-term sorption measurements are continuing. Neptunium isotherm sorptions in a CO_2 -controlled atmosphere are finished, and as much of the counting as is now possible has been completed. Counting of the samples will resume soon.

4. Plutonium and Americium Sorption Measurements (F. O. Lawrence, M. R. Cisneros, and K. W. Thomas)

Serial sorption measurements with plutonium have been started, and the first phase has been completed. The measurements are being made on GU3-916 crushed rock. The sorption ratio determined in the first phase is 260 ± 14 , which agrees quite well with the value of 250 ± 25 reported previously.¹³ The second phase, which is sorption on freshly crushed rock with the aqueous phase of a previous sorption, will be completed within the next few weeks. This will indicate whether the species of plutonium remaining in solution after a sorption experiment behave any differently than the plutonium that sorbed initially.

There has recently become available a well-characterized solution of Am(III) in carbonate solution. Batch sorptions will be run with this material as well as the material used previously for americium batch sorptions, and the results will be compared with fast-flow column experiments.

There will be available to us soon carbonate solutions of Pu(V) and of Pu(VI). Batch sorptions are planned using feed solutions made by adding a spike of the carbonate solutions to the rock-equilibrated water. A comparison will be made by using plutonium solutions prepared in our usual manner for the sorption measurements.

TABLE X
TECHNETIUM SORPTION RATIOS

Core	Traced Feed (pH)	Traced Feed Concentration (M)	Sorpton Time	Sorpton Ratios (mL/g)		
				Experimental Value (pH)	Average Value ^a	
GU-3-916	8.57	6×10^{-10}	6 wk	0.50 (8.51)	0.94 (8.57)	0.72 (0.2)
			13 wk	0.33 (8.75)	1.3 (8.70)	0.81 (0.5)
			6 months	0.81 (8.61)	0.44 (8.66)	0.62 (0.2)
			9 months	0.14 (8.81)	0.11 (8.83)	0.13 (0.02)
			12 months	0.13 (8.83)	0.32 (8.90)	0.22 (0.1)
GU-3-1301	8.67	7×10^{-10}	6 wk	0.058 (8.41)	0.022 (8.47)	0.04 (0.02)
			13 wk	0.065 (8.63)	0.002 (8.69)	0.03 (0.03)
			6 months	0.003 (8.60)	+0.004 (8.61)	0
			9 months	0.013 (8.70)	0.031 (8.72)	0.02 (0.01)
			12 months	0.17 (8.70)	0.30 (8.75)	0.23 (0.1)

TABLE X (cont)

Core	Traced Feed (pH)	Traced Feed Concentration (M)	Sorpton Time	Sorpton Ratios (ml/g)		
				Experimental Value (pH)	Average Value ^a	
G-4-1502	8.74	8×10^{-10}	6 wk	0.042 (8.60)	-0.003 (8.60)	0.02 (0.02)
			13 wk	0.06 (9.00)	-0.038 (8.81)	0.01 (0.05)
			6 months	-0.085 (8.65)	-0.09 (8.65)	0
			9 months	-0.06 (8.71)	-0.05 (8.75)	0
			12 months	0.001 (8.80)	-0.015 (8.82)	0

^aNumbers in parentheses are the standard deviation of the mean.

For the last few months one of the pieces of counting equipment (automatic NaI well counter) has been out of commission due to construction in the building and the ensuing moving of the counter. That work is completed, and the counter is back in use. We should be caught up with the backlog of samples in a month or so.

5. Sorption Measurements of Uranium and Selenium (B. P. Bayhurst and K. W. Thomas). Batch sorption measurements of uranium were carried out at a pH of 6.0 to 6.4 in a controlled partial pressure of CO₂. This gives conditions more similar to the neutral pH found in Yucca Mountain groundwaters than the pH 8.8 used previously.¹ The change from a pH of 8.8 may cause a change in the carbonate complexing of uranyl ion. We are observing R_d values 3 to 8 times higher than at pH 8.8, indicating that previous measurements gave conservative results. Similar experiments with selenium indicated no change from previous work carried out in the ambient atmosphere. The results and comparisons are given in Table XI.

6. Microbial Activity at Yucca Mountain (L. E. Hersman, F. O. Lawrence, M. R. Cisneros, and K. W. Thomas). The purpose of this research is to determine if microbial activity can influence the mobility of nuclear waste elements, especially plutonium. Of special interest are those microbial species capable of degrading drilling fluids, because these fluids are used extensively in drilling explorations at the NNWSI sites.

As reported in the last quarterly report,⁶ work was begun on developing methods for studying the anaerobic biodegradation of drilling fluids. On June 21, 1984, two 1.0-g anaerobic growth chambers containing Turco 5622 medium were inoculated with sediment. This sediment had been collected from a stagnant pond located near the Well UE-25c#1 drilling site at the NTS. Using Warburg manometers, the chambers were monitored every 2 weeks, and the results are as follows (expressed as milliliters of gas produced $\ell^{-1} \text{ day}^{-1}$):

25 June - 3.15×10^{-2} ,
9 July - 1.42×10^{-2} , and
23 July - 0.82×10^{-2} .

Originally, this experiment was designed to be conducted for 2 months; unfortunately on 6 August the redox indicator in both chambers turned pink, indicating the presence of oxygen. Because the anaerobiosis of the chambers

TABLE XI
 SORPTION RATIOS FOR URANIUM AND SELENIUM
 IN A PARTIAL CARBON DIOXIDE ATMOSPHERE

Core ^a	Element	Traced Feed (pH)	Traced Feed Concentration (M)	Sorption Time (weeks)	Sorption Ratio (ml/g)		
					Experimental Value (pH)	Average Value ^b	
G-1-2233	U	6.19	5.5×10^{-6}	8	17.7 (6.22)	16.1 (6.48)	16.9 (0.8)
	U	8.72	2.7×10^{-6}	6			5.5 (0.4) ^c
	Se	6.19	1.8×10^{-10}	8	0.8 (6.22)	1.2 (6.48)	1.0 (0.2)
	Se	8.72	1.8×10^{-11}	6			1.8 (0.1) ^c
G-1-2840	U	6.30	5.5×10^{-6}	8	3.9 (6.40)	4.5 (6.00)	4.2 (0.2)
	U	8.59	2.7×10^{-6}	6			0.5 (0.1) ^c
	Se	6.30	1.8×10^{-10}	8	1.5 (6.40)	1.9 (6.00)	1.7 (0.1)
	Se	8.59	1.8×10^{-11}	6			3.1 (0.2)
G-1-3116	U	6.32	5.5×10^{-6}	8	26.0 (6.40)	27.1 (6.02)	26.6 (0.4)
	U	8.78	2.7×10^{-6}	6			3.8 (0.1) ^c
	Se	6.32	1.8×10^{-10}	8	2.8 (6.40)	2.9 (6.02)	2.9 (0.1)
	Se	8.78	1.8×10^{-11}	6			3.1 (0.1) ^c

^aFraction size is 75 to 500 μm , wet-sieved.

^bNumbers in parentheses are the standard deviation of the mean.

^cBruce Crowe, Comp., "Research and Development Related to the Nevada Nuclear Waste Storage Investigations, January 1-March 31, 1984," Los Alamos National Laboratory report LA-10154-PR (February 1984). The measurements were made in air and are listed here as a comparison.

was compromised, the experiment was terminated. It is encouraging that the early results suggested that small quantities of gas were being produced anaerobically. In keeping with the findings of others, these data lend credence to the belief that the drilling fluids can be degraded anaerobically. Further experiments are planned to substantiate these initial data.

Final preparations were completed for a new series of plutonium adsorption experiments to study the effect of microbial activity. Unlike previous experiments where mixed bacterial cultures were used, these experiments use individual, pure cultures. To obtain pure cultures, species were subcultured (transferred) several times on nutrient agar and on drilling fluid medium. For each transfer, an individual colony was transferred to fresh medium (solid). After several transfers, pure cultures have been obtained. All are capable of degrading either ASP-700 or Turco 5622 drilling fluids. All are gram negative rods of varying sizes, and some produce extracellular capsule material. When grown on ASP-700 medium, two species produced large clear zones around each colony. These two species, plus two that do not produce clear zones, and two species capable of degrading Turco 5622 were purified for use in the adsorption experiments.

Three plutonium sorption experiments were begun during the past month. In the first, three species of bacteria were added to a 10^{-8} -M solution of plutonium with 1 g of crushed tuff. This slurry was mixed for 5 days. In the second experiment, four species of bacteria were added to a 10^{-9} -M solution of plutonium and crushed tuff. As in the first experiment, this slurry was mixed for 5 days. Unlike these two experiments, in the third experiment the crushed tuff was added to the culture of bacteria (four species) 1 wk prior to the introduction of a 10^{-9} -M solution of plutonium. This was done to provide a greater period of time for the bacteria to adsorb onto the surface of the crushed tuff. Results of these experiments will be presented in the future.

F. Dynamic Transport Processes (R. S. Rundberg, E. J. Mroz, and A. J. Mitchell)

1. Crushed-Tuff Columns. A 2-m-long column containing crushed USW G-2-2017 tuff has been prepared and the free column volume determined by eluting tritiated water at several flow rates. The average free column

volume of 22.4 ml has been reported in the previous progress report⁶ and was found not to be velocity dependent over a wide range of velocities. This result is consistent with what one should expect for a column packed with fine-grained material (75 to 500 μm). The mineral composition is approximately 20% clinoptilolite, 40% mordenite, 35% feldspar, and 5% silica phases. The intracrystalline porosity of the tuff is 17% based on the porosity of clinoptilolite (0.35) and mordenite (0.26), respectively.

Anion spiked Well J-13 water was prepared by adding 1.4 ml of 0.1-M HF, 2.8 ml of 0.1-M HCl, 3.1 ml of 0.1-M HNO₃, and 1.0 ml of 0.2-M H₂SO₄ to 1 l of Well J-13 water. The total acid added was limited to 0.93 meq/l to minimize the compositional change in the water. The resultant pH was 6.0, indicating that the buffer capacity of the bicarbonate buffer was not exceeded. The spiked solution was eluted through the column at a flow rate of 2.28×10^{-4} ml/s, which corresponds to a water velocity of 2.0 cm/s. The effluent from the column was analysed by using a DIONEX anion chromatograph. The elution curves are shown in Fig. 10.

The breakthrough results are shown in Table XII. Chloride and sulfate show the same anion exclusion with excellent agreement. Nitrate agrees with these anions but the error is much larger because of scatter in the data. The large scatter may be caused by biological activity in the column, such as algae growth that would utilize nitrate. However, this is only speculation. The fluoride did not exhibit the anion exclusion effect and in fact appeared to be slightly retarded ($R_f = 1.06$) with respect to tritiated water. The fluoride also did not elute with the initial concentration indicating some irreversible loss of fluoride. Because fluoride is the smallest of the anions, this effect may be due to some molecular sieving process. Alternatively, the water chemistry may be close to the fluorite solubility. If the effect is later shown to be actually molecular sieving, there would probably be a strong dependence on the zeolite channel diameter with fluoride preferring mordenite to clinoptilolite. The anion exclusion effect may provide a basis for verifying the sorption properties of the geologic environment in field tests. Because anions are unretarded, results would be available in a reasonable time for a large-scale tracer test, and the magnitude of the anion exclusion would be a measure of the content of zeolite and clay. Effects such as observed with fluoride in this first experiment could distinguish between sorptive minerals.

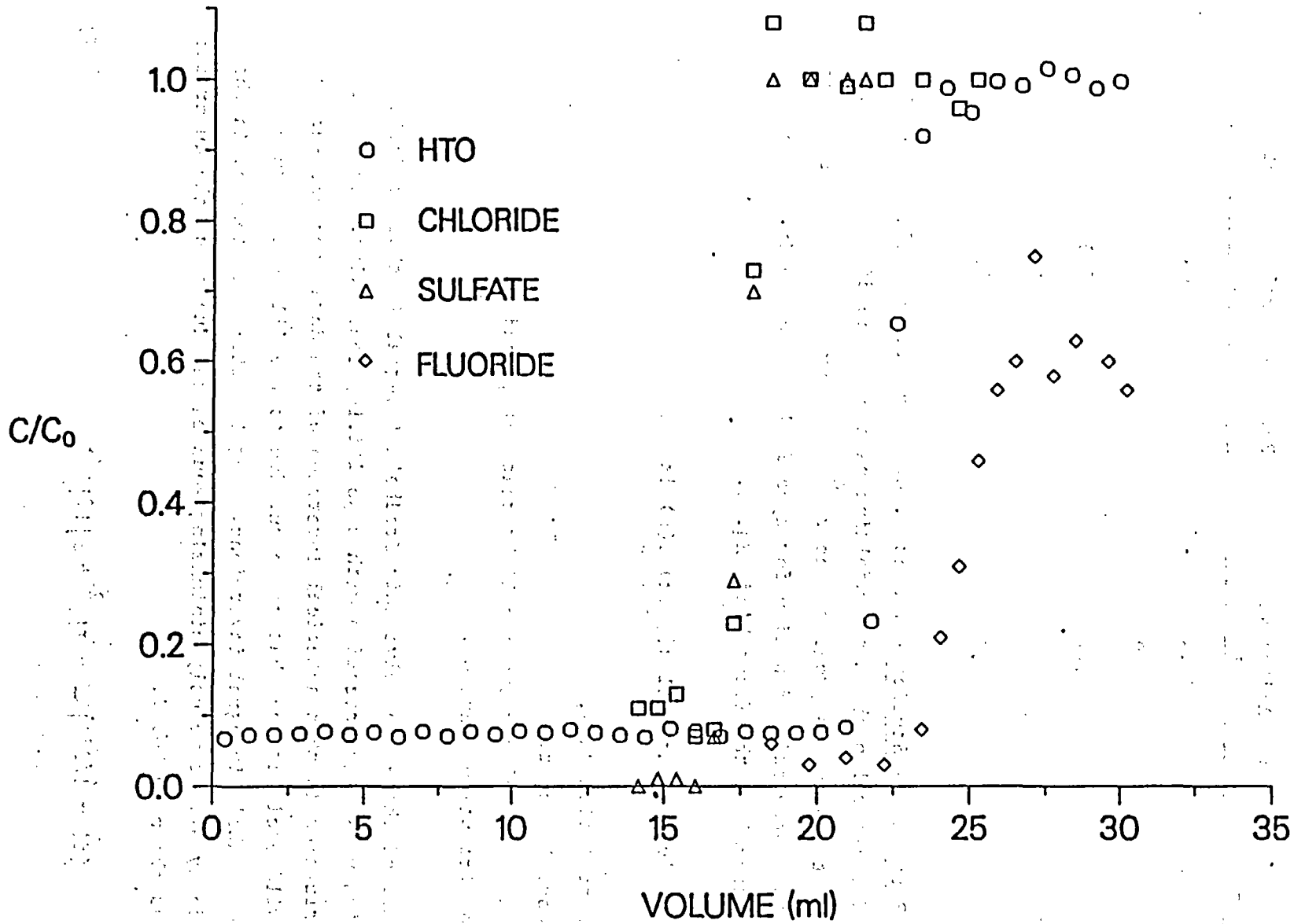


Fig. 10. Elution of anions from USW G-2-2017 crushed-tuff column.

TABLE XII
BREAKTHROUGH RESULTS

<u>Species</u>	<u>Ionic Radius Volume (ml)</u>	<u>Retention Exclusion Volume (ml)</u>
HTO	22.4	0.0
Cl ⁻	1.9	17.0
NO ₃ ⁻	1.7	17.0
SO ₄ ²⁻	1.9	17.0
F ⁻	1.5	24.0

2. Particulate Studies (S. Hodson, L. Brown, E. Nuttall, and B. J. Travis). The general problem of unfolding particle size distributions was described in the previous progress report.⁶ The form of the equation that describes the correlation function for dynamic light scattering is the Fredholm integral of the first kind, Eq. 6.

$$g(y_1) = \text{integral } k(y_1, x) f(x) dx \quad , \quad (6)$$

where

- g = correlation data,
- y = correlation time,
- k = exp (γ time) for dynamic light scattering, and
- f = distribution function.

The method chosen to solve this Fredholm integral is that of Butler et al.,¹⁶ which uses regularization with a positivity constraint. The advantage of regularization is that numerical inversion of the data does not suffer from the wild oscillations that can occur due to the ill-posed nature of first-kind Fredholm integral inversions. Regularization is imposed in the INVPOS code by simultaneously minimizing squared residuals and the quadratic function as shown in Eq. 7.

$$\pi(f) = 1/2 \|Kf - g\|^2 + \alpha \|f\|^2 \quad , \quad (7)$$

where

$||\cdot||$ denotes the vector norm ,
 $Kf = \text{integral } k(x)f(x)dx$, and
 α = smoothing factor.

In addition, the positivity constraint is introduced with the M operator, as defined in the Butler paper. It was found that even when synthetic data were inverted by using the INVPOS code that the $H(\alpha)$ function would not minimize, and, thus, no optimum smoothing factor could be determined. This condition indicates that the deviations from the fitted data are larger than the error in the measured data. The problem was then traced to the treatment of error in $H(\alpha)$. To alleviate this problem, the following equation was used.

$$H(\alpha) = g - TMTg - 2g - Tg + \epsilon \cdot c \quad , \quad (8)$$

where

T and M are matrix operators defined in the Butler paper,
 ϵ is the error vector, and
 c is essentially the deviation of the fit from the measured value of g over α .

The absolute value of each term in the dot product $\epsilon \cdot c$ was taken to ensure that the error, ϵ , is parallel to c , i.e., all errors are additive. An example of the fit to data for 60 nm polystyrene particles is shown in Fig. 11.

Monodisperse polystyrene particles with diameters from 60 nm to 1.0 μm have been acquired for testing as both calibration standards and tracers. The particle size distribution for these suspensions have been determined by electron microscopy. Fluorescent polystyrene particles have also been purchased for testing as possible colloids for use in field testing. The fluorescent particles are carboxylated so they would be expected to have a negative charge and, therefore, are not expected to adhere to mineral surfaces. The fluorescence makes them easy to detect at very low concentrations via fluorimetry.

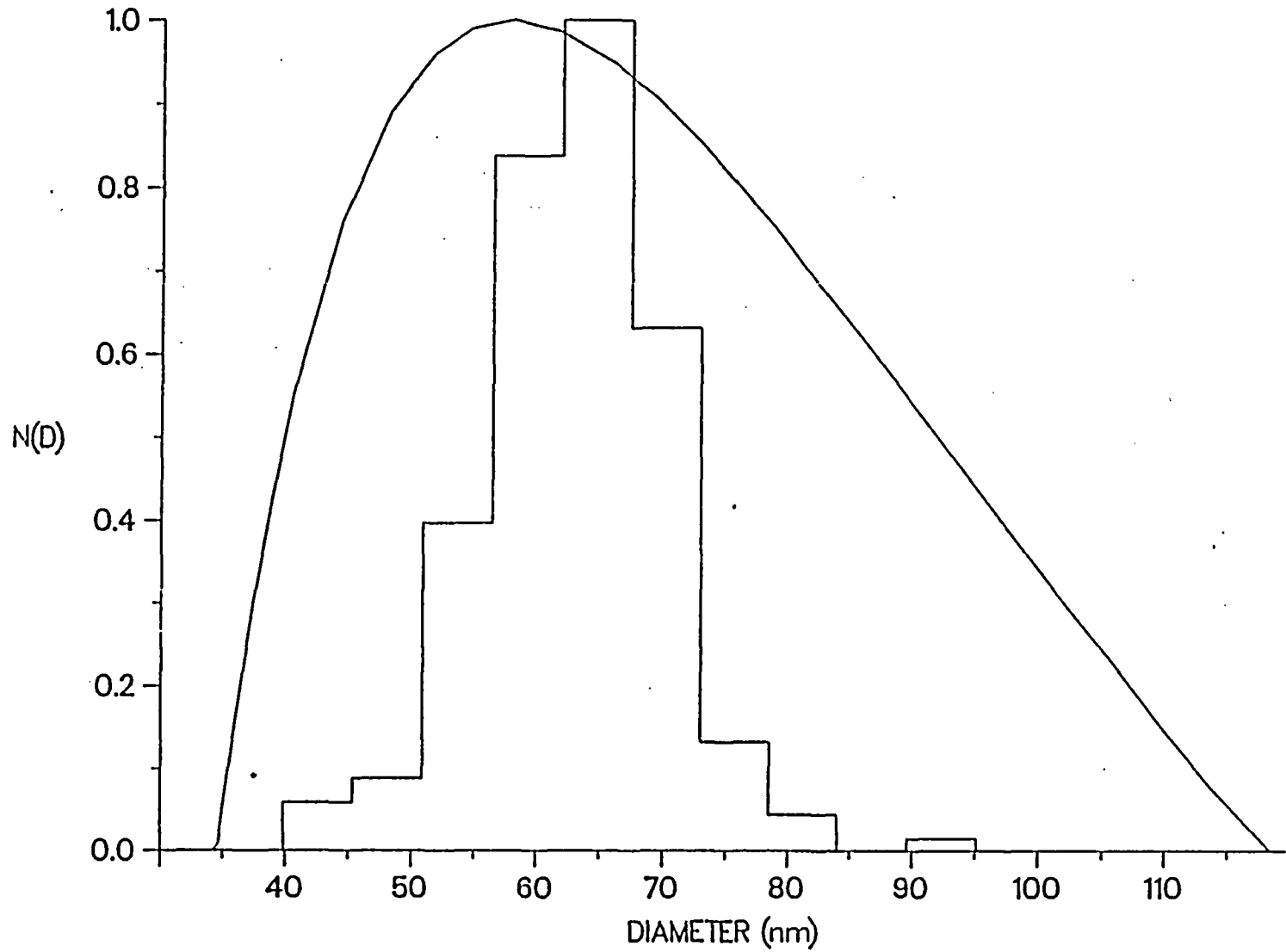


Fig. 11. Particle size distribution inverted from 60 nm polystyrene particle data and compared with input size distribution.

G. Retardation Sensitivity Analysis (B. Travis, S. Hodson, L. Brown, and E. Nuttall)

There are many recent papers on the geological disposal of waste and repository assessment, but they have not quantitatively addressed the impact of colloid formation and transport.¹⁷⁻²¹

Since about 1979, the question of colloid formation and migration has increased in importance and is now a topic of major interest in the scientific community. To date, several experimental studies have shown the presence of radioactive colloids under simulated waste disposal conditions, but their impact on repository assessment, however, has not been addressed because the existing geo-transport codes used to assess geologic waste disposal cannot treat this problem. Additional theory and equations are required to mathematically describe colloid formation and migration. The population balance equations and submodels can be added to the existing radionuclide transport theory and codes to accomplish this goal.

Through the correct use of the population balance equations coupled with the existing theory, problems of colloid formation and migration can be assessed quantitatively. The well-established theory of the population balance can be applied to the difficult radioactive colloid problem with the same success with which it has been used to treat many physical and biological particulate problems over the past 20 years.

In this section, the key experimental research on radioactive colloids is reviewed, and the population balance is developed. Its application to waste assessment is illustrated by modeling two postulated repository scenarios: (1) a near-field study and (2) a far-field problem involving colloids from when the backfill is breached and waste leakage occurs during the thermal repository, and from natural sources.

1. Colloids. Colloids were initially studied by Michael Faraday and other scientists early in the 19th century, and the name colloid was given to these extremely small particles by the Scottish chemist Thomas Graham in 1861. This class of very fine particles ranges in size, by definition, from about 1 to 1000 nm, and a single ounce of colloids may have 100 000 ft² of surface (300 m²/g). Approximately one out of every 100 of a colloidal particle's atoms or ions either is exposed to the surrounding medium or is close enough to the surface of the particle to be subjected to forces arising from interaction with the medium.²²

Colloids have many interesting properties. For example, they can change size with the larger particles growing at the expense of the smaller ones, and the particles can either coagulate or be repelled. Very stable colloid solutions can be formed that will remain for hundreds of years. India ink is an example of a rather stable colloid solution of lampblack.

There is an increasing number of references to nuclear colloids and their role in nuclear waste management. Drever²³ discusses the nature and geochemistry of colloids with emphasis on the charge surrounding colloids and its effect on suspension stability. In most natural colloids other than smectites (for example, oxides of silicon, aluminum, iron, manganese, colloidal organic matter), the surface charge results from ionization of or adsorption on the surface of the solid. In strongly acid solutions, the surface will gain a proton and be positively charged while the opposite occurs in strongly alkaline solutions. A double layer of ions surrounds colloids. The Stern layer is more or less attached to the solid surface, and outside is the Gouy layer in which the ions are free to move. The structure of the double layer is of great interest, and mathematical models are available to describe the distribution of ions within it. The stability of a colloid suspension depends on the thickness of the Gouy layer, which depends on the potential at the outside of the fixed layer and on the ionic strength of the solution. For example, as the ionic strength increases, the Gouy layer becomes compressed close to the particle. When this occurs to a large enough degree, the double-layer electrokinetic force is negligible, and the van der Waals attractive force will pull the particles together; thus rendering the suspension unstable.

Colloids also exhibit ion exchange behavior²³ as measured quantitatively in soil sciences by the cation-exchange capacity (CEC). Cation-exchange capacity is often measured by uptake and release of ammonium ions from a 1-M ammonium acetate solution at a pH of 7.0. Some typical cation-exchange capacities (meq/100 g) for a few clay minerals are:

Smectite	80-150
Vermiculite	120-200
Illite	10-40
Kaolinite	1-10
Chlorite	<10

Again, it is often pointed out that CEC values for colloidal oxyhydroxides must be interpreted with caution because the surface charge and, hence, CEC of these materials can be strongly dependent on pH. Drever suggests that the common distribution coefficient K_d can be used to represent the exchange equilibrium between the concentration of trace species on the colloid and in the solution; however, he cautions that K_d may be a function of the other ions in solution so that a distribution coefficient measured for a particular ion on a particular clay in particular solution cannot be used for calculations involving other solutions or other types of colloids.

2. Colloids in Nuclear Waste. The many radioactive colloid experimental studies now appearing in the literature illustrate the strong likelihood of nuclear colloids in the geological storage of nuclear waste.²⁴⁻²⁸

Apps et al.²⁹ recently reviewed colloid and particulate transport in the geologic storage of nuclear waste. They provided numerous references suggesting that colloid formation is strongly evident in natural systems. Olofsson et al.^{24,25,30} in their literature review of this subject suggest that the elements present in spent nuclear fuel, which are most likely to form colloid species, would be hydrolyzable elements, like the actinides and possibly strontium as well as lead and copper (representing the encapsulation material in the Swedish program). The definition of true and pseudocolloids is presented. True colloids are formed by condensation of the molecules or ions as a result of hydrolytic or precipitation processes. They consist mostly of hydroxides or polymers of iron formed by hydrolysis of the radioelements. On the other hand, pseudocolloids are formed as a result of adsorption of the radionuclide on impurities in the solution. These pseudocolloids are also referred to in our report as natural colloids. Pseudocolloids are usually much larger, up to 500 nm, than the true colloids. Pseudocolloids can be of two types, reversible and irreversible. The former are produced by reversible surface adsorption. In this case, the radionuclide can easily pass back into the solution. In the irreversible case, the element is either incorporated into the interior of the foreign particle or irreversibly sorbed on to it. A special case is the formation of pseudocolloids through interaction of nuclides with organic colloids. Such organic colloids, for example, humus substances, are present in natural waters.

The formation rates of true and pseudocolloids are quite different. True colloids form rapidly while the rate of pseudocolloid formation is basically determined by the sorption rate of radionuclides. Olofsson et al.²⁴ in their review article state that there are a lot of data available on pseudocolloidal formation rates. As an example, they point out that an equilibrium distribution of tetravalent plutonium between colloidal impurities, the vessel surface, and the solution is achieved within 3 to 5 hours. Olofsson et al.²⁴ also point out that colloids age, that is, grow in size (also coagulate), and can change properties through recrystallization of microcrystals. They present data on colloids for actinides and some other elements of interest. These data show the pH range and ionic strength where more than 10% of the radioelement is present in colloidal form under laboratory conditions.

Champ et al.²⁶ have demonstrated experimentally the existence and rapid transport of plutonium colloids. This carefully executed set of experiments, using core samples and groundwater, provides added insight into colloid formation and confirmation of rapid migration rates. The experimental work by Olofsson et al.²⁵ showed the formation and rapid nonadsorbing migration of americium colloids over a wide range of pH. In their more recent study,³⁰ they measured the diffusion rate of americium and plutonium and studied the effects of pH on the colloid formation of americium, plutonium, and neptunium. True colloids tended to form at the higher pH values. For americium, true colloids formed at a pH above 12; for plutonium, formation occurred at values above 8; and for neptunium, at pH values above 10. They point out also that colloid particles have a much slower diffusion rate than ions and molecules.

Means and Wijayarathne²⁷ discuss the role of natural colloids in the transport of heavy metals and show experimentally the very strong adsorptive strength of colloids for organic contaminants. Allard et al.²⁸ provide experimental data for the expected species of uranium, neptunium, and plutonium in neutral aqueous solutions. They point out that at low pH (below 4 to 5) the trivalent state is predominant and the hydroxide form is dominant at pH above 11 to 12. In the intermediate pH region, a mixture of different species exists. The exact chemistry is still under investigation, but this work is of value in a better understanding of the effects of pH on specie concentrations.

Avogadro et al.^{31,32} discuss the role of nuclear colloids in waste disposal. They claim that the predominating mechanisms affecting the migration of nuclear colloids are filtration and solubilization. In their most recent paper,³² reference was made to laboratory column experiments in which they showed that colloidal filtration is a major retention mechanism governing colloid transport through porous geological media. A simplified 1-D filtration model was presented and used to represent their data.

Colloid Modeling. Apps et al.²⁹ recently reviewed colloid and particulate transport in the geologic storage of nuclear waste. They provided numerous references suggesting that colloid formation is strongly evident in natural systems, but they were not able to quantitatively assess the potential formation and migration rates of nuclear colloids. The modeling was rather preliminary and made use of many simplifying assumptions which could be very important to a repository assessment. Treatment of particle sizes and the size effects was very limited.

Chiang and Tien³³ have modeled in some detail the capture of colloids within a porous medium, but did not treat radioactive colloids specifically. They point out that when Brownian diffusion is the dominant force the common trajectory calculation approach is no longer possible. Although the authors include most of the attractive and repulsive forces in their rather complete mathematical description, they neither include particle size effects nor consider radioactive decay and the migration of individual nuclides. Rather, their work is limited to modeling the processes of colloid capture in a porous medium. This work could be a very useful contribution to the population balance repository modeling by providing a colloid capture model. The capture model appears as a death term in the population balance. Guszy et al.,³⁴ Adamczyk et al.,³⁵ Spielman^{36,37} and Spielman and Goren,^{38,39} Fitzpatrick et al.,^{40,41} and Chiang and Tien³³ as well as many other researchers have modeled the capture of particles/colloids.

With the exception of the modeling by Apps et al.²⁹ and Avogadro and De Marsily³² the literature on radioactive colloids has been experimental. The absence of colloid models and the lack of quantitative assessment point clearly to the need for such modeling information. The population balance is an additional transport equation which was derived in the early 1960s^{42,43} to model particulate processes such as crystallization, but the approach has

been used successfully in many fields to model particulate systems.⁴⁴⁻⁶² These are just a few of the numerous references to the population balance.

The application of the population balance to nuclear waste colloids, though new, is a straightforward extension of this well-established modeling technique. The population balance and its applications are discussed in the following sections.

3. Population Balance. In 1962 and 1964, Randolph⁴² and Hulburt and Katz⁴³ derived the general form of the population balance. These very formal and complete derivations of the population balance in the early 1960s set the foundation for the subsequent mathematical analysis of many particulate system studies ranging in fields from engineering to biology. The population balance is a well-established transport equation that is commonly used to model systems of countable entities.⁴²⁻⁶² Randolph and Larson⁴⁵ in their book make reference to the diverse and numerous applications of the population balance. Included are processes such as crystallization, grinding, air pollution, and biological systems just to name a few. The population balance is an important addition to the common mass transport and energy transport equations.

Using a size distribution, the population balance permits a full treatment of the colloid problem from the birth of colloids to their capture on the surrounding matrix as well as modeling the gradual effects of colloid growth or dissolution. Radioactive decay of specific nuclides within the colloids is treated by assigning within the population balance a concentration property axis to each species we wish to track. The addition of these property axes allows correct treatment of the decay chain problem with full accounting of the daughter product concentrations. Also, we can model the adsorption of multiple nuclides on the same colloid (heterogeneous colloids).

Randolph and Larson⁴⁵ discuss in detail an example of using the concentration property axis within in the population balance. For each nuclide, there is a separate concentration property axis that defines the number of colloids (at a point in time/space and at a size) that have a particular concentration of, for example, plutonium. Integrating over the plutonium property axis and the size axis gives the amount of colloidal plutonium at a point in time/space.

The important factor at this stage is that the general population balance permits a correct mathematical accounting and quantitative assessment of the nuclear colloid problem. Of course, the soluble species mass transport and energy balance equations must also be included as well as the appropriate system geometry to complete an overall repository assessment model. The level of model complexity, however, is set by the desired results with the option of using simplified models and submodels to perform conservative repository assessment calculations.

Application of the population balance is further enhanced by the wealth of information and experience provided by over 20 years of frequent use in many scientific fields. This means that the solution methods and the nature of the various terms have often been studied by previous researchers, and their results can now be applied rather directly to the nuclear colloid problem without the delays of extensive research and development.

The birth, growth, and death rates of microorganisms in biochemical processes are commonly modeled with the aid of the population balance. The work by Fredrickson and Tsuchiya⁴⁷ is a good example of the interdisciplinary applications of the population balance. Randolph and Larson⁴⁵ in their book on the theory of particulate processes also give many interdisciplinary examples and applications of the population balance. Several studies using the population balance⁵⁴⁻⁶¹ range in topics from modeling gas bubbles to mineral grinding models.

4. Application to Nuclear Waste Repository Assessment-Scenarios.

In applying the population balance for repository assessment, two scenarios are considered, and the descriptive mathematical models are developed. These scenarios do not represent a specific repository or site, but rather are used to derive a quantitative description of colloid transport and release.

Scenario (A) represents perhaps a worst case near-field problem in which the backfill surrounding a single canister fails, water penetrates the canister, and radioactive colloids are released through the fractured backfill and into the surrounding geological formation where groundwater carries the colloids away from the engineered barrier. Also, the dissolved species are in high enough concentrations to precipitate into additional colloids, and adsorption of dissolved species on natural groundwater colloids is occurring. This scenario is initiated during the thermal period and leads to the far-field transport of colloids. The second scenario (B) represents

the far-field problem in that dissolved nuclides have migrated beyond the repository and are available to bond with natural groundwater colloids and be transported through the fractured/porous geological formation. Colloids from the canister and/or natural colloids that have adsorbed radionuclides may also be present. Next, we will develop the descriptive equations for each scenario.

The model for scenario (A) will require the energy, mass, and population balance transport equations. The distributed energy balance models the fluid temperature as a function a spatial position and time.⁶³

Next the mass transport equations describe the migration of dissolved species. One equation is needed for each species; thus the equation is written for the general species "i."

Mass Transport Equation:

$$\frac{\partial C_i}{\partial t} + v \nabla \cdot C_i = D \nabla^2 C_i - \lambda_i C_i - \text{sink} \quad , \quad (9)$$

where

- C_i = concentration of species "i,"
- D = effective diffusivity,
- sink = transfer of species to the colloids and rock matrix,
- t = time,
- v = fluid velocity, and
- λ = radioactive decay constant for species "i."

A sink term is required in the mass balance to represent the dynamic transfer of dissolved species to either the true or natural colloids.

Next, the additional population balance equations are required to model the formation and migration of radioactive colloids. A few assumptions are necessary at this point to clarify the number and type of population balance equations needed. These assumptions can be relaxed or changed as the descriptive scenario may require. First, only one type of natural colloid is assumed to exist, but the colloid may adsorb various nuclides. If more than one type of natural colloid should exist, we would use an additional population balance equation to describe each one. Second, we will need a set of population balance equations to describe each true colloid (plutonium,

americium, etc.). True colloids as opposed to natural colloids, are formed by precipitation of a specific radionuclide and will contain only that nuclide plus daughter products. Applying these assumptions, two types of population balances will be required, one describing natural colloids and the other modeling the true colloids.

The general form of the population balance allows for any arbitrary number of continuous property axes where particle size is just one such axis.^{42,45} In the case of nuclear waste modeling, a concentration property level axis is required for each nuclide that is adsorbed on natural colloids, and in the case of true colloids, one is required for each daughter product. In this way, the population balance can track the adsorption and decay of each nuclide of interest. Of course, if it is not necessary to track each nuclide, then the problem can be simplified. This approach is given to show the comprehensiveness of the population balance model.

True Colloid Population Balances:

$$\frac{\partial \phi_{ti}}{\partial t} + \nabla \cdot (v \phi_{ti}) - D_b \nabla^2 \phi_{ti} + \sum_{j=1}^m \frac{\partial}{\partial \xi_j} (v_j \phi_{ti}) + D_i - B_i = 0 \quad (10)$$

Natural Groundwater Colloid Population Balances:

$$\frac{\partial \phi_{nk}}{\partial t} + \nabla \cdot (v \phi_{nk}) - D_b \nabla^2 \phi_{nk} + \sum_{j=1}^m \frac{\partial}{\partial \xi_j} (v_j \phi_{nk}) + D_k - B_k = 0 \quad (11)$$

where

B = colloid birth function,

D = colloid death function,

D_b = brownian diffusion,

v = fluid or colloid velocity vector,

t = time,

ϕ = population density function,

i = property axis,

ξ = property rate function (includes growth rate and concentrate change),

i = index for nuclides which form true colloids,

j = property axis type (size and concentrations),
k = index for type of natural colloid (silicon, iron, aluminum, etc.),
m = number of property axes,
n = natural colloids, and
t = true colloids.

The energy, mass, and population balance equations together describe mathematically the near field where many physical and chemical processes are occurring simultaneously. Of course, to complete the above model the system geometry, boundary conditions, and specific terms within the equations must be defined. Submodels or kinetic expressions are used to represent the various terms in the population balance. The extensive population balance and colloid modeling literature³³⁻⁶² provides the general forms for these submodels.

Parameters within the submodels can in many cases be estimated on a conservative approach method or may require estimates from experimental data. Many experiments in numerous fields have used the population balance model, and this information can aid in modeling radioactive colloids.

The second scenario (B) is the far-field problem in which the thermal period has passed and nuclides have migrated out from the repository into the groundwater of the surrounding geological formation. Natural groundwater colloids of silicon, iron, and aluminum may be present to adsorb dissolved nuclides and, thus, provide a mechanism for rapid transport along cracks or faults. Here, as in the previous case, true colloids originating within the repository may also be present and may have migrated into the far field. The overall assessment model consists of the dissolved nuclide mass balances, a set of true colloid population balances (one for each nuclide), and the natural colloid population balance. If there is more than one type of natural colloid, then one population balance is required for each.

The mass conservation and population balance equations are essentially the same as shown previously but, of course, with different initial and boundary conditions. The problem of convective transport through fractured media should be considered in this scenario, thus, requiring equations for the fracture and for the porous medium.

Initially a rather microscopic and complex algorithm or model of colloid transport is necessary, but from this eventually could come simplified macroscopic expressions.

5. Conclusions. Colloid formation and transport form a growing area of interest and importance because they create a new and untested path for the early release of radiation from a repository.

To assess quantitatively the impact of colloids on the repository, we must enhance the existing transport models by the addition of the population balance transport equations. The population balance is an additional transport equation that, when included in the overall repository assessment model, can provide a quantitative analysis of colloids and their impact on nuclear waste disposal under geological conditions. The population balance approach is new to the modeling of nuclear waste colloids but has been used successfully in many branches of science for over 20 years.

This section shows that the comprehensive model for colloid migration can be highly coupled, requiring the simultaneous solution of the coupled-set of transport equations and involving a system of equations and submodels that describes the complex physical and chemical behavior of the colloids. However, the same can be said for radionuclide migration modeling in general. Through the use of simplifying assumptions, we have been able to develop reasonable assessment models that tell us a great deal about repository behavior. The same approach should prove viable in modeling and in assessing the importance of radioactive colloids.

The population balance is a valuable modeling tool that, with only modest effort, can be applied to the nuclear colloid problem and, thus, help to guide the study and assessment of nuclear colloids.

H. Applied Diffusion (A. E. Norris and P. L. Wanek)

The purpose of this task is to measure diffusivity values under field conditions at Yucca Mountain to ensure that values determined in laboratory experiments are reliable when used to calculate the retardation of nonsorbing radioactive wastes in water that might flow through the repository block. One aspect of this work is the development of analytical techniques for the quantitative determination of nonsorbing tracers that can be used in field experiments. Work reported previously⁶ showed that ion chromatography with an ultraviolet detector appeared to be the most suitable technique for

detecting bromide concentrations as low as 50 $\mu\text{g}/\text{l}$. Before additional data could be obtained concerning the use of bromide as a tracer in Topopah Spring Member tuff, the ion chromatograph began to malfunction. Some parts were returned to the factory for repair, and other parts were replaced with new equipment. The apparatus appears to be functioning properly once again, except for some minor leaks. When these are fixed, work will continue to measure the elution of bromide from a column containing crushed Topopah Spring Member devitrified tuff.

A newly purchased ion chromatograph was delivered this quarter. Factory service was required after delivery to get this instrument into operating condition. The sample size required for routine analyses with the new ion chromatograph is too large for compatibility with the tracer studies being performed in this task, but modifications are being made that should permit the new ion chromatograph to be used in addition to the older instrument.

III. MINERALOGY/PETROLOGY OF TUFF (D. Bish, D. Broxton, F. Byers, Jr.,

F. Caporuscio, B. Carlos, S. Levy, and D. Vaniman)

A. Iron and Manganese in Oxide Minerals and in Glasses

1. Redox Interactions. One of the main concerns at Yucca Mountain is the effect of oxidizing groundwater on the transport of radionuclides. Rock components that may affect the oxygen content of groundwater include iron-titanium oxides, glasses that contain ferrous iron, and manganese oxides. Phenocryst iron-titanium oxides occur at Yucca Mountain in reduced states to some extent, whereas groundmass iron-titanium oxides have been oxidized to hematite, pseudobrookite (Fe^{3+} -bearing phases), and rutile. In 430 samples examined, no groundmass magnetite or ilmenite has been identified. None of the common oxides observed in the groundmass contain significant Fe^{2+} . These groundmass oxides were probably originally magnetite and ilmenite that have been subsequently oxidized. Their oxidation is due to large surface area per volume (that is, extremely small grain size) and to their location along grain boundaries where water can interact with the oxides more efficiently. Also, some groundmass oxides are produced during vapor-phase alteration under conditions of high oxygen fugacity. Thus, the iron-bearing oxide minerals along or near fractures have no potential for removing oxygen from groundwater; the possible interaction with phenocrysts remains to be determined.

The thickness of vitrophyre or vitric tuff in and below the lower Topopah Spring Member varies from about 15 to 130 m in drill cores at Yucca Mountain.⁶⁴ This glass has potential for alteration, reaction, dehydration, and devitrification due to the slightly increased temperatures from an overlying repository. Oxidation of Fe^{2+} in the glass may occur more rapidly during the thermal pulse following repository loading and during the containment period, or much of the Fe^{2+} in the glass may remain available for reduction during later passage of water plus waste into the glassy tuff zones during the isolation period of repository history. The effectiveness of Fe^{2+} in glass is thus a difficult question to resolve. Preliminary studies indicate that the only appreciable Fe^{2+} in bulk rock samples from Yucca Mountain occurs in the glassy tuffs (~0.3% wt%).

The manganese oxides are a diverse series of minerals in which manganese can take on complex oxidation states. Potter and Rossman⁶⁵ have identified more than 20 valid species of tetravalent and trivalent manganese oxides. These oxides can have various amounts of water in their structures and have manganese ionic charges of 2+, 3+, 4+, 6+, and 7+ in many combinations. However, Potter and Rossman show that most of the manganese-bearing minerals that occur as dendrites in rock fractures contain Mn^{4+} as the dominant oxidation state. In a study of manganese dendrites, Potter and Rossman identify most fracture-lining dendrites as todorokite, romanechite, or a hollandite group manganese oxide (for example, cryptomelane). They also identify most underground manganese dendrites as todorokite. Potter and Rossman have found no dendrites with pyrolusite mineralogy and suggest that the term "pyrolusite dendrite" be discontinued.

The manganese oxide minerals that have been identified at Yucca Mountain, are among those that Potter and Rossman⁶⁵ specify as being typical of manganese dendrites. Todorokite $[(\text{Mn}, \text{Ca}, \text{Mg})^{2+} \text{Mn}_3^{4+} \text{O}_7 \cdot \text{H}_2\text{O}]$ has been identified⁶⁶ in the Tram Member in drill core UE-25b/#1 and cryptomelane $(\text{KMn}_8^{4+,3+} \text{O}_{16})$ has been identified in the Tram Member of drill core USW G-3.⁶⁷ X-ray diffraction studies identify a manganese oxide structure, within the Topopah Spring Member of USW GU-3, that is either lithiophorite $[(\text{Al}, \text{Li})\text{Mn}^{4+} \text{O}_2(\text{OH})_2]$ or todorokite. Further work will characterize and interpret the manganese-oxide occurrences at Yucca Mountain, but the analyses available and the studies by Potter and Rossman of similar manganese-oxide dendrites strongly suggest that Mn^{2+} is a minor or absent component in these

oxides. Manganese oxides with Mn^{2+} would buffer water Eh in a higher range than iron; depending on the actual minerals present, Eh could be controlled in the 0.2- to 0.5-V range for pH in the range from 6 to 8 (Ref. 68). For this reason, water buffered by Mn^{2+} could be effective in limiting the solubility of waste elements such as neptunium and plutonium, but not as effective in reducing uranium as would water buffered by iron. This factor, plus the relative unavailability of Mn^{2+} in either primary or secondary minerals along the flow path, limits the effective buffering of the groundwater Eh by Mn^{2+} at Yucca Mountain.

2. Retardation by Manganese Oxides. Zielinski et al.⁶⁹ and Zielinski⁷⁰ have cited hydrated manganese oxides as very strong sorbers of radionuclides. These studies propose that manganese oxides in fractures may be barriers to radionuclide migration. Concentrations of petrologically "incompatible" trace elements, such as arsenic, yttrium, and cerium, have been found in manganese oxides of the Topopah Spring Member,⁶⁷ indicating that these oxides are effective traps for incompatible elements.

Zielinski⁷⁰ lists whole-rock analyses of all major ash flows and lavas at Yucca Mountain. Values for bulk rock MnO range from <0.02 wt% in the tuff of Calico Hills to 0.32 wt% in the Tram, with an average value of 0.06 wt%. It is believed that there are three likely sources of manganese that can supply the amount necessary to produce manganese oxide fracture fill. These sources are: (1) manganese-bearing desert varnish that partially goes into solution with rain water and is reprecipitated in fractures; (2) manganese-bearing mineral phases, such as iron-titanium oxides and clinopyroxenes,⁶⁶ that contain up to 1 wt% MnO; and (3) MnO in the original glass of the ash-flow tuffs. More work needs to be done comparing the manganese content of fresh and altered ash-flow tuffs (and their mineral compositions) before the source of manganese oxide fracture fill can be identified with certainty. However, it is possible to evaluate the potential significance of manganese oxides as sorbants at Yucca Mountain based on Zielinski's work. Zielinski⁷⁰ analyzed small (3 g) samples of bulk tuff for leachable manganese, representing the manganese from "sorptive" manganese oxides. In samples from the devitrified Topopah Spring Member in drill hole USW G-1, analyses indicate 0.016 wt% manganese oxides in the bulk rock. If a repository area of 7 km² in the Topopah Spring Member is assumed, then a 10-m-thick slab of tuff with density 2.25 g/cm³ directly underlying the repository would contain more than

25 000 metric tons of manganese oxides. It is evident that the waste-element retardation potential of manganese oxides at Yucca Mountain is not trivial. It is also important to remember that this estimate is a minimum, because manganese oxides are actually concentrated along fractures rather than in the bulk rock; adequate estimates of fracture as well as bulk rock manganese oxide abundances will result from future study of large samples from exploratory mining at Yucca Mountain.

B. Zeolite Dehydration Experiments

Zeolite composition, particularly in the nature of the exchangeable cation (for example, calcium, sodium, potassium, or magnesium), has a strong effect on dehydration properties. Experiments on zeolite dehydration have begun in vacuum, in order to define the limits of the dehydration processes. Experiments are now progressing under controlled humidity in order to span the range of conditions that may be anticipated near a high-level waste repository.

Preliminary results are reported in a study by Bish.⁷¹ The samples examined in this study were all >95% clinoptilolite as determined by x-ray powder diffractometry. Natural clinoptilolites were obtained from Minerals Research, Clarkson, New York, and are as follows: #25524, Buckhorn, New Mexico; #25525, Castle Creek, Idaho; #25526 Sheaville, Oregon; and #27054, Fish Creek Mountains, Nevada. In addition, a macrocrystalline sample of Agoura, California, clinoptilolite was examined. Cation-exchanged varieties of the Castle Creek sample were prepared by mixing 2.5-g portions in 1.0-M solutions of calcium, potassium, and sodium chloride. The treatment was repeated three additional times for 16 h each at about 50°C. The solids were centrifuged and rinsed after each exchange. X-ray fluorescence analyses using fused pellets of the exchanged clinoptilolites show that the calcium and sodium exchanges were only partial. The calcium-exchanged clinoptilolite contained most of the original potassium and a minor amount of sodium; the sodium-exchanged material contained little calcium and roughly one-half of the original potassium. Harsher treatments, such as autoclaving, were not used in the cation exchanges to avoid recrystallization or alteration of the clinoptilolites.

X-ray powder diffraction (XRD) analyses were performed on an automated Siemens D-500 system employing CuK α radiation and a graphite diffracted-beam monochromator. Peak positions and intensities were measured using the Siemens first-derivative peak-search routine, and quartz and silicon external standards were used to calibrate the instrument. Data for unit-cell refinements were collected from 2 θ to 40 $^{\circ}$ 2 θ , counting for 1.0 s every 0.02 $^{\circ}$ 2 θ . Peak overlap and low intensities for most samples precluded the use of higher angle peaks in the refinements. Unit-cell parameters were refined using the least squares program of Appleman et al.⁷² Diffraction maxima were indexed with the aid of computer-calculated powder patterns; the automatic indexing feature of the Appleman program was not used. Peaks used in the cell refinements were the same as those used by Boles⁷³ with the addition of the 110, 130, -512, 530, -261, and -351 reflections.

The XRD data were collected in vacuo and at elevated temperatures using an Anton-Paar medium-temperature heater on the Siemens diffractometer. The sequence for a given sample consisted of examining a sample under room conditions (\sim 20 $^{\circ}$ C, \sim 35% relative humidity), slowly evacuating the sample chamber to \sim 0.1 torr and equilibrating for at least 30 min prior to analysis, and then heating the sample at 50 $^{\circ}$ increments from 50 to 300 $^{\circ}$ C with at least a 30-min equilibration before examination. After the 300 $^{\circ}$ C run, the heater was turned off, and the sample was cooled and re-examined in vacuo after being held at room temperature for at least 30 min. Each sample was examined one final time under room conditions, after equilibration for at least 30 min. Thirty minutes appeared to be an adequate equilibration time because the samples that were equilibrated overnight at temperature showed no significant additional changes. The temperature was measured with a platinum-resistance thermometer at a point immediately beneath the sample cavity, within the sample holder.

The XRD data demonstrate that the decreases in the unit-cell volume on heating and the ability of samples to rehydrate depend very much on the amount and nature of the exchangeable cation. The unit cells of all samples decreased in volume between 20 and 300 $^{\circ}$ C; sodium-saturated clinoptilolite underwent the greatest volume decrease (8.4%) and potassium-saturated clinoptilolite the smallest volume decrease (1.6%) of the clinoptilolites studied. The volume decrease for the calcium-saturated clinoptilolite was 3.6%. The highest percentage decrease for every sample was along the b axis,

generally making up 80 to 90% of the total volume decrease. The change in the a axis was the smallest and was usually less than 5%, although 26.5% of the contraction of the sodium-exchanged clinoptilolite was along a. The bulk of the volume contraction of many samples occurred on evacuation at room temperature, demonstrating that the observed changes were due to water loss and not to a temperature-induced phase transformation. Low-angle scattering was significantly reduced upon evacuation for every sample, and the 110 reflection of clinoptilolite at $7.45^{\circ}2\theta$ became obvious whereas it was not before. Evacuation and heating also affected the relative intensities of the clinoptilolite reflections.

These data show that the effects of heating on volume depend strongly on the exchangeable cation content. Significant reductions in the volumes of natural, mixed sodium-potassium-calcium clinoptilolites in rocks could occur in a repository environment, particularly if the clinoptilolites occurred in unsaturated, dehydrated rock. However, tests now in progress suggest that clinoptilolites occurring in partially saturated rocks at temperatures below 100°C should not decrease in volume significantly.

C. Summary of Mineralogic Data for Yucca Mountain

X-ray powder diffraction techniques have been applied to the tuffs at Yucca Mountain to obtain a three-dimensional mineralogic model. X-ray analysis is especially useful in tuff where the most abundant phases are often too fine grained for optical determination. When core was not available, data were obtained from cuttings. When core was available, approximately 15 to 20 g of material were crushed in a shatterbox to provide a large, homogeneous sample. A portion of this powder was ground in a mortar and pestle under acetone to approximately -325 mesh ($45\ \mu\text{m}$). Material from drill holes WT-1 and WT-2 was ground under acetone in an automatic Brinkmann Retsch mill with agate mortar and pestle to less than $5\ \mu\text{m}$. This fine crystallite size is necessary to ensure adequate particle statistics.⁷⁴

All diffraction patterns were obtained on a Siemens D-500 powder diffractometer with a copper-target x-ray tube and a diffracted beam monochromator. The diffractometer was run from 2.0 to 36° in the continuous scan mode at a scanning rate of $1^{\circ}/\text{min}$ for earlier samples; the data for remaining samples were collected automatically in the step scan mode with a step size of $0.02^{\circ}2\theta$ and count times per step between 1.2 and 2.0 s. Mineral

identification was accomplished by comparison of observed patterns with standard patterns produced in this laboratory and by comparison with published standards from the Joint Committee on Powder Diffraction Standards (JCPDS). Clay mineral standards were obtained from the Clay Minerals Society Source Clay Repository, and zeolite standards were recently obtained from Minerals Research Corporation, Clarkson, New York.

In contrast to qualitative identifications of the phases present in tuffs, quantitative multicomponent analysis is more difficult, time consuming, and is not straightforward due to a number of factors. These factors include variations in the degree of preferred orientation of crystallites, variations in crystallite size, variations in crystallinity, and variations in composition (crystalline solid-solution). In addition, due to the complexity of the diffraction patterns that often show peaks from at least six major phases, the method of intensity measurement also affects quantitative results. Finally, because standards are required for quantitative analysis, the choice of standards plays a critical role. In our investigation, both natural materials and computer-calculated patterns were used to standardize.

In order to eliminate or minimize the problems due to variations in the nature of the samples, samples were finely ground as described above. Variations in feldspar composition were partially overcome by choosing X-ray diffraction lines that are not significantly affected by changes in composition. Variations in the compositions of other minerals, for example, clinoptilolite, mordenite, and smectite, were not compensated for, but errors thus introduced are likely to be smaller than those introduced by orientation effects and by problems with peak overlap. All of our analyses presently use integrated peak intensities rather than peak heights to compensate for crystallinity variations.

Integrated intensities for all but drill hole USW G-2 samples were obtained using the Siemens first derivative peak search routine; this algorithm yields accurate integrated intensities for resolved peaks. Data for USW G-2 samples employed peak heights, and the results are not as accurate or precise as later data.

Most of our data on overlapping peaks were obtained using the first derivative routine that divides the intensity of overlapping peaks at the midpoint between the peaks. Closely overlapping but partially resolved peaks

are a problem mainly with rocks containing tridymite, cristobalite, quartz, and alkali feldspar. Overlapping peaks of these phases are now deconvoluted by using a Gaussian peak profile, and this technique was used for data from WT-1 and WT-2. Completely overlapping peaks of mordenite and clinoptilolite or of alkali feldspars were not deconvoluted. Instead, nonoverlapping peaks were used for mordenite and clinoptilolite. Peaks of the alkali feldspars were chosen that are relatively insensitive to compositional changes; therefore, overlapping peaks could be used. In many tuff samples, there are at least four separate feldspar species present: groundmass and phenocryst feldspar, both of which have exsolved separate feldspar. The resultant diffraction pattern is so complex that it is usually difficult to determine the exact nature of the individual feldspar phases.

The technique employed in our laboratory for quantitative analysis is known as the matrix-flushing method or the external standard method.⁷⁵ This technique requires the use of reference intensities, which as Chung⁷⁵ pointed out, vary depending on instrumental conditions and design. We have determined the reference intensity ratios (RIR), the ratio of the integrated intensity of a given reflection of a phase to the integrated intensity of the 113 reflection of Linde A corundum in a 1:1 mixture, by weight, for several phases found in Yucca Mountain tuffs, but many minerals could not be isolated in pure form. Smectite from drill hole USW G-1-1415 was isolated by centrifugation; clinoptilolite was obtained from the Nevada Test Site in drill hole UE-4P-1660, and quartz crystals were obtained from Hot Springs, Arkansas.

The value of the RIR for calcite was taken from Chung.⁷⁵ Calculated RIR values were used for the remaining phases, the data coming mainly from Borg and Smith.⁷⁶ Where possible, RIR values were obtained for more than one peak per phase, for example, the RIR for the quartz 100 reflection is 0.95 and the RIR for the 101 reflection is 4.32. We have recently obtained pure samples of sanidine, cristobalite, clinoptilolite, mordenite, analcime, biotite, and labradorite, and RIR values will be experimentally determined for all of these phases in the near future. Estimates of the percentage of glass in samples were based on the intensity of the "amorphous hump," and precision is poorer for glass-containing samples than for those containing no glass.

To analyze the X-ray data, we solve the following equation that is derived by Chung:⁷⁷

$$X_i = \left(\frac{k_i}{I_i} \sum_{i=1}^n \frac{I_i}{k_i} \right)^{-1}, \quad (12)$$

where X_i is the unknown weight fraction of phase i in a mixture, k_i is the RIR for phase i , and I_i is the integrated intensity of the appropriate line of phase i . Equation (12) is derived using the constraint that $\sum X_i = 1$, and the resultant equation "flushes" out the absorption coefficients by ratioing the k_i values.

Quantitative x-ray diffraction data for samples from 11 drill holes at Yucca Mountain are summarized in Bish and Vaniman.⁷⁸ A three-dimensional summary of these data is included in that report, based on 21 mineralogic cross-sections using the geologic cross-sections compiled by Scott and Bonk.⁷⁹ Several points concerning the x-ray data are summarized below.

1. Glass. Glasses occur both above and below the potential repository host rock at Yucca Mountain (the welded devitrified Topopah Spring Member). A vitrophyre is the first different primary lithologic type that would be encountered in transport downward from a repository in the overlying devitrified Topopah Spring. Vitric nonwelded glasses occur both above and below the devitrified Topopah Spring unit. These nonwelded and poorly consolidated glasses are more abundant than the vitrophyre across most of Yucca Mountain, although the lower nonwelded vitric zone thins and disappears to the east where the stratigraphic dip and structural displacements bring the vitric material closer to the static water level. The vitric nonwelded material may have important paleohydrologic significance because the preservation of nonwelded glass can be interpreted as an indication that the past water level has been no higher than the deepest occurrence of vitric pumice.⁸⁰ Glasses are also preserved in some dense rock types (for example, lavas) well below the static water level.

2. Silica Polymorphs. The silica polymorphs are abundant throughout Yucca Mountain. The polymorphs present include quartz, tridymite, and cristobalite. Slight variations in solubility and thermodynamic properties occur among the silica polymorphs. Experimental studies indicate that silica concentrations in solution will be controlled by cristobalite rather than quartz.⁸¹ Cristobalite is ubiquitous above the water table except in drill hole UE-25a#1, where cristobalite does not occur below the Topopah Spring

unit. Elsewhere, cristobalite persists to depths greater than 500 m above sea level. There is also a relatively clear correlation between the loss of tridymite and the first appearance of abundant quartz with increasing depth. This transition takes place within the Topopah Spring unit and represents a major transition in the mineralogy of the proposed repository host rock. This transition in part reflects the passage from zones of common vapor-phase crystallization (tridymite) to zones of vapor-poor devitrification (quartz) within the Topopah Spring.

3. Smectite. Previous studies have noted that smectite is a ubiquitous alteration product at Yucca Mountain, but one that is typically found in relatively small quantities.⁸² Although this statement is generally true, the data summarized in Bish and Vaniman⁷⁸ indicate that two zones of abundant smectite can be mapped out across Yucca Mountain. These zones occur at the top of the vitric nonwelded base of the Tiva Canyon Member with about 7 to 35% smectite and at the top of the basal vitrophyre of the Topopah Spring Member (5 to 45% smectite). The sorptive potential of this thin (generally <1 m) lower interval is high and may provide an important supplement to the sorptive behavior of the more abundant zeolitized zones. The thermal stability of this smectite zone and the probable time-temperature-hydration history of the layer under repository conditions are being studied as an important part of the retardation modeling of Yucca Mountain.

Jones⁸³ attempted to use clay-mineralogic criteria as evidence of past variations of water table elevation in alluvium north of Frenchman Flat, NTS. He found no sepiolite or palygorskite in the alluvium, minerals apparently indicative of a relatively long-standing water table. Neither of these minerals has been identified in the tuffs from Yucca Mountain. Jones⁸³ also proposed that variations in the smectite 001 spacing would reflect changes in the water-table elevation. He found slightly more expanded (statistically significant?) basal spacings for smectites up to 50 m above the present water table and suggested that this may be showing the effects of increased hydration. It is well documented that smectite basal spacings are a function of the interlayer cation and the partial pressure of water in contact with the smectite.^{84,85} Therefore, it is doubtful that the variations seen by Jones can be attributed to variation in water table level, unless secondarily. The smectites in Yucca Mountain typically show no systematic trends in $d(001)$ with depth near the water table^{66,67,86} and have basal

spacings representative of mixed sodium-calcium interlayers. The only apparent change in phase assemblage near the water table in Yucca Mountain is the alteration of vitric Calico Hills tuff and lower Topopah Spring Member.

4. Clinoptilolite and Mordenite. There is a general correlation of zeolitized material with the nonwelded zones between ash flows. Exceptions to this relationship are also common (for example, the occurrence of zeolitized tuff in the welded Tram Member of drill hole USW G-3). Indeed, the first zeolitized interval below the proposed repository horizon occurs within the densely welded Topopah Spring Member, at the contact between devitrified and vitrophyre lithologies. The origins of this particular interval may be very different from the deeper zeolitized intervals⁸⁷ being coupled in part with water liberation at elevated temperatures during early devitrification. Zeolites may also form along fractures crossing the devitrified intervals.⁸⁸ These various occurrences point out the complexities of zeolite formation at Yucca Mountain and are a caveat against simplified models for open-system zeolitization.

Although phillipsite and erionite were reported to occur in Yucca Mountain tuffs,^{89,90} we have found no evidence for the presence of these two zeolites in our analyses. Heiken and Bevier⁸⁹ reported erionite in samples JA-15, JA-32, and JA-33BC and phillipsite in JA-13. These analyses were based primarily on electron microprobe data, although the discussion of JA-32 included the XRD identification of "erionite." Sykes et al.⁹⁰ reported the occurrence of erionite in YM-34 based on scanning electron microscope (SEM) examination.

We have since re-examined all of the above samples by x-ray diffraction and found no evidence for the occurrence of erionite or phillipsite. These analyses agree with those published in Carroll et al.⁸⁶ Minimum detection limits for phases such as erionite, phillipsite, mordenite, and clinoptilolite are on the order of 1%. In addition, the x-ray patterns of these zeolites are distinctive, and their identification by XRD is usually unambiguous. We have recently conclusively identified by XRD very poorly crystallized erionite in a fracture in drill core UE-25a#1-1296. The erionite was mixed with clinoptilolite and occurred in a form common for mordenite in fractures.

There are several explanations for the previous erionite and phillipsite identifications. All of the JA erionite and phillipsite analyses relied upon electron microprobe data. It is difficult, if not impossible, to obtain reliable chemical data for hydrous, finely intergrown materials using this method, and identifications based upon analyses of such materials are suspect. Furthermore, it is possible for several different zeolites to yield similar chemical analyses, particularly erionite and mordenite. The tentative identification of erionite in YM-34 was based on the morphology observed with the SEM. However, we have observed identical morphologies in mordenite-rich tuffs containing no erionite.⁶⁶ The fibrous material in YM-34 was likely mordenite even though no mordenite was obvious in the XRD pattern; mordenite has since been identified in fractures using the SEM when no mordenite peaks appeared in the XRD patterns of bulk material.⁸⁸ The identity of the mordenite was established by examining small scraped samples by XRD.

5. Analcime and Albite. Few drill holes have penetrated deep enough to intersect analcime-bearing zones, and fewer still are deep enough to contain authigenic albite. Analcime typically first occurs at a depth of about 250 m above sea level but appears as high as 600 m above sea level in drill hole USW G-2. The shallower occurrence of analcime in USW G-2 agrees with other evidence of major hydrothermal alteration up to the 600-m elevation, possibly attributable to higher-temperature alteration along the Claim Canyon cauldron rim.⁹¹ Authigenic albite has been found only in drill holes USW G-1 and G-2 and Well UE-25b#1. The authigenic albite occurs only below 500 m above sea level, and may generally occur at much greater depths throughout most of the exploration block. As with analcime, the shallowest occurrence of authigenic albite is in USW G-2 near the Claim Canyon cauldron rim.

IV. TECTONICS AND VOLCANISM (B. M. Crowe, D. T. Vaniman, and D. B. Curtis)

A. Mechanism of Emplacement of Shallow Intrusions

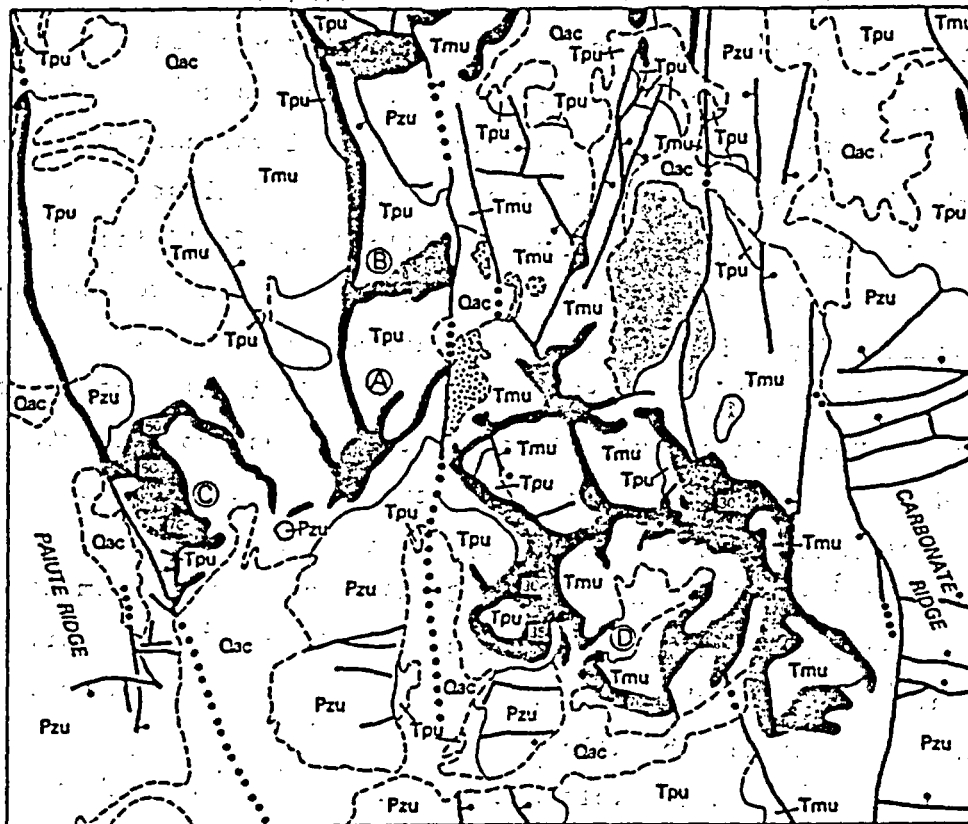
Crowe et al.⁹² summarized evidence concerning the subsurface geometry of basalt feeder systems in the southern Great Basin. They suggested that the prevalent intrusion structure exposed in dissected basalt centers is narrow dikes. However, a number of exceptions were noted. These include, the Palute Ridge area in the Halfpint Range of the eastern NTS region.⁹²

A recently discovered additional locality of shallow basalt intrusions is in the Funeral Mountains, east of the Amargosa Valley.* The Paleozoic and Cenozoic rocks of the Paiute Ridge area are intruded by sills, discordant intrusions and saucer-shaped bodies within the floor of a northwest-trending graben (Fig. 12). These intrusions are locally associated with scoria cones and lava flows, indicating magma was extruded at the surface.

The potential effects of sill and lopolithic intrusions on disruption of a repository were not considered in volcanic consequence analyses. Such effects could considerably change the results of consequence analyses for the Yucca Mountain site because of the greater potential for magma-waste contamination in an intrusion. Evidence against formation of sills and lopoliths beneath basalt centers includes the following: (1) dikes are the most common feeder structures exposed at eroded basalt centers; sills and lopoliths are rare;⁹² (2) no basalt intrusions were noted in alluvium or bedrock in drill holes VH-1 or VH-2, both of which were located adjacent to the the Red and Black Cone basalt centers in Crater Flat; (3) a 10 Myr. basalt that intruded the Tiva Canyon Member of the Paintbrush tuff at the western edge of the exploration block formed a narrow dike; there is no outcrop evidence that sills or sill-like intrusions were fed from the dike; and (4) formation of shallow intrusions beneath or within a waste repository need not increase the consequences of repository disruption. The intruding basalt could crystallize within the repository tunnel without incorporating waste within magma that was fed to the surface.

Several factors suggest shallow intrusions may be possible at the Yucca Mountain site. First, and most importantly, stress measurements in drill hole USW G-2 show a normal faulting stress regime with the magnitude of the least principal stress being close to the value at which slip could occur.⁹³ Crowe et al.⁹² presented field evidence indicating that the Paiute Ridge intrusions were emplaced contemporaneously with extensional faulting. They further suggested that extensional faulting may have favored formation of lopolithic intrusions. Second, data on the frequency of occurrence of intrusion structures are biased by the level of erosional dissection of basalt centers. It is possible that shallow intrusions are more common in the geologic record but are rarely exposed by erosion.

* This information was provided by W. J. Carr (1983).



0 5 10
KILOMETERS

-  BASALT INTRUSION
-  CONE SCORIA AND CONDUIT PLUGS
-  BASALT LAVA FLOW

Fig. 12. Generalized geologic map of the Paiute Ridge area of the Halfpint Range. Numbers represent the dip of the inward-directed intrusion walls. Modified from Ref. 92.

B. Volcanic Patterns Through Time: DV-PR Volcanic Zone

Volcanic fields of the Death Valley-Pancake Range volcanic zone are divided into two types.⁹⁴ Type I fields are large-volume volcanic fields with a range of basalt types including basanite, alkali olivine basalt, and hawaiite. These basalt fields, which include the basalt of the Greenwater Range, the basalt of the Reville Range, and the basalt of Lunar Crater are long-lived fields that were active over several million years. The volume of magma associated with the fields is $>10 \text{ km}^3$ for the composite field with

individual eruptive centers producing magma exceeding 2 km^3 in volume. Volcanic centers are clustered along major, generally northeast-trending structures resulting in volcanic fields with high scoria cone densities (10^{-1} to 10^2 vents/ km^2). The Greenwater field is a bimodal volcanic field with basalts interbedded with rhyolite domes and related pyroclastic rocks that comprise the Greenwater Formation. The Reveille Range field includes local trachyte plugs that may have evolved through fractionation from the more voluminous basalt. Type II volcanic fields are small-volume fields with the composite field volume being less than 2 km^3 and individual centers of 0.1 km^3 or less. Volcanic activity in these fields was sporadic with basalt centers formed during brief cycles of activity separated by longer periods of inactivity. Individual centers are widely distributed, resulting in a low cone densities (10^{-3} to 10^{-4} vents/ km^2). Basalt types are predominately hawaiite with lesser amounts of alkali basalt and hypersthene-hawaiite. Type II volcanic fields in the DV-PR include the southern Death Valley area, the NTS region, and the Kawich Valley.

The important question for volcanic hazard studies is whether there is a time progression to the evolution of Type I volcanic fields. Could Type II fields evolve toward Type I volcanic fields through time? Such a temporal change would result in greatly increased rates of volcanism and, therefore, an increase in the projected hazards of future volcanism. In order to answer these questions, we examine the temporal patterns of volcanism in the NTS region and contrast these patterns with those of long-lived, Type I volcanic fields in the DV-PR volcanic zone. Only the volcanic patterns of the NTS region are described in this quarterly report. Volcanic patterns of Type I volcanic fields of the volcanic belt will be described in the next quarterly report.

The basaltic rocks of the NTS area are divided into three episodes, with each episode spanning several million years and including basalt of many eruptive centers. The volume relations of these episodes vs time are shown on Fig. 13. The oldest episode of basaltic volcanism includes the basalts of the silicic episode (BSE) that erupted during the waning phase of silicic volcanic activity (11 to 8.5 Myr). These basalts form bimodal basalt-rhyolite centers that crop out in a northwest-trending zone extending from the south moat zone of the Timber Mountain caldera to Stonewall Mountain. Volumes of basaltic magma from the basalts of the silicic episode are large

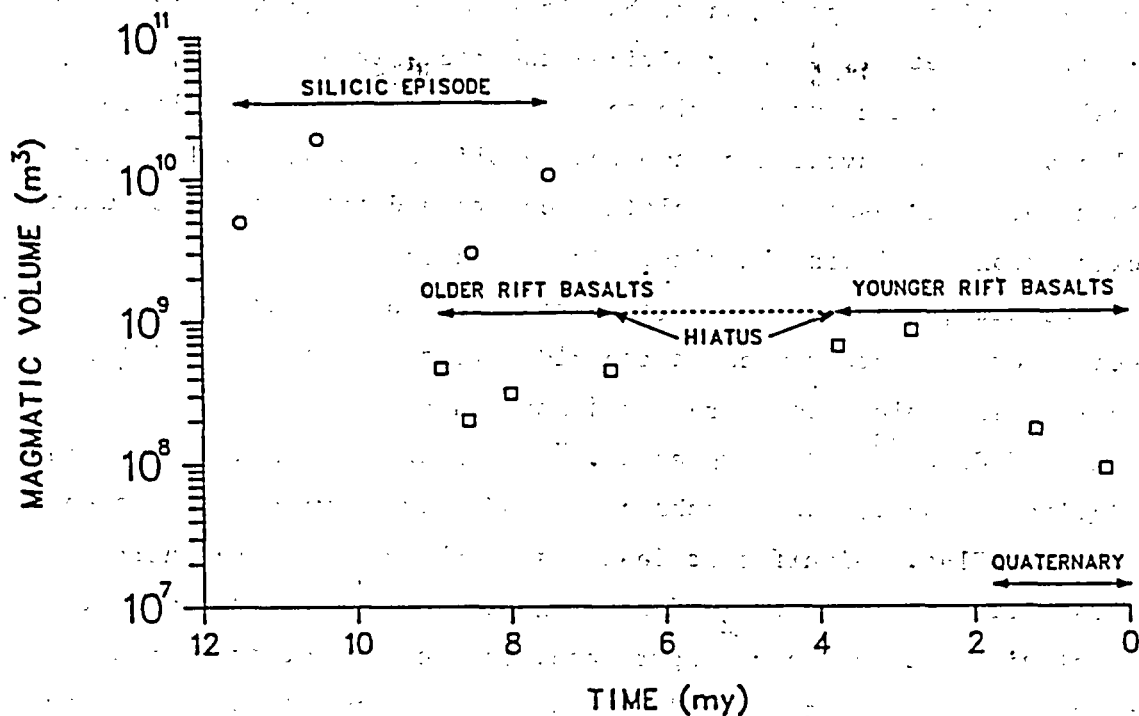


Fig. 13. Plot of magmatic volume (dense rock equivalent) vs time for the basalt episodes of the NTS region. Circles: basalts of the silicic episode; squares: older and younger rift basalts.

with individual centers exceeding 10 km^3 . The basalts of the silicic episode were replaced gradationally in time by the older rift basalts. These basalts are either distinctly younger than or are spatially separate from the silicic volcanic centers. They consist of small volume ($<1 \text{ km}^3$) monogenetic Strombolian centers that erupted during the probable peak of extensional faulting. Basalts of this episode range in age from about 9 to 6.5 Myr. Magma volumes declined drastically at the transition between episodes then stabilized at low but generally uniform rates (Fig. 13). There was a brief but important pause in volcanic activity between 6.5 and 3.7 Myr. This hiatus was followed by eruption of the younger rift basalts. These basalts form widely scattered, small-volume centers identical to those of the older rift basalts. They are separated from the older rift basalts on the basis of their younger age (3.7 Myr to recent) and their enrichment in incompatible trace elements with the exception of rubidium.⁹⁴

The mineralogical composition of basaltic rocks of the NTS region was summarized by Crowe et al.⁹⁴ They divided the rocks into four major petrological groups including aphyric to moderately porphyritic olivine basalt, plagioclase porphyritic clinopyroxene-olivine basalt, feldspathic clinopyroxene-olivine basalt to basaltic andesite and trachyte, and quartz-bearing clinopyroxene-olivine basalts. Trace phases in the basalts include apatite, kaersutite, and phlogopite (late stage). These phases occur in all basalt cycles but are more common in the older rift basalts. No distinct variations in basalt mineralogy are noted through time.

Vaniman and Crowe⁹⁵ and Crowe et al.⁹⁴ emphasized the hawaiite affinity of the majority of the volcanic rocks of the NTS region with emphasis on the basalt of Crater Flat. Significant features of these rocks are their alkaline classification on a $(Na_2O+K_2O)/SiO_2$ diagram,⁹⁴ the presence of groundmass olivine and calcic clinopyroxene, the scarcity of groundmass calcium-poor pyroxene, and their andesine-normative composition. Vaniman and Crowe⁹⁵ further noted that the majority of analyzed hawaiites exhibit the straddle-type association of Miyashiro⁹⁶ where compositions range from slightly nepheline to slightly hypersthene normative and the calculated parental compositions straddle the diopside-olivine join in the basalt tetrahedron diagram. An important petrological feature of these rocks is the increase in normative hypersthene or nepheline with decreasing magnesium number ($Mg/Mg + Fe^{2+}$). This suite of straddle-type hawaiites represents one distinctive group of basalts probably derived by fractionation from a representative parental basalt. This hawaiite basalt group is a major petrologic rock type throughout the Great Basin.

We now recognize two other petrological groups of basalts in the NTS region based on the addition of major and trace element data from a much more comprehensive sampling population. These two groups are hypersthene hawaiite and basaltic andesite. Hypersthene hawaiites are nearly identical in many petrological features to the straddle-type hawaiites. They are classified as alkaline on the total alkalis vs SiO_2 diagram and have andesine normative compositions. They differ from the hawaiites in several important ways. First, the rocks have higher contents of normative hypersthene (7 to 16%). As a result, these rocks cluster toward the center of the ol-hy-di triangle of the basalt tetrahedron. Second, calcium-poor clinopyroxene is more common as a groundmass phase. Third, and more importantly, the hypersthene

hawaiites show decreasing normative hypersthene with decreasing magnesium number, the exact opposite of the straddle-type hawaiites (Fig 14). This suggests that the hypersthene hawaiites were derived from a differing parental magma than that of the straddle-type hawaiites. However, we have not yet calculated model compositions of the parental magmas to the hypersthene hawaiites. Hypersthene hawaiites are represented in the basalt analyses of Best and Brimhall⁹⁷ but were classified with the hawaiite group. Our more detailed work in the NTS region shows that while the compositions of some of these rocks can overlap, they represent differing petrological groups.

The basaltic andesite group comprises basaltic andesite and subordinate basalt that show increasing normative quartz with decreasing magnesium number. These rocks occur with large-volume centers, have both alkaline and subalkaline affinities,⁹⁴ and commonly contain phenocrysts or megacrysts of mottled plagioclase and resorbed bipyridinal quartz. Basaltic andesites are common throughout the Great Basin and were recognized as a separate rock group by Best and Brimhall.⁹⁷

The BSE exhibit a diversity of basalt types including all of the three major basalt groups. In marked contrast, all basalts of the Older Rift basalts are straddle-type basalts. These rocks are some of the most strongly unsaturated (nepheline normative) of the NTS region, exhibit only a narrow range of compositional variation, and include the only known occurrence of a parental basalt in the region (magnesium number from 0.69 to 0.74). The Younger Rift basalts repeat the pattern of petrological diversity of the BSE with some significant differences. First, the most voluminous petrological type of this episode is the straddle-type basalt. Second, the basalt to basaltic andesite of Buckboard Mesa is remarkably poor in normative diopside. Third, all of the basalts are of small volume.

V. TUFF LABORATORY PROPERTIES (J. Blacic)

The purpose of this work is to investigate the time-dependent mechanical properties of Yucca Mountain tuffs. During this quarter, the creep deformation experiment samples from the tuff of Calico Hills were completed, and the first experiment on samples from the Topopah Spring Member was begun. Because of the long time spans involved in these experiments, the data can not be presented yet. Brittle microcracking has been shown to be a process of

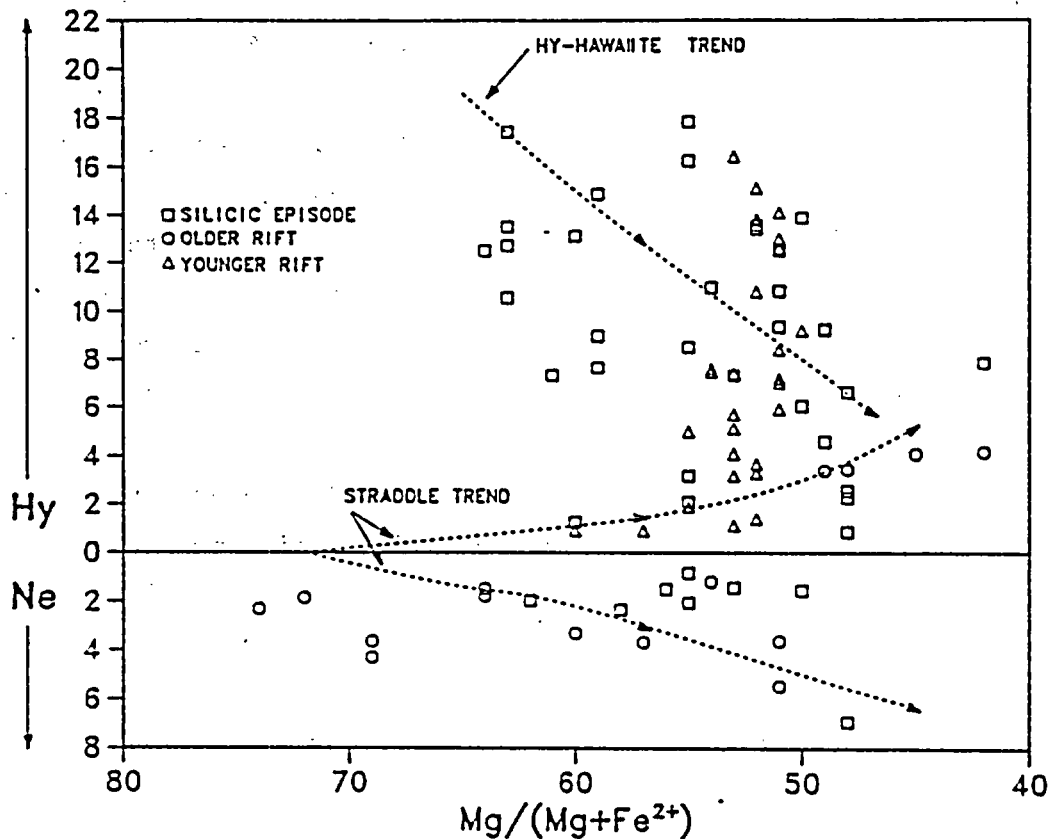


Fig. 14. Normative hypersthene and nepheline values plotted vs magnesium number for the basalt episodes of the NTS region.

potential concern for long-term tunnel or borehole stability in the tuff of Calico Hills. It is not yet known whether such processes may be significant in the Topopah Spring Member. Unfortunately, this project is being terminated at the end of this fiscal year, and very few data will be obtained for samples from the Topopah Spring Member.

A. History

The potential significance of time-dependent strength reduction (creep) of repository host rock was first brought to the attention of the NNWSI and national nuclear waste storage communities about 5 years ago. Our concern was based on long experience in experimental rock mechanics and on geologic observations of naturally altered rock, which had been subjected to long-term

heat and moisture conditions, anticipated to be artificially induced in the near field of a repository. The processes involved are microcracking, subcritical propagation of cracks, frictional sliding along cracks and joints, and mineral alteration, dissolution, and precipitation. All of these processes, particularly their interactions, are not well characterized. However, we believe that these processes would dominate the long-term response of rock subjected to the hot, wet, and stressed conditions induced by the waste, just as they do in nature. Because of the low rates of these processes at repository temperatures, they are easily overlooked in short engineering-type tests and their importance is frequently underestimated. Ultimately, the application of our knowledge of these phenomena will require a large time extrapolation from the laboratory time scale. This means that the mechanisms of the processes must be thoroughly understood if the effects are to be incorporated into predictive models. In order to further evaluate these phenomena, we formulated an approach to the problem in basically three parts.

First, we carried out a brief survey of existing data on the time-dependent deformation of potential hard rock repository media (granite, basalt, and welded tuff). This survey⁹⁸ also attempted to assess some implications of the data for repository design and was written largely with the intention of explaining to the uninitiated the significance of brittle creep phenomena for repository considerations.

Second, we performed a set of exploratory tests on a range of tuff types from Yucca Mountain in order to evaluate, in a rough way, the effect of extended exposure of tuffs to hydrothermal conditions similar to those likely to be encountered in the near-field of a repository. In these tests, samples from the Topopah Spring, Calico Hills, Bullfrog, and Tram stratigraphic units were subjected to a range of confining pressure, pore pressure, and temperature conditions for times ranging from 2 to 6 months. A number of thermo-mechanical and transport property measurements were made at ambient conditions before and after the hydrothermal exposure. Although the number of combinations of tuff types and exposure conditions was too large to allow a complete, statistically valid separation of sample inhomogeneity and exposure effects, we were able to reach the following conclusions.^{99,100}

(1) After hydrothermal exposure, there were statistically significant changes in compressive strength, tensile strength, porosity and matrix permeability,

and insignificant changes in grain density and thermal properties. (2) The observed changes appear to be related to subtle surface modifications of mineral grains although we were able to detect some dissolution reactions and alteration of clay and zeolite minerals. (3) These geochemical reactions were detectable at the limit of our capabilities and thus point up, again, the difficulty in evaluating the importance of these processes in short engineering-type tests.

Third, when the results of the soak tests were becoming apparent, we designed and built a prototype apparatus capable of obtaining the type of time-dependent strength data required. This device is capable of making accurate sample strain measurements at precisely controlled stress, temperature, and pressure conditions maintained for long times (months). It also has the capability of simultaneously allowing measurement of matrix permeability change.

B. Current Research

Over the last 13 months, creep experiments have been performed on Calico Hills tuff samples. Unexpected phenomena have been encountered, one of which has had the result of slowing the rate of progress on this work. The combined high porosity and low permeability of this tuff results in very long saturation times for the 5.4- by 11-cm-cylindrical samples we are using. Nominal saturation times of from 2 to 5 weeks have added substantially to the experiment times that were originally anticipated. In all, one failed, and four successful tests were performed, ranging from 1 to 3 months in duration each. This data base is inadequate to attain the goal of formulating a constitutive equation for this tuff, but some conclusions of importance are possible at this point.

(1) Hydration/dehydration strains of Calico Hills zeolitized tuff are large and are strongly time dependent. Hydration-state changes appear capable of generating compressive stresses of 20 to 60 MPa (hydration) and tensile stresses (dehydration) beyond the tensile strength of any rock within the thermal field of a repository. In creep tests at stresses below about 85% of the ultimate failure stress, samples first exhibit primary creep at nearly logarithmically decreasing rates, but then the sense of axial strain reverses, and the samples elongate against the applied axial stress. This appears

to be due to very slow swelling from incomplete saturation and hydration of zeolite and clay minerals. The maximum rate of swelling coincides with the onset of dilational microcracking in tests in which the axial stress is increased in steps. This implies that microcracking produces additional pathways for water to penetrate the innermost regions of the sample and produce an increased rate of hydration swelling. In other words, brittle microcracking, water permeation, and mineral hydration strain are coupled phenomena in this rock.

(2) Creep deformation of Calico Hills zeolitized tuff appears to be characterized by a steady-state strain rate component as low as $1 \times 10^{-10} \text{ s}^{-1}$. This result offers hope that a predictive model of mechanical strength can be formulated that will be valid over the long time extrapolation required for performance assessment, although the complicated coupling of hydration straining, microcracking, and water transport phenomena need to be sorted out before this can be realized.

In May 1984 we stopped work on Calico Hills tuff and began tests on Topopah Spring welded tuff. One or, at most, two tests on Topopah Spring tuff are possible by the September 30 termination date. These will be insufficient to adequately characterize the time-dependent processes in this tuff, but perhaps some indications will be possible.

The important question at this point is whether or not Topopah Spring tuff also exhibits important time-dependent variations in key properties. Unfortunately, we do not have the data to answer this question. We can get some idea of the potential magnitude of including time effects if we make some assumptions. First, assume that the effect of strain rate on uniaxial compressive strength of Topopah Spring welded tuff is the same as that for Grouse Canyon welded tuff for which some data exist. A similar argument for the mechanical behavior of welded tuffs was also made in the Johnstone et al.¹⁰¹ draft report. Blacic⁹⁸ showed that at 50 to 100 yr the strength may be reduced by something between 3/4 and 1/2 depending on moisture effects. This does not include any additional weakening due to elevated temperatures. Assuming a weakening factor of 2/3 for the sake of argument, the factor of safety calculations of Johnstone et al.¹⁰¹ can be used to estimate the extent of a weakened zone under the above assumptions. Fig. 15 shows calculated

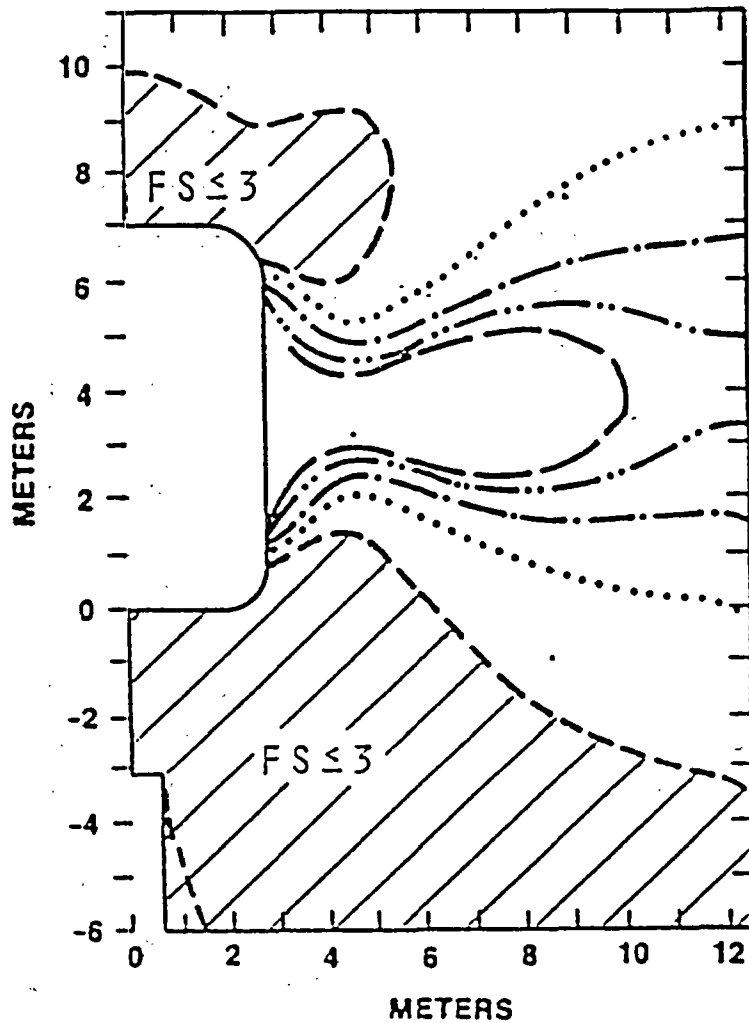


Fig. 15. Matrix factor of safety for Topopah Spring Member (average properties) at 50 yr (Johnstone et al., 1983).

contours of factors of safety for Topopah Spring tuff at 50 yr after waste emplacement, assuming time-independent average properties. If we now make our assumption of a 2/3 reduction in strength at 50 yr due to time effects, then the $FS = 3$ contour will actually be reduced to $FS = 1$. One can see from the figure that there is now a large region in the roof, floor, and around the waste emplacement hole for which the rock is in a state of incipient failure at that time. While this is a very qualitative argument, it fairly indicates the potential magnitude of including time effects on strength.

VI. SEALING MATERIALS EVALUATION (D. M. Roy and C. J. Duffy)

Cementitious materials (grouts, mortars, concretes) are being proposed as one major type of potential sealing material for a nuclear waste repository sited in the felsic tuffs of Yucca Mountain. Introduction of any sealing materials will, in general, cause reactions between the host rock and the sealant to occur because of chemical differences and the reactive nature of the fine minerals and glasses in the tuff.

The purpose of this project is to evaluate the chemical stability of potential sealing materials based upon laboratory studies conducted at a series of conditions that represent a range of credible temperature conditions for a repository at Yucca Mountain. These are supplemented by evaluation based upon thermodynamic considerations and by durable analogues from other sources.

Different concrete-type sealing materials are being evaluated for their potential chemical compatibility with the tuff rock chemistry. Two approaches to sealant-host rock compatibility were examined. The first utilized indigenous sands and gravel in the formulation of the sealant, while the second approach chose to utilize more conventional concrete materials, but to control the "bulk" chemical composition of the concrete so that it approached more closely the tuff composition.

A. Experimental Results

During this quarter, work has been carried out on a new cementitious grout mixture (84-12) having lower calcium sulfate content, which addresses the concern of some scientists that the introduction of sulfate into water in the repository might adversely affect waste element solubility. Work was also completed on a previously prepared, higher sulfate grout (82-22). Both formulations were developed with the objective of minimizing the chemical potential differences between the bulk tuff composition and the bulk grout composition without the extensive use of locally derived (local to the NTS) tuffaceous materials. Ongoing work is demonstrating that these tuffaceous materials with their glassy components are susceptible to devitrification and hence rapid chemical alteration under the temperature conditions anticipated as approaching the maximum credible for this repository design.

The formulation 82-22 was prepared initially. As formulated, 82-22 exhibited expansive behavior based upon the development of ettringite that was formed by the chemical reactions between flyash and hemihydrate. The preliminary studies on this formulation revealed that sulfate was released during the alteration of this phase. Concern over the effects of the introduction of sulfate in the groundwater prompted the development of the lower sulfate 84-12 formulation to minimize the release of sulfate.

Throughout the experiments described herein, the ratio of solids to fluid has been maintained at 1:10 in both the 150 and 200°C experiments. In all of the experiments Well J-13 groundwater was used as the mineralizing fluid. In these tests, no large-scale concrete test specimens were prepared. Therefore, to approximate the concrete that would be anticipated for usage in a sealing system, a mechanical mixture of -16+30 mesh graded crushed tuff and cementitious grout was used. The ratio of tuff (welded Topopah Spring Member) to grout was maintained at 2:1.

Hydrothermal treatment was conducted in either a rocking autoclave or an internally stirred Parr vessel. The former apparatus had a volume of 300 ml while the latter had a volume of 1 l. In the rocking autoclave, sampling was conducted with a pneumatically operated valve, to minimize throttling, into a Teflon-lined collection chamber. The Parr vessel was sampled with a manually operated valve and also collected into a Teflon-lined collection chamber. All reactions were conducted on a sampling schedule approximating $t = 2^n$ where n equals 0 to 10 days.

The pH of all liquid samples was measured at room temperature before they were stabilized with HCl to a pH of 1 to 2. Analyses of the fluids were accomplished with a combination of a direct current plasma atomic emission spectrometer and ion chromatography. Solids recovered from the charge at the termination of the experiment were characterized by X-ray Diffraction (XRD) and Scanning Electron Microscopy/Energy Dispersive X-Ray (SEM/EDX).

Of the 15 cations and anions that were routinely analyzed, only calcium, sodium, silicon, and sulfate with occasional potassium were detected in appreciable concentrations. Experiments with 82-22 at both 150 and 200°C and 84-12 at 200°C are complete at this writing. The final 150°C experiment with 84-12 is still in progress, but pH values from the recovered fluid phase samples are available.

1. Grout Mixture 82-22. The 150°C experiment established a pH value of approximately 9.5 for the initial 200 h of the experiment, but dropped to 8.5 by 800 h. The pH exhibited an unusually large jump to 9.9 after the vessel had been cooled to room temperature. The 200°C experiment established a pH of about 8.5 that persisted for nearly 500 h before dropping to 6.5. The pH increased only slightly when the experiment was quenched to room temperature. The lower pH obtained at 200°C may be due to more extensive reaction.

With the exception of silicon, the ionic species in the 150°C experiments appear to be more concentrated than in the 200°C experiment. Additionally, the 150°C data suggest a substantial wash-off of fines during the initial hours of the experiment. At both elevated temperatures, the calcium, silicon, and sulfate show an initial increase in concentration followed by a steady decrease. These behaviors suggest the formation of a solid phase occurring at temperature removing the ionic species from solution at a rate faster than it can be replaced by dissolution of the cement. Observed calcium and sulfate concentrations suggest that anhydrite may control sulfate solubility. Sodium exhibits a continual increase in concentration in the fluids in a manner similar to that anticipated for depletion of sodium from the solids, that is asymptotically approaching a fixed value.

2. Grout Mixture 84-12. The recorded pH for the 84-12 formulation at 150°C currently in progress averaged 9.7 during the initial 100 h after which it exhibited a drop to about 8.5 at 200 h. The 200°C experiment established a pH of 9.4 and maintained it for the duration of the experiment. As for the 82-22 formulation, the calcium and sulfate concentrations mimic each other, with the sulfate concentration approaching twice that of the calcium. Silica exhibits a steady decrease in solution concentration with time, but exhibits an unusual increase in concentration in the quenched sample. This seeming retrograde solubility behavior for silica is atypical for silicate phases in these systems. Sodium too, exhibits atypical behavior. The concentrations show a steady decrease to about 200 h followed by a slight increase in concentration to the termination of the experiment. An unanticipated sharp increase in concentration is observed in the quenched sample.

B. Comparison of the 82-22 and 84-12 Formulations

Comparisons of the data for the 200°C experiments show relatively small differences in the compositions of calcium, sodium, and sulfate in the fluid phases in contact with the two formulations in combination with tuff. The 84-12 formulation exhibits a generally lower concentration of silicon than the 82-22 formulation, possibly reflecting the physical properties of the silica-rich admixtures that were utilized in the formulation. The pH values of liquids in contact with both formulations, appear to decrease with time, except for the 84-12 mixture at 200°C (based on a single point at 600 h, which is slightly higher again). The alteration of the two concretes appears to be slightly different. The 82-22 formulation maintains a pH value almost 1 unit lower than the 84-12 mixture. It is not clear to what extent this could be related to the differences in agitation in the two different types of pressure vessels used for these experiments.

Bulk phases were determined by X-ray diffraction on each of the mixtures of grout and tuff that remained in the reaction vessels. The X-ray diffraction patterns of these products are all dominated by the mineralogy of the tuff (which comprises 66% of the solids). A plagioclase feldspar that best matches an oligoclase dominated the diffraction patterns. Additionally, quartz is present in all of the patterns as a principal component of the grout and possibly as a phase in the tuff. The 82-22 grout formulations at 150°C contain calcite (which has been confirmed by SEM/EDX on morphological and chemical basis). Similarly, calcite was identified in the 200°C 84-12 formulation but not in the 200°C 82-22 formulation. Well-crystallized tobermorite can be recognized in the SEM/EDX characterization of the 150°C 82-22 sample and is confirmed by XRD. A trace of poorly crystalline tobermorite was observed in the 200°C 84-12 formulation that ran for 600 h. This may be persisting metastably because the equivalent experiment at 200°C with the 82-22 mixture does not contain detectable tobermorite.

C. Conclusions

No major differences were found between the chemical behavior of grout mixtures 82-22 and 84-12. Despite the lower sulfate content of mixture 84-12, solutions in contact with it showed similar sulfate content to those in contact with mixture 82-22. This is probably due to control of sulfate by anhydrite precipitation in both grouts. Grout 84-12 may, however, be a more

appropriate grout for use in Yucca Mountain because its use would introduce less total sulfate. Also, if removal of sulfate from the fault seals were leach rate controlled, the lower sulfate content in grout 84-12 would probably give up its sulfate more slowly.

REFERENCES

1. B. M. Crowe and D. T. Vaniman, Comps., "Research and Development Related to the Nevada Nuclear Waste Storage Investigations, January 1--March 30, 1984," Los Alamos National Laboratory report LA-10154-PR (February 1984).
2. A. E. Ogard and J. F. Kerrisk, "Groundwater Chemistry Along Flow Paths Between a Proposed Repository Site and the Accessible Environment," Los Alamos National Laboratory report LA-10188-MS (November 1984).
3. R. K. Waddell, "Two-Dimensional, Steady-State Model of Groundwater Flow, Nevada Test Site and Vicinity, Nevada-California," US Geological Survey, Water Resources Investigation 82-4085 (1982).
4. L. V. Benson, J. H. Robison, R. K. Blankennagel, and A. E. Ogard, "Chemical Composition of Ground Water and the Locations of Permeable Zones in the Yucca Mountain Area, Nevada," US Geological Survey open file report USGS-OFR-83-854 (1983).
5. W. R. Daniels, B. R. Erdal, and D. T. Vaniman, Comps., "Research and Development Related to the Nevada Nuclear Waste Storage Investigations, July 1--September 30, 1982," Los Alamos National Laboratory report LA-9577-PR (1983).
6. R. Rundberg, A. E. Ogard, and D. T. Vaniman, Comps., "Research and Development Related to the Nevada Nuclear Waste Storage Investigations, April 1--June 30, 1984," Los Alamos National Laboratory report LA-10297-PR (in press).
7. Ki-Tae Kim and B. J. Burley, "A Further Study of Analcime Solid Solutions in the System $\text{NaAlSi}_3\text{O}_8 - \text{NaAlSiO}_4 - \text{H}_2\text{O}$, with Particular Note of an Analcime Phase Transformation," Mineralogical Magazine 43, pp. 1035-1045 (1980).
8. F. Birch, "Compressibility; Elastic Constants," in Handbook of Physical Constants, S. P. Clark, Jr., Ed., Geol. Soc. Amer. Mem. 97, Chap. 7, pp. 97-174 (1966).
9. B. J. Skinner, "Thermal Expansion," in Handbook of Physical Constants, S. P. Clark, Jr., Ed., Geol. Soc. Amer. Mem. 97, Chap. 6, pp. 75-96 (1966).

10. H. C. Helgeson, J. M. Delany, H. W. Nesbitt, and D. K. Bird, "Summary and Critique of the Thermodynamic Properties of Rock Forming Minerals," Amer. J. Sci. 278-A, 229 (1978).
11. G.K. Johnson, H. E. Flotow, P. A. G. O'Hare, and W. S. Wise, "Thermodynamic Studies of Zeolites: Analcime and Dehydrated Analcime," Amer. Mineral. 67, 736-748 (1982).
12. T. W. Newton, "The Kinetics of the Oxidation-Reduction Reactions of Uranium, Neptunium, Plutonium, and Americium in Aqueous Solutions," TID report 26506, 55 (1975).
13. K. Wolfsberg and D. T. Vaniman, Comps., "Research and Development Related to the Nevada Nuclear Waste Storage Investigations, October 1--December 31, 1983," Los Alamos National Laboratory report LA-10032-PR (1984).
14. D. Rai and J. L. Ryan, "Crystallivity and Solubility of Pu(IV) Oxide and Hydrated Oxide in Aged Aqueous Suspensions," Radiochim. Acta 30, 213 (1982).
15. R. J. Silva and H. Nitsche, "Thermodynamic Properties of Chemical Species of Waste Radionuclides," US Nuclear Regulatory Commission report NUREG/CP-0052 (1983).
16. J. P. Butler, J. A. Reeds, and S. V. Dawson, "Estimating Solutions of First Kind Integral Equations With Nonnegative Constraints and Optimum Smoothing," SIAM J. Numer. Anal. 18, 381 (1981).
17. C. Klingsberg and J. Duguid, "Isolating Radioactive Wastes," Amer. Scientist 70, 182-190 (1982).
18. T. H. Pigford, "Geological Disposal of Radioactive Waste," Chem. Eng. Prog. 78, No. 3, 18-26 (March 1982).
19. S. Gonzales, "Host Rocks for Radioactive-Waste Disposal," Amer. Scientist 70, 191-200 (1982).
20. Sandia National Laboratories, "Technical Report, Technical Assistance for Regulatory Development: Review and Evaluation of the Draft EPA Standard 40CFR191 for Disposal of High-Level Waste," Vols. 2-4, Sandia National Laboratories report SAND82-1557/NUREG/CR-3235 (April 1983).
21. N. R. Ortiz and R. M. Cranwell, "Technical Report, Risk Assessment Methodology for High Level Waste: Assessing Compliance with the EPA Draft Standard Including Uncertainties," Sandia National Laboratories SAND82-0596 (June 1982).
22. The Encyclopedia Americana International Edition, 1975.
23. J. I. Drever, "The Geochemistry of Natural Water," in Colloid Properties (Prentice Hall, New York, 1982), pp. 78-89.

24. U. Olofsson, B. Allard, K. Andersson, and B. Torstenfelt, "Formation and Properties of Radiocolloids in Aqueous Solution-A Literature Survey," Programradet for Radioaktivt Avfall, National Council for Radioactive Waste, Report Proav 4.25, Department of Nuclear Chemistry, Chalmers University of Technology, Goteborg, Sweden (June 1981).
25. U. Olofsson, B. Allard, K. Andersson, and B. Torstenfelt, "Formation and Properties of Americium Colloids in Aqueous Systems," in Scientific Basis for Nuclear Waste Management, Vol. 4, S. Topp, Ed. (Elsevier Science Publishing Company, New York, 1982).
26. D. R. Champ, W. F. Merritt, and J. L. Young, "Potential for the Rapid Transport of Plutonium in Groundwater as Demonstrated by Core Column Studies," in Scientific Basis for Nuclear Waste Management, Vol. 5, Werner Lutze, Ed. (North-Holland Publishing Company, New York, 1982), pp. 745-754.
27. J. Means and R. Wijayarathne, "Role of Natural Colloids in the Transport of Hydrophobic Pollutants," Science 215, 968-970 (February 19, 1982).
28. B. Allard, H. Kipatsi, and J. O. Liljenzin, "Expected Species of Uranium, Neptunium, and Plutonium in Neutral Aqueous Solutions," J. Inorg. Nucl. Chem. 42, 1015-1027 (1980).
29. J. A. Apps, C. L. Carnahan, P. C. Lichtner, M. C. Michel, D. Perry, R. J. Silva, O. Weres, and A. F. White, "Status of Geochemical Problems Relating to the Burial of High-Level Radioactive Waste, Lawrence Berkeley Laboratory report LBL-15103/NUREG/CR-3062 (March 1983).
30. U. Olofsson, B. Allard, B. Torstenfelt and K. Andersson, "Properties and Mobilities of Actinide Colloids in Geologic Systems," in Scientific Basis for Nuclear Waste Management, Vol. 5, Werner Lutze, Ed. (North-Holland Publishing Company, New York, 1982), pp. 755-764.
31. A. Avogadro and F. Lanza, "Relationship between Glass Leaching Mechanism and Geochemical Transport of Radionuclides," in Scientific Basis for Nuclear Waste Management, Vol. 5, Werner Lutze, Ed. (North-Holland Publishing Company, New York, 1982), pp. 103-112.
32. A. Avogadro and G. De Marsily, "The Role of Colloids in Nuclear Waste Disposal," in Scientific Basis for Nuclear Waste Management, Vol. 7, Gary L. McVay, Ed. (North-Holland Publishing Company, New York, 1982), pp. 495-506.
33. H. Chiang and C. Tien, "Deposition of Brownian Particles in Packed Beds," Chem. Eng. Sci. 17, No. 8, 1159-1171 (1982).
34. C. J. Guzy, E. J. Bonano, and E. J. Davis, "The Analysis of Flow and Colloid Particle Retention in Fibrous Porous Media," J. Col. Inter. Sci. 95, No. 2, 523-543 (October 1983).
35. Z. Adamczyk, T. Dabros, J. Czarnecki, and T. G. M. Van De Ven, "Particle Transfer to Solid Surfaces," Advan. Col. Inter. Sci. 19, 183-252 (1983).

36. L. A. Spielman, "Particle Capture from Low-Speed Laminar Flows," *Ann. Rev. Fluid Mechanics* 19, 297-319 (1977).
37. L. A. Spielman, "Viscous Interactions in Brownian Coagulation," *J. Col. Inter. Sci.* 33, No. 4, 562-571 (August 1970).
38. L. A. Spielman and S. L. Goren, "Capture of Small Particles by London Forces from Low-Speed Liquid Flows," *Environ. Sci. Tech.* 4, No. 2, 135-140 (February 1970).
39. L. A. Spielman and S. L. Goren, "Progress in Induced Coalescence and a New Theoretical Framework for Coalescence by Porous Media," *Indust. Eng. Chem.* 62, No. 10, 10-24 (October 1970).
40. J. H. Fitzpatrick, L. W. Zitnay, and L. A. Spielman, "Advances in the Design of Granular Bed Filters," *World Filter Congress, Paris, France, May 14-17, 1974* (Halsted Press, Div. of John Wiley and Sons, New York, 1974).
41. J. H. Fitzpatrick and L. A. Spielman, "Filtration of Aqueous Latex Suspensions Through Beds of Glass," *J. Col. Inter. Sci.* 43, 350-369 (1973).
42. A. D. Randolph, "A Population Balance for Countable Entities," *Can. J. Chem. Eng.* 42, 280-281 (1962).
43. H. M. Hulburt and S. Katz, "Some Problems in Particle Technology," *Chem. Eng. Sci.* 19, 555-574 (1964).
44. H. E. Nuttall, "Computer Simulation of Steady-State and Dynamic Crystallizers," Ph.D. thesis, University of Arizona (1971).
45. A. D. Randolph and M. A. Larson, Theory of Particulate Processes (Academic Press, New York-London, 1971).
46. A. D. Randolph and E. T. White, "Modeling Size Dispersion in the Prediction of Crystal-Size Distribution," *Chem. Eng. Sci.* 32, 1067-1076 (1977).
47. A. G. Fredrickson and H. M. Tsuchiya, "Continuous Propagation of Microorganisms," *AIChE J.* 9, No. 4, 459-468 (1963).
48. S. K. Bhatia and D. D. Perlmutter, "A Population Balance Approach to the Modeling of Solid Phase Reactions," *AIChE J.* 25, No. 2, 298-306 (1979).
49. N. A. Clontz and W. L. McCabe, "Contact Nucleation of Magnesium Sulfate Heptohydrate," *Chem. Eng. Progr. Symp. Ser.* 110 67, 6-17 (1971).
50. M. Volmer and A. Weber, *Zeitschrift Fur Physikalische Chemie (Leipzig)* 119, 277 (1926).
51. A. E. Nielson, Kinetics of Precipitation (Macmillan, New York, 1964).

52. M. D. Cise, "Crystal Growth and Nucleation Kinetics of the Potassium Sulfate System in a Continuous-Flow, Seeded Crystallizer," Ph.D. thesis, University of Arizona (1971).
53. A. D. Randolph, "Effects of Crystal Breakage on Crystal Size Distribution in a Mixed Suspension Crystallizer," *Ind. Eng. Chem. Fundam.* 8, No. 1, 58-63 (1969).
54. M. A. Larson and A. D. Randolph, *Chem. Eng. Progr. Sym. Ser.* 65, No. 95, 1-13 (1969).
55. W. Pasiuk-Bronikowska and K. J. Rudziński, "Mathematical Model of Bubble Gas Desorption from Liquids," *Chem. Eng. Sci.* 35 (1980).
56. C. Kiparissides and W. R. Ponnuswamy, "Application of Population Balance Equations to Latex Reactors," *Chem. Eng. Commun.* 10, No. 4-5, 283-291 (1981).
57. J. P. Barone, W. Furth, and S. Loynaz, "Simplified Derivation of the General Population Balance Equation for a Seeded, Continuous Flow Crystallizer," *Can. J. Chem. Eng.* 58, No. 1, 137-138 (1980).
58. J. A. Herbst and D. W. Fuerstenau, "Scale-up Procedure for Continuous Grinding Mill Design Using Population Balance Models," *Int. J. Miner. Process.* 7, No. 1., 1-33 (1980).
59. V. K. Gupta, D. Hodouin, and M. D. Everell, "An Analysis of Wet Grinding Operation Using a Linearized Population Balance Model for a Pilot Scale Grate-Discharge Ball Mill," *Powder Technol.* 32, No. 2, 233-244 (1982).
60. R. C. Griffiths, G. Paramo, and R. L. Merson, "Preliminary Investigation of Lactose Crystallization using the Population Balance Technique," *AIChE Symp. Ser.* 78, No. 218, 118-128 (1982).
61. B. Waldie and D. Wilkinson, "Modeling of Product Particle Size Distributions from Formation Processes," *Inst. Chem. Eng. Symp. Ser.* 69, 49-62 (1983).
62. W. S. Weng and T. L. Chen, "Population Balance and Residence Time Distribution Models for Well-Mixed Reactor and Regenerator Systems," *Chem. Eng. Sci.* 35, No. 4, 915-924 (1980).
63. R. B. Bird, W. E. Stewart, and E. N. Lightfoot, Transport Phenomena (John Wiley & Sons, Inc., New York, 1962).
64. D. L. Bish, A. E. Ogard, and D. T. Vaniman, "Mineralogy-Petrology and Groundwater Geochemistry of Yucca Mountain Tuffs," in Scientific Basis for Nuclear Waste Management VII, 1983 Symposium, G. L. McVay, Ed. (Materials Research Society, Boston 1984), pp. 283-291.
65. R. M. Potter and G. R. Rossman, "Mineralogy of Manganese Dendrites and Coatings," *Amer. Mineral.* 64, 1219-1226 (1979).

66. F. Caporuscio, D. Vaniman, D. Bish, D. Broxton, B. Arney, G. Heiken, F. Byers, R. Gooley, and E. Semarge, "Petrologic Studies of Drill Cores USW-G2 and UE25b-1H, Yucca Mountain, Nevada," Los Alamos National Laboratory report LA-9255-MS (July 1982).
67. D. Vaniman, D. Bish, D. Broxton, F. Byers, G. Heiken, B. Carlos, E. Semarge, F. Caporuscio, and R. Gooley, "Variations in Authigenic Mineralogy and Sorptive Zeolite Abundance at Yucca Mountain, Nevada, Based on Studies of Drill Cores USW GU-3 and G-3," Los Alamos National Laboratory report LA-9707-MS (June 1984).
68. R. M. Garrells and C. L. Christ, Solutions, Minerals and Equilibria (Freeman, Cooper and Co., San Francisco, 1965).
69. R. A. Zielinski, D. A. Lindsey, and J. N. Rosholt, "The Distribution and Mobility of Uranium in Glassy and Zeolitized Tuff, Keg Mountain Area, Utah, USA," *Chem. Geol.* 29, 139-162 (1980).
70. R. A. Zielinski, "Evaluation of Ash-flow Tuffs as Hosts for Radioactive Waste: Criteria based on Selective Leaching of Manganese Oxides," US Geol. Survey open file report 83-480 (1983).
71. D. L. Bish, "Effects of Composition on the Thermal Expansion/Contraction of Clinoptilolite," Clays and Clay Minerals (in press).
72. D. E. Appleman, D. E. Handwerker, and H. T. Evans, Jr., "A FORTRAN IV Version of The Least Squares Refinement of Crystal Unit Cells with Powder Diffraction Data by an Automatic Computer Indexing Method," *Prog. Ann. Meeting Amer. Cryst. Assoc.*, Cambridge, Massachusetts, 42-43 (1963).
73. J. R. Boles, "Composition, Optical Properties, Cell Dimensions, and Thermal Stability of Some Heulandite-Group Zeolites," *Amer. Mineral.* 57, 1463-1493 (1972).
74. H. P. Klug and L. E. Alexander, X-Ray Diffraction Procedures for Polycrystalline and Amorphous Materials, (John Wiley & Sons, New York, 1974), 966 pp.
75. F. H. Chung, "Quantitative Interpretation of X-Ray Diffraction Patterns of Mixtures. I. Matrix-Flushing Method for Quantitative Multicomponent Analysis," *J. Appl. Crystal.* 7, 519-525 (1974a).
76. I. Y. Borg and D. K. Smith, "Calculated X-Ray Powder Patterns for Silicate Minerals," *Geol. Soc. Amer. Mem.* 122, 896 (1969).
77. F. H. Chung, "Quantitative Interpretation of X-Ray Diffraction Patterns of Mixtures. II. Adiabatic Principle of X-Ray Diffraction Analysis of Mixtures," *J. Appl. Crystal.* 7, 526-531 (1974b).
78. D. L. Bish and D. T. Vaniman, "Mineralogic Summary of Yucca Mountain, Nevada," Los Alamos National Laboratory report (in preparation).
79. R. Scott and J. Bonk, "Geological Map of Yucca Mountain with Cross Sections," US Geol. Survey open file report USGS-OFR-84-494 (1984).

80. D. L. Hoover, "Genesis of Zeolites, Nevada Test Site," in "Nevada Test Site," Geol. Soc. Amer. Mem. 110, 275-284 (1968).
81. G. Knauss, V. M. Oversby, and T. J. Wolery, "Post Emplacement Environment of Waste Packages," in Scientific Basis for Nuclear Waste Management VII, 1983 Symposium, G. L. McVay, Ed (Material Research Society, Boston, 1984), pp. 301-308.
82. D. L. Bish, D. T. Vaniman, F. M. Byers, and D. Broxton, "Summary of the Mineralogy-Petrology of Tuffs of Yucca Mountain and the Secondary-Phase Thermal Stability in Tuffs," Los Alamos National Laboratory report LA-9321-MS (1982).
83. B. F. Jones, "Mineralogy of Fine-Grained Alluvium from Borehole U11g, Expl. 1, Northern Frenchman Flat Area, Nevada Test Site," U.S. Geol. Survey report for US Department of Energy, Nevada Operations Office (1982).
84. F. H. Gillery, "Adsorption-Desorption Characteristics of Synthetic Montmorillonoids in Humid Atmospheres," Amer. Mineral. 44, 806-818 (1959).
85. H. Suquet, C. De La Calle, and H. Pezerat, "Swelling and Structural Organization of Saponite," Clays and Minerals, 23, 1-9 (1975).
86. P. I. Carroll, F. A. Caporuscio, and D. L. Bish, "Further Description of the Topopah Spring Member of the Paintbrush Tuff in Drill Holes UE25a-1 and USW-G1 and of the Lithic Rich Tuff in USW-G1, Yucca Mountain, Nevada," Los Alamos National Laboratory report LA-9000-MS (November 1981).
87. S. S. Levy, "Studies of Altered Vitrophyre for the Prediction of Nuclear Waste Repository-Induced Thermal Alteration at Yucca Mountain, Nevada," in Scientific Basis for Nuclear Waste Management VII, 1983 Symposium, G. L. McVay, Ed. (Materials Research Society, Boston 1984b) pp. 959-966.
88. B. A. Carlos, "Fracture Mineralogy of Samples above the Static Water Level in Drill Core USW G-4, Yucca Mountain, Nevada," Los Alamos National Laboratory report (in preparation)
89. G. H. Heiken and M. L. Bevier, "Petrology of Tuff Units from the J-13 Drill Site, Jackass Flats, Nevada," Los Alamos National Laboratory report LA-7563-MS (February 1979).
90. M. L. Sykes, G. H. Heiken, and J. R. Smyth, "Mineralogy and Petrology of Tuff Units from the UE25a-1 Drill Site, Yucca Mountain, Nevada," Los Alamos National Laboratory report LA-8139-MS (November 1979).
91. D. L. Bish and E. Semarge, "Mineralogic Variations in a Silicic Tuff Sequence: Evidence for Diagenetic and Reactions," Abst. 19th Ann. Clay Min. Soc. Mtg., Hilo, Hawaii, August 8-14, p. 42 (1982).
92. B. Crowe, B. S. Self, D. Vaniman, R. Amos, and F. Perry, "Aspects of Potential Magmatic Disruption of a High-Level Radioactive Waste Repository in Southern Nevada," J. Geol. 91, pp. 259-276 (1983).

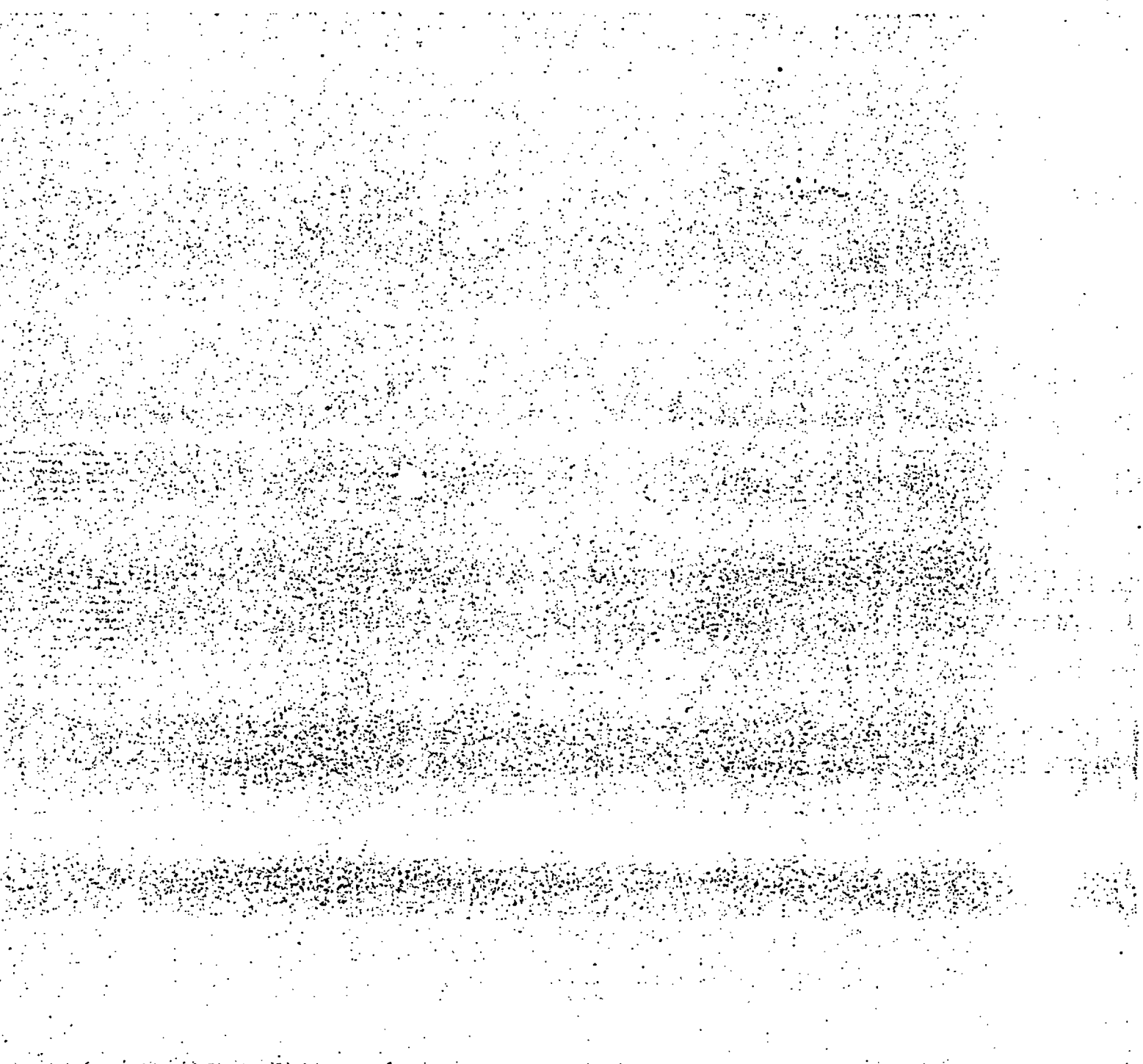
93. J. M. Healy, S. M. Hickman, M. D. Zoback, and W. L. Ellis, "Report on Televiewer Log and Stress Measurements in Core Hole USW-G1, Nevada Test Site, December 13-22, 1981," US Geological Survey open file report USGS-OFR-84-15 (1984).
94. B. M. Crowe, D. T. Vaniman, and W. J. Carr, "Status of Volcanic Hazard Studies for the Nevada Nuclear Waste Storage Investigations," Los Alamos National Laboratory report LA-9325-MS (March 1983).
95. D. T. Vaniman and B. M. Crowe, "Geology and Petrology of the Basalts of Crater Flat: Applications to Volcanic Risk Assessment for the Nevada Nuclear Waste Storage Investigations," Los Alamos National Laboratory report LA-8845-MS (1981).
96. A. Miyashiro, "Nature of Alkalic Volcanic Rock Series," Contrib. Mineral. Petrol. 66, 91-104 (1978).
97. M. G. Best and W. H. Brimhall, "Late Cenozoic Alkalic Basaltic Magmas in the Western Colorado Plateaus and the Basin and Range Transition Zone and Their Bearing on Mantle Dynamics," Geol. Soc. Am. Bull. 85, 1677-1690 (1974).
98. J. D. Blacic, "Importance of Creep Failure of Hard Rock in the Near Field of a Nuclear Waste Repository," in Near-Field Phenomena in Geologic Repositories for Radioactive Waste (N.E.A., Paris, 1981), pp. 121-129.
99. J. D. Blacic, J. Carter, P. Halleck, P. Johnson, T. Shankland, R. Andersen, K. Spicochi, and A. Heller, "Effects of Long-Term Exposure of Tuffs to High-Level Nuclear Waste-Repository Conditions: Preliminary Report," Los Alamos National Laboratory report LA-9174-PR (1982).
100. J. D. Blacic, D. T. Vaniman, D. L. Bish, C. J. Duffy, and R. C. Gooley, "Effects of Long-Term Exposure of Tuffs to High-Level Nuclear Waste-Repository Conditions: Final Report," Los Alamos National Laboratory report LA-9330-MS (1984).
101. J. K. Johnstone, R. R. Peters, and P. F. Gnirk, "Unit Evaluation at Yucca Mountain: Summary Report and Recommendation," Sandia National Laboratories report SAND83-0372 (1984).

Printed in the United States of America
Available from
National Technical Information Service
US Department of Commerce
5285 Port Royal Road
Springfield, VA 22161

Microfiche (A01)

NTIS		NTIS		NTIS		NTIS	
Page Range	Price Code						
001-025	A02	151-175	A08	301-325	A14	451-475	A20
026-050	A03	176-200	A09	326-350	A15	476-500	A21
051-075	A04	201-225	A10	351-375	A16	501-525	A22
076-100	A05	226-250	A11	376-400	A17	526-550	A23
101-125	A06	251-275	A12	401-425	A18	551-575	A24
126-150	A07	276-300	A13	426-450	A19	576-600	A25
						601-up*	A99

*Contact NTIS for a price quote.



Los Alamos